# Doctoral Thesis

# Novel Synthesis of $Li_2S$-Graphene Composite for Advanced Lithium-Sulfur Batteries

($Li_2S$-グラフェン複合体の新規合成及び革新的リチウム-硫黄二次電池への適用)

Graduate School of Engineering
Yokohama National University
(国立大学法人　横浜国立大学大学院　工学府)

Zhe　Li
(喆　　李)

September 2016

# Novel Synthesis of $Li_2S$-Graphene Composite for Advanced Lithium-Sulfur Batteries

A Dissertation Submitted to Yokohama National University for the Partial Fulfillment of the Requirements for the Degree of Doctor of Engineering

**Submitted by**
Zhe Li
13SA592

September 2016

Department of Materials Science and Engineering
Yokohama National University
Yokohama, Japan

**Contents:**

## Acknowledgement

My sincere thanks go to all those people who have made my dissertation possible. Because of them, my doctoral study experience in Japan will become the one that I will cherish forever.

My deepest gratitude is to my supervisors, **Professor Masayoshi Watanabe** and **Professor Kaoru Dokko**, Department of Chemistry and Biotechnology, Yokohama National University, Japan, for their immense knowledge, continuous encouragement and invaluable guidance at all the stages of my research. Their support and patience help me to overcome the research issues and finish the dissertation, and, most importantly, they teach me how to do the research deeply. I also appreciate a lot for providing me an opportunity to join this high-level research group with such good experiment conditions.

I would like to express my sincere gratitude to **Dr. Hisashi Kokubo**, Department of Chemistry and Biotechnology, Yokohama National University, Japan, for his encouraging suggestion and various forms of support and care during my study.

I would like to acknowledge **Professor Masayoshi Watanabe, Professor Yoshihiro Kubota, Professor Mahito Atobe, Professor Kaoru Dokko** and **Associate Professor Satoshi Inagaki**, for their constructive and insightful comments as members of my thesis committee.

**Dr. Shiguo Zhang** has always been there to give practical advice in all the time of research. I am deeply grateful to him for helping me to enrich my ideas and improve my knowledge by numerous discussions on my research topic.

I am also deeply thankful to **Dr. Tomohiro Yasuda**, **Dr. Kazuhide Ueno**, **Dr. Morgan L. Thomas, Dr. Yutaro Kamei, Dr. Ce Zhang, Dr. Heejoon Moon, Mr. Ryoichi Tatara, Ms. Azusa Yamazaki, Mr. Shoshi Terada, Ms. Yumi Kobayashi, Mr. Kohei Ikeda, Ms. Ai Ikoma** and **other Li-S group members**, for their kind cooperation, enlightening instructions and helpful suggestions during this work. I also appreciate **Dr. Zhengjian Chen, Dr. Jiaheng Zhang, Dr, Miao Xu, Dr. Xiaofeng Ma, Mr. Jiazhi Wang** and **Ms. Caihong Wang** for their sincere concern and warm encouragement in my daily life.

I am indebted to the secretaries who assist the lab to run so efficiently, and all the lab members for the sleepless nights that we worked together for the research seminar, and for all the happiness that we have had in the past three years.

I also appreciate the financial support from China Scholarship Council (CSC) during my study at Yokohama National University.

Last but not the least, I would like to express my sincere appreciation to my family and friends for all of their love and support.

# Synopsis

The development of high-energy-density lithium-sulfur batteries is of profound importance for the long-term necessity of cheap and high-performance energy-storage devices for society and environment. However, the well-documented lithium anode issue may hinder its practical applications. As an alternative to sulfur cathodic materials, lithium sulfide ($Li_2S$) has recently attracted considerable attention, because of its high theoretical specific capacity, the pre-expansion of the active material that counters the large volume change issues associated with the $Li_2S$/S redox reactions, and, importantly, the possibility to address the safety concerns by using lithium-free anodes. Various efforts have been made to synthesize a highly efficient $Li_2S$/carbon composite; however, the electronically and ionically insulating nature and very high melting point of $Li_2S$ strongly complicate the synthetic procedures, making it difficult to achieve high utilization and realize the projected capacity.

In this work, for the first time, a very simple method was proposed by one-pot pyrolysis of a mixture of graphene nanoplatelet aggregates (GNAs) and low-cost lithium sulfate ($Li_2SO_4$). This in situ formed $Li_2S$/graphene nanocomposite, combined with a discharge-product-insoluble electrolyte developed by our group (where the discharge product is $Li_2S_x$: $x$ = 8–4), demonstrated excellent Li–S battery performance exceeding that of a mixture of commercial $Li_2S$ and GNAs. This simple, low-cost, and efficient strategy may open the way to further design and preparation of advanced $Li_2S$/carbon composite cathodes for Li–S batteries.

To remove the Li metal issues from the current Li-S cell configuration, simple and advanced lithium-ion sulfur cells are fabricated for the first time, by combining a thick $Li_2S$ cathode (three-dimensional porous current collector, $Li_2S$ loading: 2.2 mg/cm$^2$) with a solvate ionic liquid-based electrolyte and a graphite anode, without any complicated cell architecture. Such solvate ionic liquid (IL) electrolytes actually have a triple function. First, solvate ILs with high $Li^+$ transference numbers and high Li-ion concentration are compatible with the cathode of a Li-S battery. Second, they are compatible with the graphite electrodes, and $Li^+$ can reversibly intercalate/deintercalate into the graphite anode without cointercalation of solvent molecules. Third, the shuttle effect is significantly suppressed because polysulfides have very low solubility in solvate ILs. As a result, this triple-function electrolyte-based full cell demonstrated a stable and reversible charge and discharge behavior, along with a very high Coulombic efficiency.

Additionally, a suitable Li-free anode is vital for the achievement of the high-energy-density full cell with a prolonged cycling property. In this sense, amorphous silicon anode could be an ideal candidate for this battery configuration owing to its high theoretical specific capacity (3580 mAh/g) and good cycling behavior enabled by the relaxation of the physical stress. Another simple and advanced lithium-ion sulfur cell is then fabricated, by combining a thick $Li_2S$ cathode (three-dimensional porous current collector, $Li_2S$ loading: 2.2 $mg/cm^2$) with a solvate ionic liquid-based electrolyte and an amorphous silicon (Si nanoflake powder) anode. This $Li_2S$/Si full cell demonstrated a good charge and discharge behavior at 1 C rate. We believe that the present research could trigger new attempts to fabricate the $Li_2S$ cathode/Li-free anode cells.

# Chapter One

General Introduction

## 1.1.Lithium-Sulfur (Li-S) Batteries

Since Sony commercialized the Li-ion batteries (LIBs), LIBs have dominated the rechargeable battery market for more than two decades due to their light weight, high voltage and good environmental compatibility when compared with other kinds of batteries.[1, 2] The LIBs are typically comprised of a graphite anode and a lithium transition-metal oxide cathode, and operate based on the intercalation–deintercalation mechanism. Although LIBs have enabled the personal electronics revolution and altered the way we interact with people and information, they only deliver energy densities of less than 387 Wh/kg, which cannot satisfy the rapidly increasing power demands for portable electronics, electric vehicles (EVs) and hybrid electric vehicles (HEVs) (**Fig. 1.1**).[3, 4] Furthermore, with the development of stationary energy storage system supplied by sustainable and renewable sources (such as wind and solar), the "beyond Li-ion" rechargeable devices with high energy density and long cycle life have been urgently required.

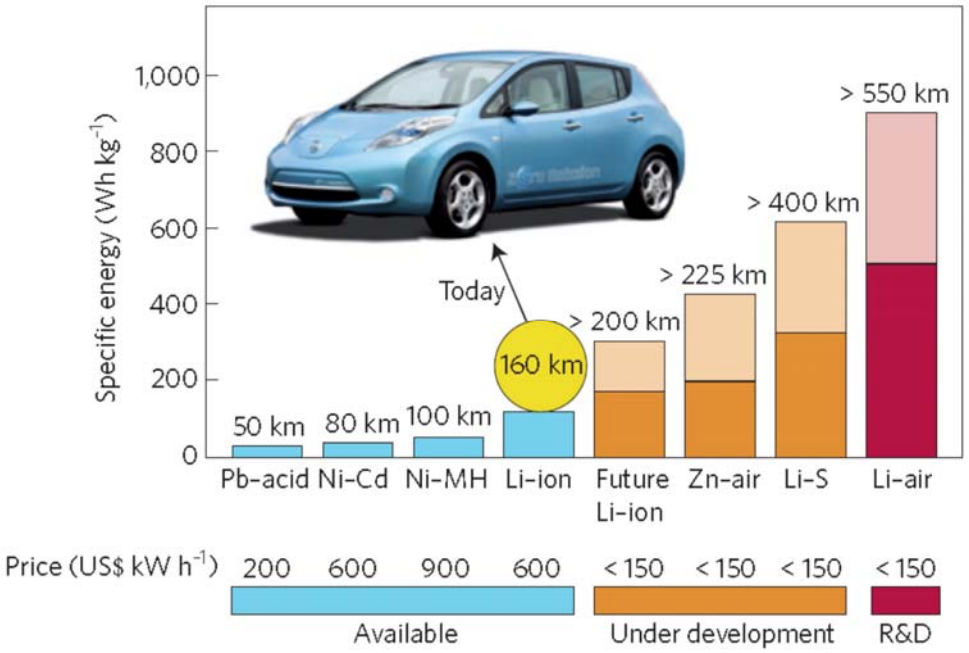


Fig. 1.1. Practical specific energies for some rechargeable batteries, along with estimated driving distances and pack prices.[3]

In this regard, lithium–sulfur (Li–S) battery, a promising "beyond Li-ion" device, has been attracting the ever-growing attention of researchers.[5-12] This battery operates on the basis of the lithium/sulfur redox reaction ($16Li + S_8 \rightarrow 8Li_2S$), which is totally different from the intercalation–deintercalation mechanism for the LIBs. The sulfur is an abundant and environmentally friendly resource, and can offer a theoretically large specific capacity of 1672 mAh/g. Additionally, lithium-sulfur battery benefits from the merits including a relatively low and safe operating voltage, the enormous potential for a high cyclability, a wide operating temperature region and a high theoretical specific energy (2600 Wh/Kg), which make it become the most promising star for next-generation rechargeable battery.[5]

### 1.1.1. Fundamental Lithium-Sulfur (Li-S) Chemistry

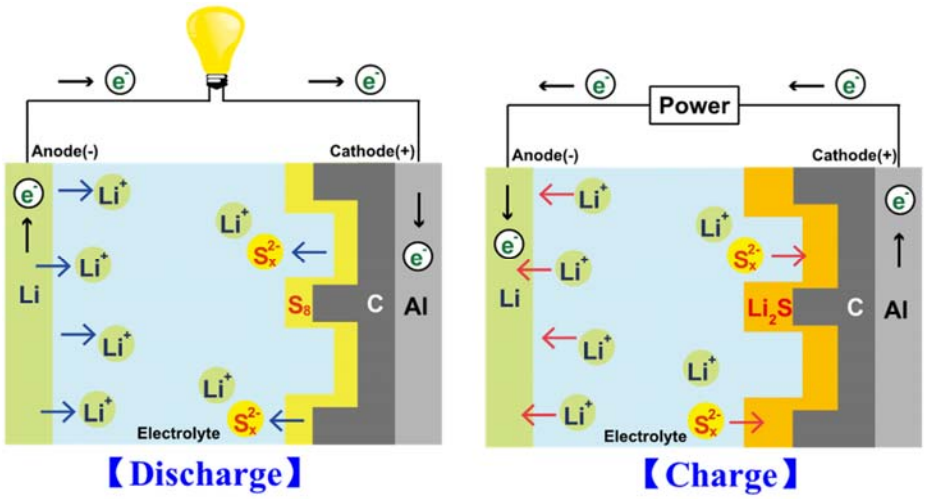


Fig. 1.2. Schematic illustration of Li–S battery configuration with its operations.

The Li–S battery is composed of a sulfur cathode, an electrolyte (polymer or liquid) and a lithium anode. **Fig. 1.2** displays the schematic illustration of Li–S battery configuration with its operations. Since the sulfur is at the charged state, this Li–S cell will begin with the discharge. During the discharge process, lithium anode could be oxidized to lithium ions and generate the electrons, while sulfur at the cathode side could be reduced to lithium sulfide through taking the electrons and lithium ions. According to the phase change of the discharge

product, this reduction process could be divided into four steps,[13] as shown in **Fig. 1.3**.

Step I: From sulfur (solid phase) to $Li_2S_8$ (liquid phase).

$$S_8 + 2Li \rightarrow Li_2S_8 \quad (1)$$

Step II: From $Li_2S_8$ (liquid phase) to low-order lithium polysulfide (liquid phase).

$$Li_2S_8 + 2Li \rightarrow Li_2S_{8-n} + Li_2S_n \quad (2)$$

Step III: From low-order lithium polysulfide (liquid phase) to $Li_2S_2$ or $Li_2S$ (solid phase).

$$2Li_2S_n + (2n-4)Li \rightarrow nLi_2S_2 \quad (3)$$

$$Li_2S_n + (2n-2)Li \rightarrow nLi_2S \quad (4)$$

Step IV: From $Li_2S_2$ (solid phase) to $Li_2S$ (solid phase).

$$Li_2S_2 + 2Li \rightarrow 2Li_2S \quad (5)$$

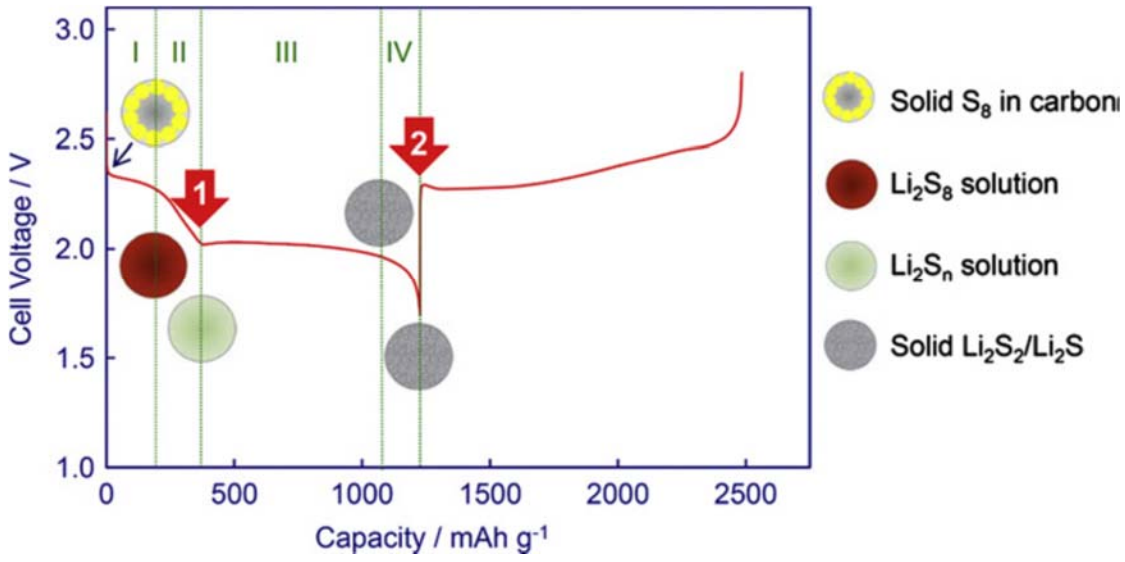


Fig. 1.3. A typical discharge and charge voltage profile of the first cycle of Li-S cells.[13]

In this four-step discharge, the step III with the discharge plateau at 1.9-2.1 V versus $Li/Li^+$ provides the majority of capacity for Li–S battery. While the sulfur

is electrochemically reduced step by step, the chemical reactions based on lithium polysulfides can also occur in organic electrolytes, as generally exhibited by the following equations [(6) and (7)]. During the charge process, lithium sulfide can be converted to elemental sulfur via the lithium polysulfide intermediates.[13]

$$Li_2S_n + Li_2S \rightarrow Li_2S_{n-m} + Li_2S_{1+m} \quad (6)$$

$$Li_2S_n \rightarrow Li_2S_{n-1} + 1/8S_8 \quad (7)$$

### 1.1.2. Main Issues and challenges of Li-S Batteries

The basic Li–S chemistry was investigated from more than 30 years ago, with a research about the reversible lithium polysulfide redox reactions.[12, 14] Although considerable advances in Li–S batteries have been made in recent years, their commercialization is still hindered by several serious issues and challenges.

(i) For the electrolyte, linear, cyclic, polymeric and short-chain ethers have been studied as potential candidates for Li–S batteries,[15] whereas the commonly used carbonate-based electrolytes in Li-ion batteries (ethylene carbonate (EC), diethyl carbonate (DEC), propylene carbonate (PC), and dimethyl carbonate (DMC)) are not compatible with Li–S batteries in most of cases, due to the strong nucleophilic reactivity of polysulfide anions to the carbonate solvents.[16] Among ether solvent-based electrolytes, the electrolyte depending on a solvent mixture of 1,3-dioxolane (DOL) and 1,2-dimethoxyethane (DME) (1 M LiTFSA in DOL/DME (1:1 v/v)), has generally been considered as the baseline for Li–S batteries.[15] DOL could help to form a protective solid–electrolyte interphase (SEI) layer on the surface of the Li metal anode through disruption of cyclic structures, while DME with a low viscosity and relatively high dielectric constant is a good solvent for lithium polysulfides, which could enable the sufficient redox reactions.

Although this DOL/DME-based electrolyte has a high conductivity, a low viscosity and good SEI-forming properties, its high polysulfide solubility can

result in a severe redox shuttle effect between the sulfur cathode and Li anode.[12] When the lithium polysulfides are formed at the cathode side, they can be dissolved into the DOL/DME-based electrolyte, and then diffuse to the Li metal anode side. Those dissolved lithium polysulfides can be electrochemically and chemically reduced to low-order lithium polysulfides and $Li_2S_2$ or $Li_2S$ on Li anode. When the concentration of lithium polysulfides gets higher at anode, the formed lithium sulfides will recombine with other dissolved lithium polysulfides, which can then diffuse back to the cathode side and be oxidized again. The lithium polysulfides repeatedly shuttle between the cathode and anode, resulting in a significant loss of active material, reaction with the lithium anode, fast capacity fading, and low Coulombic efficiencies.[12, 13, 15]

Different from the conventional DOL/DME-based electrolyte, novel electrolytes based on molten complexes comprised of equimolar mixtures of LiTFSA and triglyme (G3) or tetraglyme (G4), were proposed by our group.[17-24] Because those glyme–Li salt equimolar complexes behave like ionic liquids (ILs), such as a low volatility, a high thermal stability and a wide electrochemical window, they are considered to be a new type of IL, named solvate ILs.[17, 23] Note that the solvate ILs have the high $Li^+$-ion concentration and high Li transference number, and can suppress the dissolution of lithium polysulfides due to the solvation properties of ILs. However, the intrinsically high viscosity of ILs becomes a disadvantage for its application in Li–S batteries. Adding the appropriate low-viscosity and low-polar cosolvents into solvate ILs is an effective way to reduce the viscosity of the electrolyte.[17] Also, it can enhance the conductivity and $Li^+$ transport properties, while still inhibiting the dissolution of lithium polysulfides and giving rise to high Coulombic efficiency for the batteries.[17] For example, the solvate IL, $[Li(G4)_1][TFSA]$, can be diluted by a low-polar hydrofluoro ether, 1,1,2,2-tetrafluoroethyl 2,2,3,3-tetrafluoropropylether (HFE). We found that the solubility of lithium polysulfides became even lower in the $[Li(G4)_1][TFSA]$/HFE electrolyte, while the conductivity and $Li^+$ transport properties were improved.[15, 17] As a result, $[Li(G4)_1][TFSA]$/HFE-based Li–S battery exhibited a higher discharge capacity, a better cycling stability, a higher

Coulombic efficiency and rate capability (**Fig. 1.4**).[17] Although this solvate IL diluted by HFE has the limitation of easy evaporation, this type of polysulfide-insoluble electrolyte is a very promising candidate for Li–S batteries.

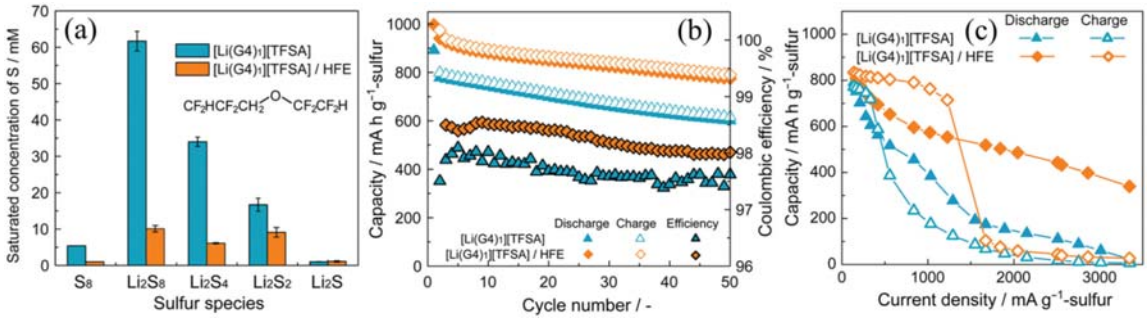


Fig. 1.4. (a) Comparison of $S_8$ and $Li_2S_n$ solubility limits in $[Li(G4)_1][TFSA]$ and $[Li(G4)_{11}][TFSA]$/HFE (molar ratio of Li[TFSA]/G4/HFE = 1:1:4) at 30 °C. The structure of HFE is shown in the inset. (b) Dependences of the discharge and charge capacities and coulombic efficiencies on cycle number. (c) Comparison of discharge and charge rate capabilities for Li–S cells with $[Li(G4)_1][TFSA]$ and $[Li(G4)_1][TFSA]$/HFE. Sulfur/Ketjen black (KB) composites were used as the electrode materials with a sulfur content of 60 wt% in the cathode composites.[17]

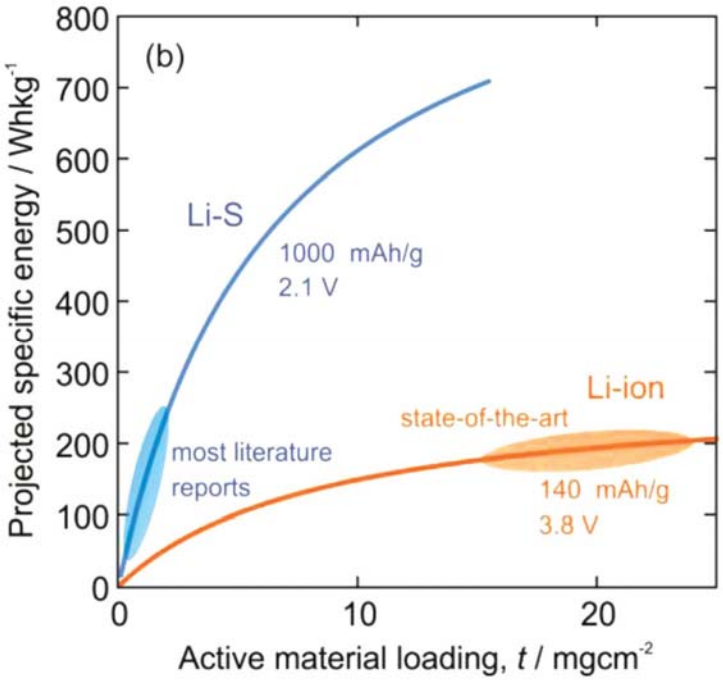


Fig. 1.5. Corresponding practical energy density as a function of active material loading and several assumed parameters. For the sulfur case, the assumption that a 125 μm thick Li foil

was used required us to stop the curve at ≈15.6 mg/cm$^2$ as this corresponds to the point where Li metal is no longer in excess.[25]

(ii) For the sulfur cathode, the active sulfur and its discharge product (lithium sulfide, $Li_2S$) are electronically and ionically insulating in nature, and have relatively low weight density. In most of cases, conductive carbon or polymer should be added into the sulfur cathode to increase the electronic conductivity and thus improve the electrochemical utilization of poorly conducting sulfur.[13] First, to ensure the high energy density of Li–S batteries, the content of the active sulfur in cathode material and the sulfur loading are required to be high.[10, 26-29] For example, Prof. Pope and Prof. Aksay investigated the relationship between the practical energy density and active material loading through defining some battery parameters and assumptions, as shown in **Fig. 1.5**.[25] From their result, it is distinct that the sulfur loading on cathode is indeed a vital parameter, which can reflect the potential for a Li–S battery to realize an energy density higher than the state-of-the-art Li-ion batteries. However, the sulfur loading in the most of reported cathodes is usually low (< 2.0 mg/cm$^2$), limiting the energy density of the Li-S batteries.[29] Second, the low weight density of sulfur cathode material and the pore structure of conductive carbon, will increase the electrolyte uptake, resulting in a lower practical energy density for Li-S batteries. Finally, the active sulfur is known to undergo a large volume expansion/contraction (ca. 80%) during discharge–charge, and this induces an unstable electrochemical contact over long cycles and degrades the structural integrity of the cathode. [9, 13]

(iii) For the anode, besides the well-documented redox shuttle effect mentioned above, Li metal is very reactive and prone to dendrite formation during the charging especially at high current densities (**Fig. 1.6**).[9, 30] This brings about the internal short circuit of the cell that causes serious problems for the safe use of Li-S batteries and hinders their large-scale practical applications.

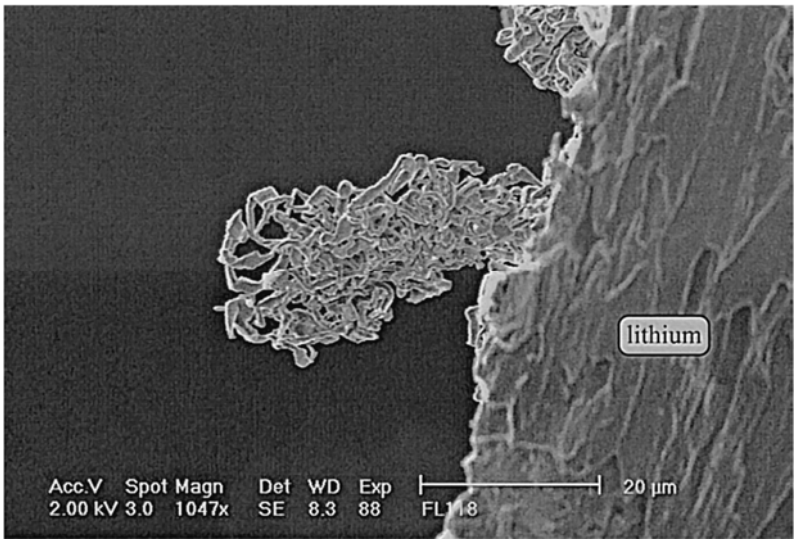


Fig. 1.6. Lithium dendrite formation in a lithium battery after one charge at 2.2 mA/cm$^2$.[30]

### 1.1.3. $Li_2S$ Cathode Architecture

To circumvent the issues and face the challenges mentioned above, extensive efforts have been undertaken to investigate the lithium sulfur battery (sulfur as cathode and metallic lithium as anode). For example, the development of advanced composite cathodes or new potential electrolytes could help to solve the problems associated with the sulfur cathode, by improving the electronic conductivity of the cathode materials, optimizing the carbon material structure, suppressing the shuttle effect, accommodating the volume change and exploiting the three-dimensional (3D) porous current collectors.[5, 15, 31-36] However, the issue about lithium dendrite formation at anode side still remain.

As an another problem-solving strategy, displacing the sulfur by $Li_2S$ active material could enhance the mechanical stability of the composite cathode during cycling and enable us to design the high-density cathode with high active material loading, since the volume of the active material experiences the shrinkage ($Li_2S \rightarrow S$) rather than expansion ($S \rightarrow Li_2S$) in the first charging process.[24, 37, 38] Also, $Li_2S$ could offer an acceptable theoretical specific capacity of 1166 mAh/g, representing a promising cathode-active material.[9, 39] Note that the well-documented safety hazards from the lithium metal anode in liquid

electrolytes could be solved, by combining the $Li_2S$ cathode with Li-free anodes (such as graphite, high-capacity tin and silicon) to construct a lithium-ion full cell configuration.[9, 39]

Generally speaking, $Li_2S$ is electrochemically inactive, and a high overpotential exists for the large-sized $Li_2S$ particles during the initial charging process, due to the electronically and ionically insulating nature.[40, 41] In this case, the $Li_2S$ cathode must first be electrochemically activated by applying a high charging cutoff voltage to overcome the barrier, which can enhance the utilization of $Li_2S$ markedly. Yang et al. have investigate the $Li_2S$ activation mechanism in detail by means of in-situ X-ray diffraction, electrochemical characteristics and the model for this initial charging.[40] They found that this initial barrier is from the phase nucleation of polysulfide, while the height of the barrier is attributed to the slow charge transfer at $Li_2S$ surface and the poor lithium ion diffusion in $Li_2S$. After this $Li_2S$ activation, all the subsequent cycles exhibit similar charge/discharge behaviors with the conventional sulfur cathodes, and the barrier of lithium extraction from insulating $Li_2S$ does not exist anymore.[40, 41]

## 1.2 Preparation of $Li_2S$-Carbon Composite

Similar with the sulfur, $Li_2S$ is neither electronically nor ionically conductive, which make it hard to realize the high utilization and deliver the high capacity. Continuous efforts have been made to face this problem by adding the conductive additives and improving the electrochemical contact between $Li_2S$ and conductors.[5, 9, 39] However, due to its high melting point (938℃), it is difficult to incorporate $Li_2S$ into porous conductive hosts through the established melting–diffusion method, which is used for sulfur cathode material. Hence, many approaches have been proposed recently for the preparation of $Li_2S$-carbon composite, by which a high reversible capacity could be obtained. In this section, several typical approaches will be introduced.

### 1.2.1. Ball-Milling Method

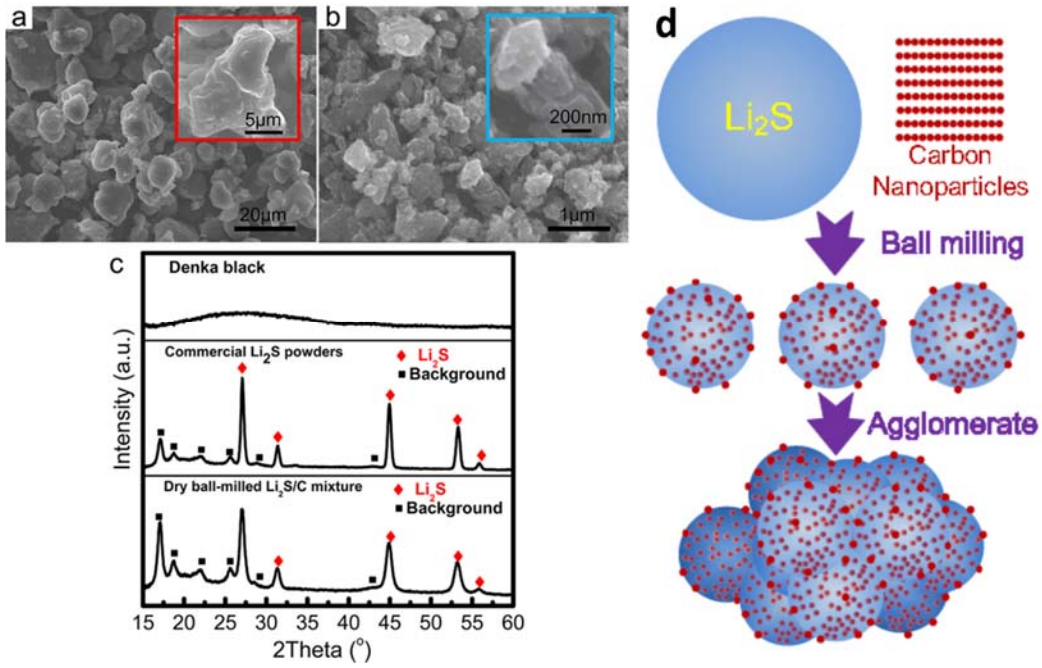


Fig. 1.7. Scanning electron microscope (SEM) images of (a) bulk $Li_2S$ powder and (b) ball-milled $Li_2S$−carbon black composite. The insets in (a) and (b) show enlarged views of $Li_2S$ particles before and after ball mill. (c) X-ray diffraction (XRD) patterns of carbon black, $Li_2S$ powder and ball-milled $Li_2S$−carbon black composite. The black squares correspond to peaks from the glass substrate and tape cover used to prevent the exposure of $Li_2S$ to air. (d) Schematic illustration of the high-energy ball-milling process.[42]

A ball mill operates based on the principle of attrition and impact force, and is extensively used for grinding materials (wet or dry) and reducing the particle size. Moreover, ball-milling method is found to be an effective way to fabricate the amorphous materials. $Li_2S$-C composite cathodes can be prepared simply via direct ball-milling of commercial $Li_2S$ powder with carbon materials.[40, 42-47] Based on this method, Prof. Yuegang Zhang's group produced a nanostructured $Li_2S$-carbon black composite at a rotation speed of 1060 cycles per minute.[42] As shown in **Fig. 1.7**, the particle size of $Li_2S$ can be decreased from 10-30 μm to 200-500 nm. Although the ball-milled $Li_2S$−carbon black composite exhibited some agglomeration, the carbon black was homogeneously distributed on the surface of $Li_2S$ particles. X-ray diffraction (XRD) analysis (**Fig. 1.7(c)**) also confirmed the vital role of high-energy ball mill. The XRD peak of ball-milled composite matched very well with the bulk $Li_2S$, indicating that no impurities

are generated during the ball-milling process. In agreement with the SEM results, the peaks are considerably broadened when compared with bulk $Li_2S$, due to the decrease in particle size of the $Li_2S$. This method could also increase the contact between $Li_2S$ cathode and electrolyte, and further improve the reaction kinetics of $Li_2S$. As a result, this ball-milled $Li_2S$−carbon black composite cathode with a high $Li_2S$ content (67.5 wt%) can deliver a very high discharge capacity of 1144 mAh/g-$Li_2S$ (98% of the theoretical value).[42] Kaiser et al. used four different carbon sources (carbon black (CB), activated carbon (AC), graphene (GP) and multi-walled carbon nanotube (MWCNT)) to mill with microsized $Li_2S$ powder in a planetary ball mill at 100 rpm, and the obtained $Li_2S$-C composites were investigated to find the suitable carbon sources.[44] Also, in their work, three-dimensional (3D) multi-layered Ni foam was employed to fabricate a binder-free and high-mass-loading composite cathode (active material loading: ~5 mg/cm$^2$). Electrochemical performance testing revealed that $Li_2S$-MWCNT composite cathode had the capacity retention of 50.7% after 100 cycle, which is higher than $Li_2S$-GP (40.9%), $Li_2S$-AC (25%) and $Li_2S$-CB (21.3%). This excellent cycling performance of $Li_2S$-MWCNT composite can be explained by its morphology, where the highly conductive MWCNT was well dispersed, and covered the surface of $Li_2S$.[44]

Although ball mill is a very simple and efficient approach in reducing the particle size and improving the distribution of carbon, it inevitably produces a wide particle size distribution and random morphology of $Li_2S$.

### 1.2.2. Solution-Based Route

The solution-based route was proposed based on the high solubility of $Li_2S$ in anhydrous ethanol, by which $Li_2S$ nanoparticles can be homogeneously deposited onto the conductive carbon matrix.[48-55] For example, Wu et al. have developed a multi-walled carbon nanotube (MWCNT)-linked $Li_2S$ composite through this versatile method.[48] **Fig. 1.8** displays schematic illustration of the nanoporous $Li_2S$ and MWCNT-linked nano-$Li_2S$ composite synthesis.[48] In this synthesis, $Li_2S$ was first dissolved into anhydrous ethanol to obtain a $Li_2S$ solution, followed by the addition of MWCNT and evaporation of ethanol. Thus,

$Li_2S$ can nucleate and grow heterogeneously on the surface of MWCNT. Finally, this composite was annealed under Ar atmosphere at 400 ℃. Interestingly, the $Li_2S$ particles intimately connected with MWCNT exhibited a particle size of 10 nm, which is quite smaller than that of commercial $Li_2S$. This MWCNT-linked $Li_2S$ composite (20 wt% MWCNT) could give high discharge capacities of up to 1050 mAh/g-S at C/20 and 800 mAh/g-S at C/2, and demonstrate a stable electrochemical performance for over 100 cycles. Following to this discovery, Wu et al. have also developed $Li_2S$-graphene composite, $Li_2S$-C nanocomposite (polyvinylpyrrolidone (PVP) as a carbon precursor), hierarchical C-$Li_2S$-C nanocomposite, graphene-$Li_2S$-carbon nanocomposite (C-coated $Li_2S$ nanoparticles on graphene) and so on.[49-51, 53] The solution-based route can be used not only for the preparation of $Li_2S$-carbon composite, but also for the development of a free-standing and binder-free cathode. Wang et al. reported a slurryless nano-$Li_2S$/reduced graphene oxide cathode paper, which is synthesized by drop coating of the reduced graphene oxide paper through the solution of $Li_2S$ (in anhydrous ethanol).[52] After vacuum heating, the ethanol (solvent) was removed, while $Li_2S$ particles can nucleate and grow uniformly onto the reduced graphene oxide paper with a size of 25-50 nm. This paper can act as the cathode directly without using the metal current collectors, and delivered a high discharge capacity of 816.1 mAh/g-$Li_2S$ after 150 cycles at 0.1 C, and 597 mAh/g-$Li_2S$ at 7 C, indicating a superior electrochemical performance.

For the physical methods described above (ball-milling method and solution-based route), commercial bulk $Li_2S$ powders were employed as the starting material, which may not be an attractive candidate for practical application because of its high cost.

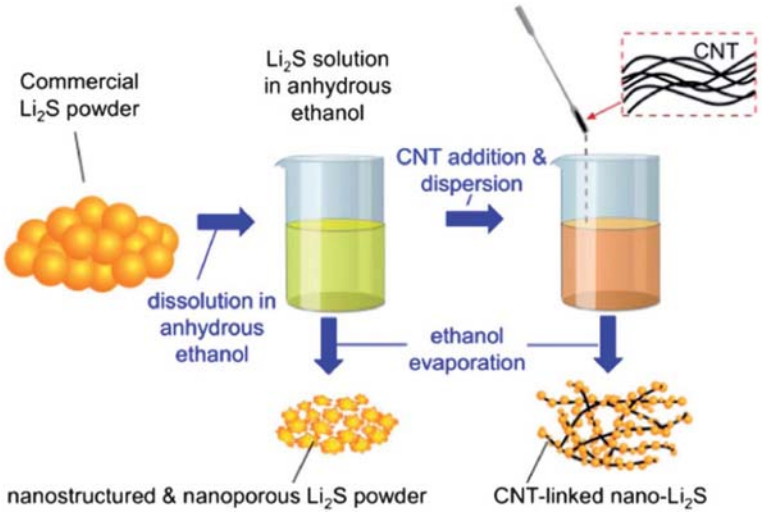


Fig. 1.8. Schematic illustration of the nanoporous $Li_2S$ and MWCNT-linked nano-$Li_2S$ composite synthesis.[48]

### 1.2.3. Chemistry Approach

Chemistry approaches were also implemented to synthesize $Li_2S$-C composites by various reactions. Nan et al. have synthesized durable carbon-coated $Li_2S$ core−shell ($Li_2S$@C) spheres successfully, as shown in **Fig. 1.9**.[37] The sulfur solution (in toluene) was added into lithium triethylborohydride ($LiEt_3BH$) solution (in tetrahydrofuran, THF). The chemical reaction ($S + 2LiEt_3BH = Li_2S + 2Et_3B + H_2$) could then occur. By altering the reaction time and the amount of toluene, $Li_2S$ spheres with three different sizes (2 μm, 1 μm, and 500 nm) could be obtained. After the heat treatment (500 °C, 0.5 h), the organics in $Li_2S$ spheres could form the carbon and cover parts of the $Li_2S$ particle surface. The $Li_2S$ spheres after the heat treatment were finally coated with carbon by using the chemical vapor deposition (CVD) method. The protective and conductive carbon shell could enhance the conductivity of the $Li_2S$ spheres and inhibit the dissolution of polysulfides. Consequently, $Li_2S$@C spheres cathodes exhibited high specific capacity (an initial discharge capacity of 972 mAh/g-$Li_2S$ at 0.2 C) and excellent cycling performance. By employing the reaction between sulfur and $LiEt_3BH$, $Li_2S$-graphene nanosheets composite,[56] $Li_2S$/GO@C nanospheres ($Li_2S$/graphene oxide nanospheres with conformal carbon coating),[57] carbon-coated Nano$Li_2S$ (Nano$Li_2S$@carbon) composite and carbon cage encapsulating

nano-cluster $Li_2S$ have been developed recently.[58, 59] Besides the $LiEt_3BH$, another organolithium reagent, n-butyllithium was also adopted to prepare the $Li_2S$-C composite. Prof. Yi Cui's group reported a $Li_2S$/ordered mesoporous carbon (CMK-3) electrode, which is made from the lithiation of sulfur/CMK-3 electrode by n-butyllithium in hexane.[60] During the lithiation process, $Li_2S$ can be formed within the pores of the CMK-3.

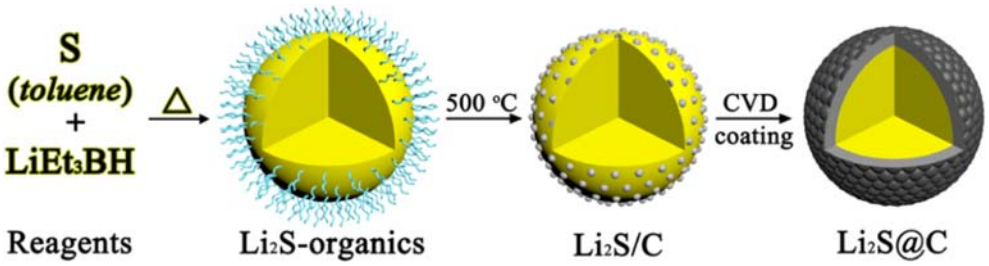


Fig. 1.9. Schematic illustration of the preparation process for the $Li_2S$@C spheres.[37]

Thermal treatment of lithium polysulfide-carbon (or carbon precursor) composites could provide a novel route to create $Li_2S$-C composites. Prof. Lynden A. Archer's group proposed a $Li_2S$-C composite by thermal treatment of a $Li_2S_3$-polyacrylonitrile (PAN) composite.[61] **Fig. 1.10** shows the synthesis route for $Li_2S$-C composite. A $Li_2S_3$ solution in DMF was first prepared by the reaction between $Li_2S$ and elemental sulfur, followed by mixing with the PAN solution in DMF. Here, the codissolution of the $Li_2S_3$ and PAN in DMF will benefit the homogenous dispersion. After heating at 100 °C to remove the DMF, the obtained $Li_2S_3$-PAN composite was then treated in furnace at 300 °C for 2 h. In this step, the PAN will form ring-like structures by cyclization, while the $Li_2S_3$ will convert to $Li_2S$ and elemental sulfur. Finally, the composite will be kept for 30 min at 600 °C to carbonize the PAN. Due to the uniform dispersion of $Li_2S$ throughout the composite, the cathode based on this $Li_2S$-C composite could deliver a stable discharge capacity of 500 mAh/g-$Li_2S$ with a Coulombic efficiency of nearly 100% at current density of 200 mA/g. Moreover, Han et al. prepared the $Li_2S$-reduced graphene oxide (rGO) nanocomposites with a unique 3D pocket structure, by thermal treatment of $Li_2S_6$-partially reduced graphene oxide (p-rGO) composite for 1 h at 700 °C.[62]

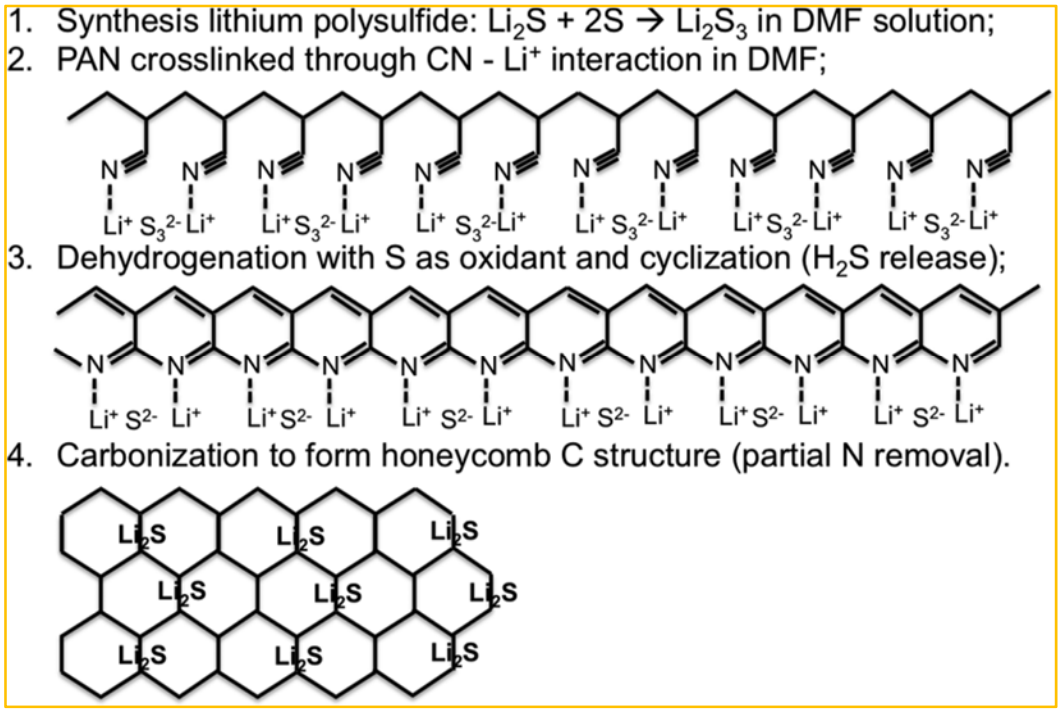


Fig. 1.10. Synthesis route for $Li_2S$-C composite.[61]

Besides the methods mentioned above, other methods such as the reaction between hydrogen sulfide ($H_2S$) and lithium naphthalenide (Li-NAP),[63] the utilization of a lithiated graphite electrode to reduce the $Li_2S_6$,[64] the pyrolysis of the mixture of lithium sulfate and resorcinol–formaldehyde aerogel,[65] and lithiation of sulfur/microporous carbon (S/MC) composite by stabilized lithium metal powder (SLMP),[66] were also reported to synthesize $Li_2S$-C composites. For most of chemistry approaches, they can enable the $Li_2S$-C composite with a good electrochemical performance. Nevertheless, these costly, dangerous, complex procedures are difficult to handle and unsuitable for large-scale production.

## 1.3. $Li_2S$ Cathode/Li-free Anode Batteries

Up to now, intensive research efforts have been devoted to preparing highly efficient $Li_2S$-carbon composites and improving the electrochemical performance of $Li_2S$/Li half cells. Note that the main purpose of designing and preparing the $Li_2S$/carbon composite is to construct the full lithium-ion cell configuration by combination of $Li_2S$ cathode and safe Li-free anode. However,

relatively little emphasis has been placed on these full cells. In previous works, $Li_2S$ cathodes have been coupled with graphite, Si and Sn anodes to realize the rechargeable full cells, which will be introduced in this section.

### 1.3.1 Graphite Anode-Based Full Cell

Low-cost graphite is a very promising candidate as the anode for a full cell, which is based on the well-established $Li^+$ intercalation/deintercalation chemistry, and has been applied in the commercial Li-ion batteries. Graphite with a layered structure can accommodate one Li per six C atoms to form $LiC_6$. Additionally, the electrochemical $Li^+$ intercalation and deintercalation reactions can only involve a very limited volume change,[67] which will benefit the full cell for outstanding cycling performance. However, the electrochemical $Li^+$ intercalation and deintercalation of graphite are highly electrolyte-selective. For example, although the electrolyte relying on ether solvents such as tetrahydrofuran, 1,3-dioxolane (DOL), and 1,2-dimethoxyethane (DME) is the most frequently utilized liquid electrolyte in Li–S battery, it is incompatible with graphite anode in Li-ion batteries due to the cointercalation of solvent into graphite, resulting in the destruction of the graphite crystalline structure.[68] Ethylene carbonate (EC)-based electrolyte has been used extensively in practical Li-ion batteries,[69] in which the formed solid electrolyte interphase (SEI) on the graphite surface can inhibit the cointercalation of solvent molecules into the graphite, and guarantee the successful $Li^+$ intercalation process.[19] However, in general, EC will adversely react with the polysulfides produced during the charge and discharge of Li-S battery.[16]

Hence, to construct the $Li_2S$/graphite full cells (graphite|electrolyte|$Li_2S$), one way is to employ the special $Li_2S$ cathodes, which can be compatible with the carbonate-based electrolytes. For example, $Li_2S$ was incorporated into microporous carbons by vacuum infusion of sulfur (vapor) at high temperature, followed by a lithiation process (spraying stabilized lithium metal powder (SLMP)).[66] **Fig. 1.11** shows schematic illustration of synthesis route for this $Li_2S$/microporous carbon composite electrode. In this case, this $Li_2S$ cathode can be paired with a graphite anode in this conventional Li-ion cell electrolyte (1.0

M $LiPF_6$ + EC/DEC (1:1, v/v)), and exhibited a high Coulombic efficiency (close to 100%) and good cycling performance. Unfortunately, this microporous carbon can only support 30% active material, and the full cell shows a low discharge plateau (ca. 1.6 V), both of which will decrease the energy density.[66]

Another way is also developed by constructing a very complicated full cell configuration with a two-phase electrolyte system, [graphite | electrolyte 1 (carbonate) || electrolyte 2 (ether) | $Li_2S$]. In this full cell, the carbonate electrolyte (compatible with the graphite anode) and the ether electrolyte (compatible with the $Li_2S$ cathode) is separated by a ceramic lithium super ionic conductor film (LISICON).[70] Hence, a more suitable electrolyte that can match the requirements of $Li_2S$ cathode and graphite anode simultaneously still need to be developed.

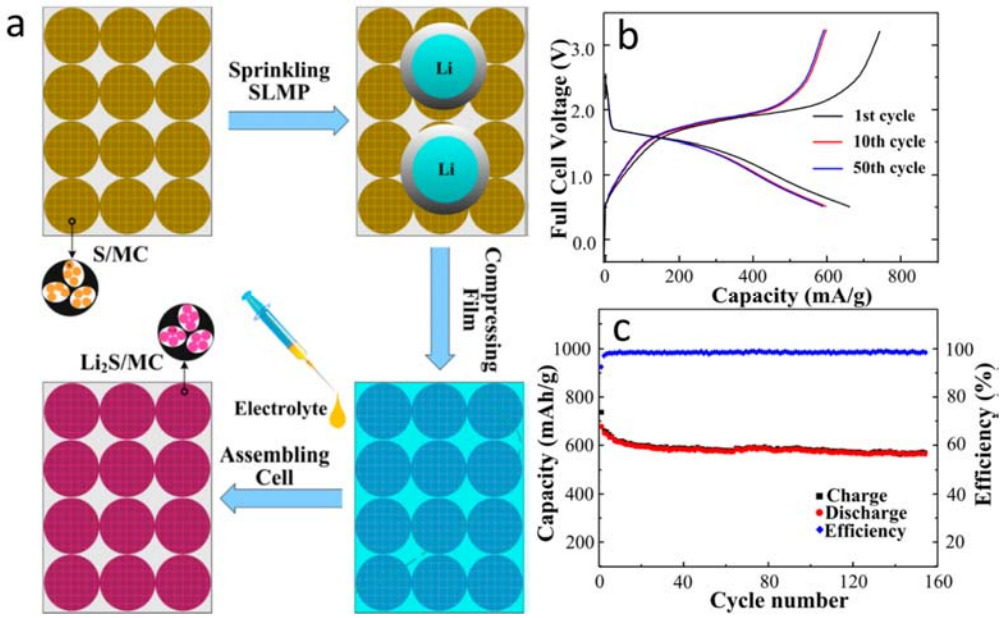


Fig. 1.11. (a) Schematic illustration of synthesis route for a $Li_2S$/microporous carbon (MC) composite electrode. (b) discharge/charge profiles of the full cell with a $Li_2S$/MC cathode and a graphite anode in the 1st, 10th, and 50th cycles. (c) Cycling performance and Coulombic efficiency curves. The specific capacity is based on the mass of $Li_2S$.[66]

### 1.3.2 Si Anode-Based Full Cell

Among the various anode materials, Si as a Li-alloying metal is one of the most promising candidates owing to the wide abundance and extremely high capacity. However, the large volume change of Si during the lithiation and delithiation process may cause the mechanical degradation (cracking or pulverization) and then the poor electrochemical properties.[71, 72] A lithium metal-free full cell comprised of a $Li_2S$/mesoporous carbon composite cathode and a silicon nanowire anode was reported by Prof. Yi Cui's group, as shown in **Fig. 1.12**.[60] This full cell can manifest a first discharge capacity of 423 mAh/g with an average discharge voltage of ~1.7 V. However, the corresponding capacity retention over 20 cycles is not good, showing a fast capacity fade. Hence, the high-energy-density $Li_2S$/Si full cell with a prolonged cycling property still need to be developed.

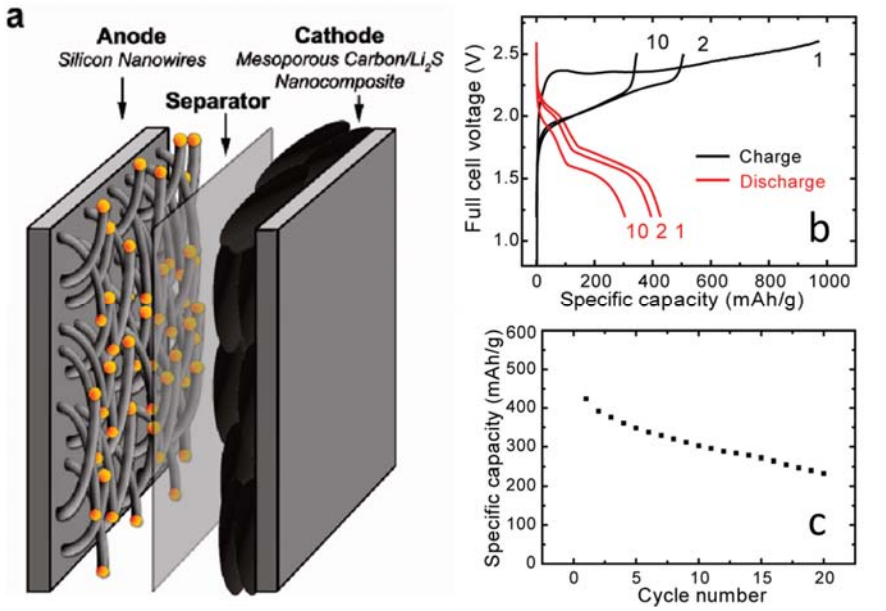


Fig. 1.12. (a) Schematic illustration of $Li_2S$/Si battery structure. (b) discharge/charge profiles of the full cell with a $Li_2S$/CMK-3 mesoporous carbon nanocomposite cathode and a silicon nanowire anode. (c) Cycling performance of this full cell. The current rate is C/3 (389 mA/g), and the specific capacity is based on the mass of $Li_2S$.[60]

### 1.3.3 Sn Anode-Based Full Cell

Tin can also alloy with Li, and deliver a theoretical capacity of 994 mAh/g when convert to $Li_{4.4}Sn$. Although this gravimetric capacity of Sn anode is lower than

that of Si, Sn-based anode is still attractive owing to its high volumetric capacity of 2000 mAh/cm$^3$, which is close to Si.[71] However, as with the other Li-alloying materials, its mechanical degradation from the large volume changes during cycling can lead to an unstable electrochemical contact and then a poor capacity retention.[71] To solve the volume change issue of Sn, a Sn-C nanocomposite (1:1 in weight) was selected as an anode by Hassoun et al.,[73] in which the Sn nanoparticles are in a protective amorphous carbon matrix. **Fig. 1.13** displays the schematic illustration of $Li_2S$/Sn-C battery consisting of a $Li_2S$/C cathode, a PEO-based gel polymer electrolyte and a Sn-C nanocomposite anode.[73] At cathode side, $Li_2S$ will convert to elemental sulfur with the release of lithium ions ($2.2Li_2S/C = 2.2S + C + 4.4Li^+ + 4.4e^-$). When the lithium ions arrive at anode side, an alloying reaction with Sn will occur ($4.4Li^+ + Sn/C + 4.4e^- = Li_{4.4}Sn + C$). Though this full cell exhibited a lower discharge capacity at C/5, the stability was excellent, along with a high Coulombic efficiency.

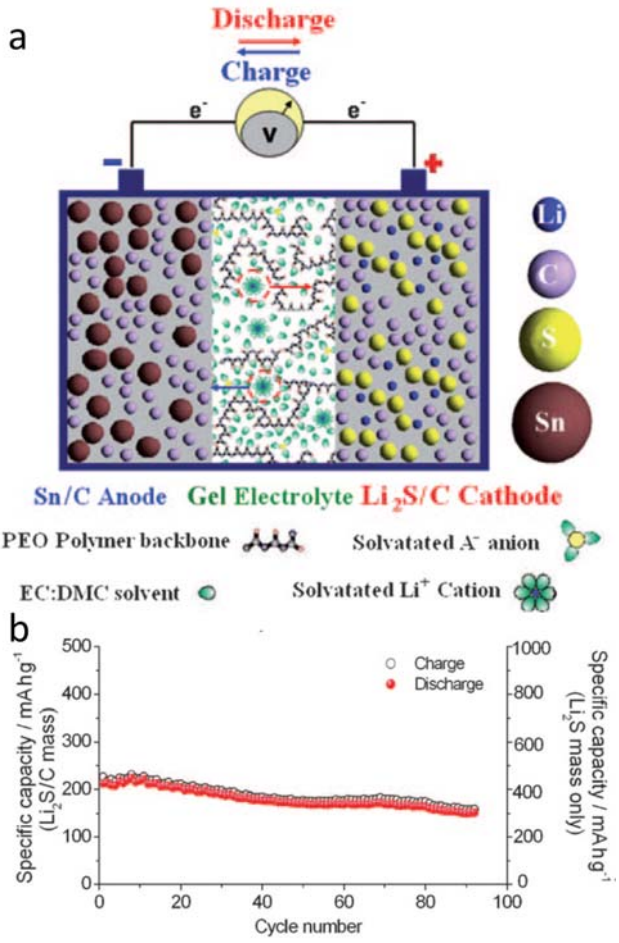

Fig. 1.13. (a) Schematic illustration of $Li_2S$/Sn-C battery structure. (b) Cycling performance of this full cell with a $Li_2S$/C cathode, a PEO-based gel polymer electrolyte and a Sn-C nanocomposite anode. The current rate is C/5 and the voltage range is 0.2-4.6 V. PEO: poly(ethylene oxide).[73]

## 1.4. Outline of This Study

In recent years, the preparation of highly efficient $Li_2S$-carbon composite and improvement of its electrochemical performance in $Li_2S$/Li half cells have been widely studied. In this study, different from other methods (**Chapter 1.2**), a facile, low-cost, scalable and environmentally friendly method is developed for the first time to prepare the $Li_2S$-C composite. Moreover, for the $Li_2S$ research, relatively little emphasis has been placed on the high-safety full cells, consisting of a $Li_2S$ cathode and a Li-free anode. Therefore, to take advantage of this $Li_2S$-C composite and remove the Li metal issues from the current Li-S cell configuration, another important aim of this work is to apply the obtained highly efficient $Li_2S$-C composite to the high-performance lithium-ion sulfur batteries (full cell). An outline for the main contents of this work is summarized as follows.

In chapter 2, one-pot synthesis of a $Li_2S$/graphene composite through direct pyrolysis of a mixture of graphene nanoplatelet aggregates (GNAs) and low-cost lithium sulfate ($Li_2SO_4$) was proposed. The GNAs have two functions: part of them serve as a reductant to reduce $Li_2SO_4$ and create $Li_2S$ at elevated temperature ($Li_2SO_4 + 2C \rightarrow 2CO_2 \uparrow + Li_2S$); meanwhile, GNAs are etched in situ into thin graphene sheets via this chemical reaction. The special layered structure of these residual graphene sheets can act as a highly conductive two-dimensional (2D) host to immobilize the active $Li_2S$ by intimate contact, improving the electrochemical utilization of $Li_2S$. When used as a cathode for Li–S batteries, in combination with a discharge-product-insoluble electrolyte (solvate ionic liquid), this $Li_2S$/graphene composite demonstrates excellent electrochemical performance with faster reaction kinetics, lower polarization, and better cycling performance and rate capability.

In chapter 3, a novel ball-milled $Li_2S$/graphene composite (LS-G BM) was introduced. This simple and efficient approach (high-energy ball milling) can not only reduce the particle size of the $Li_2S$/graphene composite, but also enhance the reaction kinetics of $Li_2S$. To improve the electrochemical performance of the LS-G BM cathode at high $Li_2S$ loading, carbon fiber paper was employed in place of the traditional aluminum foil current collector.

In chapter 4, lithium-ion sulfur batteries were constructed by combining a thick $Li_2S$ cathode, a solvate ionic-liquid-based electrolyte, and a graphite anode. In this system, solvate ionic liquid (IL), acting as a single-phase electrolyte, can enable the effective $Li^+$ intercalation and deintercalation of graphite electrodes and simultaneously inhibit the severe shuttle effect of lithium polysulfides. The composition of solvate ILs was further optimized by varying the molar ratio between G4 and LiTFSA. The ionic conductivity and the $Li^+$ intercalation/deintercalation properties of the electrolytes were found to greatly affect the battery performance.

A suitable Li-free anode is vital for the achievement of the high-energy-density full cell with a prolonged cycling property. Amorphous silicon anode could be an ideal candidate for this battery configuration owing to its high theoretical specific capacity. In chapter 5, a full cell is proposed by combining Si anode with a solvate ionic-liquid-based electrolyte and a thick $Li_2S$ cathode. After 200 cycles, this $Li_2S$/Si full cell can still maintain a discharge capacity of 292 mAh/g at 1 C, showing a good rate capability and cycle stability.

In chapter 6, concluding remarks on each chapter have been made individually based on results and discussion to underpin the prime achievements of the chapter. A future prospect of lithium-ion sulfur batteries was provided. Also, the improvement of battery energy density still need to be further studied for satisfying the practical applications.

## 1.5. References

[1] D. Bresser, S. Passerini, B. Scrosati, *Chem. Commun.* **2013**, *49*, 10545.
[2] M. Barghamadi, A. Kapoor, C. Wen, *J. Electrochem. Soc.* **2013**, *160*, A1256.
[3] P. G. Bruce, S. A. Freunberger, L. J. Hardwick, J. M. Tarascon, *Nat. Mater.* **2012**, *11*, 19.
[4] A. Manthiram, Y. Fu, Y. S. Su, *Acc. Chem. Res.* **2013**, *46*, 1125.
[5] A. Manthiram, Y. Fu, S. H. Chung, C. Zu, Y. S. Su, *Chem. Rev.* **2014**, *114*, 11751.
[6] X. Ji, K. T. Lee, L. F. Nazar, *Nat. Mater.* **2009**, *8*, 500.
[7] R. Xu, J. Lu, K. Amine, *Adv. Energy Mater.* **2015**, *5*, 1500408.
[8] M. K. Song, E. J. Cairns, Y. Zhang, *Nanoscale* **2013**, *5*, 2186.
[9] Y. Son, J. S. Lee, Y. Son, J. H. Jang, J. Cho, *Adv. Energy Mater.* **2015**, *5*, 1500110.
[10] S. Urbonaite, T. Poux, P. Novák, *Adv. Energy Mater.* **2015**, *5*, 1500118.
[11] G. Xu, B. Ding, J. Pan, P. Nie, L. Shen, X. Zhang, *J. Mater. Chem. A* **2014**, *2*, 12662.
[12] A. Rosenman, E. Markevich, G. Salitra, D. Aurbach, A. Garsuch, F. F. Chesneau, *Adv. Energy Mater.* **2015**, *5*, 1500212.
[13] S. S. Zhang, *J. Power Sources* **2013**, *231*, 153.
[14] H. Yamin, A. Gorenshtein, J. Penciner, Y. Sternberg, E. Peled, *J. Electrochem. Soc.* **1988**, *135*, 1045.
[15] S. Zhang, K. Ueno, K. Dokko, M. Watanabe, *Adv. Energy Mater.* **2015**, *5*, 1500117.
[16] J. Gao, M. A. Lowe, Y. Kiya, H. D. Abruña, *J. Phys. Chem. C* **2011**, *115*, 25132.
[17] K. Dokko, N. Tachikawa, K. Yamauchi, M. Tsuchiya, A. Yamazaki, E. Takashima, J. W. Park, K. Ueno, S. Seki, N. Serizawa, M. Watanabe, *J. Electrochem. Soc.* **2013**, *160*, A1304.
[18] H. Moon, T. Mandai, R. Tatara, K. Ueno, A. Yamazaki, K. Yoshida, S. Seki, K. Dokko, M. Watanabe, *J. Phys. Chem. C* **2015**, *119*, 3957.
[19] H. Moon, R. Tatara, T. Mandai, K. Ueno, K. Yoshida, N. Tachikawa, T. Yasuda, K. Dokko, M. Watanabe, *J. Phys. Chem. C* **2014**, *118*, 20246.
[20] J. W. Park, K. Yamauchi, E. Takashima, N. Tachikawa, K. Ueno, K. Dokko, M. Watanabe, *J. Phys. Chem. C* **2013**, *117*, 4431.
[21] N. Tachikawa, K. Yamauchi, E. Takashima, J. W. Park, K. Dokko, M. Watanabe, *Chem. Commun.* **2011**, *47*, 8157.
[22] K. Ueno, J. W. Park, A. Yamazaki, T. Mandai, N. Tachikawa, K. Dokko, M. Watanabe, *J. Phys. Chem. C* **2013**, *117*, 20509.
[23] K. Yoshida, M. Nakamura, Y. Kazue, N. Tachikawa, S. Tsuzuki, S. Seki, K. Dokko, M. Watanabe, *J. Am. Chem. Soc.* **2011**, *133*, 13121.
[24] Z. Li, S. Zhang, C. Zhang, K. Ueno, T. Yasuda, R. Tatara, K. Dokko, M. Watanabe, *Nanoscale* **2015**, *7*, 14385.
[25] M. A. Pope, I. A. Aksay, *Adv. Energy Mater.* **2015**, *5*, 1500124.

[26] X. B. Cheng, H. J. Peng, J. Q. Huang, L. Zhu, S. H. Yang, Y. Liu, H. W. Zhang, W. Zhu, F. Wei, Q. Zhang, *J. Power Sources* **2014**, *261*, 264.
[27] S. H. Chung, A. Manthiram, *Electrochem. Commun.* **2014**, *38*, 91.
[28] S. H. Chung, A. Manthiram, *Electrochim. Acta* **2013**, *107*, 569.
[29] D. Lv, J. Zheng, Q. Li, X. Xie, S. Ferrara, Z. Nie, L. B. Mehdi, N. D. Browning, J. G. Zhang, G. L. Graff, J. Liu, J. Xiao, *Adv. Energy Mater.* **2015**, *5*, 1402290.
[30] F. Orsini, A. Du Pasquier, B. Beaudoin, J. Tarascon, M. Trentin, N. Langenhuizen, E. De Beer, P. Notten, *J. Power Sources* **1998**, *76*, 19.
[31] J. Lim, J. Pyun, K. Char, *Angew. Chem. Int. Ed.* **2015**, *54*, 3249.
[32] L. Sun, M. Li, Y. Jiang, W. Kong, K. Jiang, J. Wang, S. Fan, *Nano Lett.* **2014**, *14*, 4044.
[33] H. Wang, Y. Yang, Y. Liang, J. T. Robinson, Y. Li, A. Jackson, Y. Cui, H. Dai, *Nano Lett.* **2011**, *11*, 2644.
[34] N. Jayaprakash, J. Shen, S. S. Moganty, A. Corona, L. A. Archer, *Angew. Chem.* **2011**, *123*, 6026.
[35] X. Yang, L. Zhang, F. Zhang, Y. Huang, Y. Chen, *ACS nano* **2014**, *8*, 5208.
[36] M. Hagen, S. Dörfler, P. Fanz, T. Berger, R. Speck, J. Tübke, H. Althues, M. J. Hoffmann, C. Scherr, S. Kaskel, *J. Power Sources* **2013**, *224*, 260.
[37] C. Nan, Z. Lin, H. Liao, M. K. Song, Y. Li, E. J. Cairns, *J. Am. Chem. Soc.* **2014**, *136*, 4659.
[38] Z. W. Seh, H. Wang, P. C. Hsu, Q. Zhang, W. Li, G. Zheng, H. Yao, Y. Cui, *Energy Environ. Sci.* **2014**, *7*, 672.
[39] S. K. Lee, Y. J. Lee, Y. K. Sun, *J. Power Sources* **2016**, *323*, 174.
[40] Y. Yang, G. Zheng, S. Misra, J. Nelson, M. F. Toney, Y. Cui, *J. Am. Chem. Soc.* **2012**, *134*, 15387.
[41] Y. Fu, Y. S. Su, A. Manthiram, *Adv. Energy Mater.* **2014**, *4*, 1300655.
[42] K. Cai, M. K. Song, E. J. Cairns, Y. Zhang, *Nano Lett.* **2012**, *12*, 6474.
[43] L. Chen, Y. Liu, M. Ashuri, C. Liu, L. L. Shaw, *J. Mater. Chem. A* **2014**, *2*, 18026.
[44] M. R. Kaiser, X. Liang, H. K. Liu, S. X. Dou, J. Z. Wang, *Carbon* **2016**, *103*, 163.
[45] L. Chen, Y. Liu, F. Zhang, C. Liu, L. L. Shaw, *ACS Appl. Mater. Interfaces* **2015**, *7*, 25748.
[46] J. Liu, H. Nara, T. Yokoshima, T. Momma, T. Osaka, *J. Power Sources* **2015**, *273*, 1136.
[47] S. Jeong, D. Bresser, D. Buchholz, M. Winter, S. Passerini, *J. Power Sources* **2013**, *235*, 220.
[48] F. Wu, A. Magasinski, G. Yushin, *J. Mater. Chem. A* **2014**, *2*, 6064.
[49] F. Wu, J. T. Lee, E. Zhao, B. Zhang, G. Yushin, *ACS Nano* **2016**, *10*, 1333.
[50] F. Wu, J. T. Lee, A. Magasinski, H. Kim, G. Yushin, *Part. Part. Syst. Charact.* **2014**, *31*, 639.

[51] F. Wu, H. Kim, A. Magasinski, J. T. Lee, H. T. Lin, G. Yushin, *Adv. Energy Mater.* **2014**, *4*, 1400196.
[52] C. Wang, X. Wang, Y. Yang, A. Kushima, J. Chen, Y. Huang, J. Li, *Nano Lett.* **2015**, *15*, 1796.
[53] F. Wu, J. T. Lee, F. Fan, N. Nitta, H. Kim, T. Zhu, G. Yushin, *Adv. Mater.* **2015**, *27*, 5579.
[54] G. Zhou, E. Paek, G. S. Hwang, A. Manthiram, *Adv. Energy Mater.* **2016**, *6*, 1501355.
[55] M. Wu, Y. Cui, Y. Fu, *ACS Appl. Mater. Interfaces* **2015**, *7*, 21479.
[56] K. Zhang, L. Wang, Z. Hu, F. Cheng, J. Chen, *Sci. Rep.* **2014**, *4*, 6467.
[57] Y. Hwa, J. Zhao, E. J. Cairns, *Nano Lett.* **2015**, *15*, 3479.
[58] Z. Lin, C. Nan, Y. Ye, J. Guo, J. Zhu, E. J. Cairns, *Nano Energy* **2014**, *9*, 408.
[59] L. Suo, Y. Zhu, F. Han, T. Gao, C. Luo, X. Fan, Y. Hu, Sheng, C. Wang, *Nano Energy* **2015**, *13*, 467.
[60] Y. Yang, M. T. McDowell, A. Jackson, J. J. Cha, S. S. Hong, Y. Cui, *Nano Lett.* **2010**, *10*, 1486.
[61] J. Guo, Z. Yang, Y. Yu, H. D. Abruna, L. A. Archer, *J. Am. Chem. Soc.* **2013**, *135*, 763.
[62] K. Han, J. Shen, C. M. Hayner, H. Ye, M. C. Kung, H. H. Kung, *J. Power Sources* **2014**, *251*, 331.
[63] X. Li, C. A. Wolden, C. Ban, Y. Yang, *ACS Appl. Mater. Interfaces* **2015**, *7*, 28444.
[64] Y. Fu, C. Zu, A. Manthiram, *J. Am. Chem. Soc.* **2013**, *135*, 18044.
[65] Z. Yang, J. Guo, S. K. Das, Y. Yu, Z. Zhou, H. D. Abruña, L. A. Archer, *J. Mater. Chem. A* **2013**, *1*, 1433.
[66] S. Zheng, Y. Chen, Y. Xu, F. Yi, Y. Zhu, Y. Liu, J. Yang, C. Wang, *ACS nano* **2013**, *7*, 10995.
[67] Y. Ma, B. Ding, G. Ji, J. Y. Lee, *ACS nano* **2013**, *7*, 10870.
[68] D. Lv, P. Yan, Y. Shao, Q. Li, S. Ferrara, H. Pan, G. L. Graff, B. Polzin, C. Wang, J. G. Zhang, J. Liu, J. Xiao, *Chem. Commun.* **2015**, *51*, 13454.
[69] D. Aurbach, Y. Talyosef, B. Markovsky, E. Markevich, E. Zinigrad, L. Asraf, J. S. Gnanaraj, H. J. Kim, *Electrochim. Acta* **2004**, *50*, 247.
[70] L. Wang, Y. Wang, Y. Xia, *Energy Environ. Sci.* **2015**, *8*, 1551.
[71] C. M. Park, J. H. Kim, H. Kim, H. J. Sohn, *Chem. Soc. Rev.* **2010**, *39*, 3115.
[72] H. Wu, G. Zheng, N. Liu, T. J. Carney, Y. Yang, Y. Cui, *Nano Lett.* **2012**, *12*, 904.
[73] J. Hassoun, B. Scrosati, *Angew. Chem. Int. Ed.* **2010**, *49*, 2371.

# Chapter Two

Preparation of $Li_2S$/Graphene Composite by One-Pot Pyrolysis of Lithium Sulfate and Graphene Nanoplatelet Aggregates

**Abstract**

Lithium sulfide ($Li_2S$) as a cathodic material in Li–S batteries can not only deliver a high theoretical specific capacity of 1166 mAh/g, but also is essential for batteries using Li-free anode materials such as silicon and graphite. Various efforts have been made to synthesize a highly efficient $Li_2S$–carbon composite; however, the electronically and ionically insulating nature and high melting point of $Li_2S$ strongly complicate the synthetic procedures, making it difficult to realize the expected capacity. Herein, a very simple method is proposed to prepare $Li_2S$/graphene composites by one-pot pyrolysis of a mixture of graphene nanoplatelet aggregates (GNAs) and low-cost lithium sulfate ($Li_2SO_4$). For the first time, the entire pyrolysis process is clarified by thermogravimetry-mass spectrometry, wherein GNAs were found to partly serve as a carbon source to reduce $Li_2SO_4$ to $Li_2S$, while the remaining GNAs formed thin graphene sheets as a result of this in-situ etching, as a highly conductive host can immobilize the generated $Li_2S$ by intimate contact. Consequently, the obtained $Li_2S$/graphene composite, combined with a $Li_2S_x$ -insoluble (x = 4-8) electrolyte developed by our group, exhibits excellent electrochemical behavior for Li–S batteries

Part of the work presented in this chapter has been published as:

Zhe Li, Shiguo Zhang, Ce Zhang, Kazuhide Ueno, Tomohiro Yasuda, Ryoichi Tatara, Kaoru Dokko, Masayoshi Watanabe, One-pot pyrolysis of lithium sulfate and graphene nanoplatelet aggregates: in situ formed $Li_2S$/graphene composite for lithium–sulfur batteries, Nanoscale, 2015, 7, 14385-14392.

## 2.1. Introduction

Conventional Li-ion batteries (LIBs), which typically consist of a graphite anode and a lithium transition-metal oxide cathode and operate according to the intercalation–deintercalation mechanism, have dominated the rechargeable battery market for more than two decades. However, they deliver energy densities of no more than 387 Wh/kg,[1] which is insufficient to meet the rapidly increasing power requirements for portable electronics and electric vehicles. Moreover, the development of large-scale grid-based energy storage systems for sustainable and renewable sources (such as wind and solar) has triggered the development of novel rechargeable electrochemical devices with higher energy density, lower cost, and longer cycle life than conventional LIBs.[2, 3] Lithium–sulfur (Li–S) batteries, a promising "beyond Li-ion" technology, have attracted considerable attention recently.[4-12] Sulfur is naturally abundant and environmentally friendly, and, importantly, can deliver a theoretical specific capacity of 1672 mAh/g and a theoretical energy density of 2600 Wh/kg or 2800 Wh/L when fully discharged, which are far greater than those of state-of-the-art LIBs.[13] Although considerable advances in Li–S batteries have been made, their commercialization is still hindered by several serious issues. Polysulfides are likely to be soluble and to diffuse from the cathode and dissolve in most electrolytes, which can act as a redox shuttle, resulting in a significant loss of active material, reaction with the lithium anode, fast capacity fading, and low Coulombic efficiencies.[14] The paired Li metal anode in Li–S batteries is reactive and prone to dendrite formation, posing some potential safety hazards. Furthermore, the active sulfur is known to undergo a large volume expansion/contraction (ca. 80%) during discharge–charge, and this induces an unstable electrochemical contact over long cycles and degrades the structural integrity of the cathode.

As an alternative active material, lithium sulfide ($Li_2S$) could deliver an acceptable theoretical specific capacity of 1166 mAh/g while overcoming most of the problems associated with the sulfur cathode.[4] For example, $Li_2S$ can be paired with some high-capacity Li-free anodes such as tin and silicon,[15, 16]

avoiding the formation of lithium dendrites. In addition, $Li_2S$ (the fully lithiated state of sulfur) is at the maximum volume, so volumetric shrinkage instead of expansion occurs during the initial charge process, making the cathode mechanically stable. However, as with the sulfur cathode, $Li_2S$ is neither electronically nor ionically conductive, making it difficult to achieve high utilization and realize the projected capacity. Various efforts have been made to ameliorate this problem by improving the contact between $Li_2S$ and electronic conductors. Because its high melting point (938 °C) makes it impossible to incorporate $Li_2S$ into porous conductive hosts using the established melting–diffusion method for sulfur, most $Li_2S$/C composite cathodes were fabricated via direct high-energy ball-milling of commercial $Li_2S$ powder with carbon materials, which inevitably produces a wide particle size distribution and random morphology of $Li_2S$ and thus poor cell performance.[17-20] A solution-based route has also been pursued by dispersing carbon hosts into an ethanol–$Li_2S$ solution,[21, 22] which is still a physical mixing process. Thermal treatment of a $Li_2S_3$–polyacrylonitrile composite could result in the formation of a $Li_2S$/C composite via chemical reactions at elevated temperatures, although this step was accompanied by the release of harmful $H_2S$.[23] For the methods described above, commercial bulk $Li_2S$ powders were employed as the starting material, which may not be an attractive candidate for practical application because of its high cost. Other wet chemistry approaches were also implemented to synthesize $Li_2S$/C composites by means of the reaction between sulfur and organolithium reagents such as lithium triethylborohydride ($LiEt_3BH$)[15, 24, 25] or *n*-butyllithium.[16] Nevertheless, these costly, dangerous, complex procedures are difficult to handle and unsuitable for large-scale production.

In this work, we demonstrated a facile, low-cost, scalable, and environmentally friendly method for one-pot synthesis of a $Li_2S$/graphene composite through direct pyrolysis of a mixture of graphene nanoplatelet aggregates (GNAs) and low-cost lithium sulfate ($Li_2SO_4$). The GNAs have two functions: Part of them serve as a reductant to reduce $Li_2SO_4$ and create $Li_2S$ at elevated temperature ($Li_2SO_4 + 2C \rightarrow 2CO_2 \uparrow + Li_2S$);[26] meanwhile, GNAs are etched in situ into thin

graphene sheets via this chemical reaction. The special layered structure of these residual graphene sheets can act as a highly conductive two-dimensional (2D) host to immobilize the active $Li_2S$ by intimate contact, facilitating the transport of electrons in the cathode[27-30] and improving the electrochemical utilization of poorly conducting $Li_2S$. When used as a cathode for Li–S batteries, in combination with a discharge-product-insoluble electrolyte developed by our group (where the discharge product is $Li_2S_x$: $x$ = 4-8),[7, 8, 11, 31] this $Li_2S$/graphene composite demonstrates excellent electrochemical performance with faster reaction kinetics, lower polarization, and better cycling performance and rate capability than the physical mixture of commercial $Li_2S$ and GNAs.

## 2.2. Experimental

*Preparation of $Li_2S$/graphene composite:* A $Li_2SO_4$/graphene nanoplatelet aggregates (GNAs) composite was first obtained via a solvent/nonsolvent precipitation method. GNAs (Strem Chemicals, 0.48 g) and $Li_2SO_4 \cdot H_2O$ (1.60 g) were dispersed into ultrapure water (70 mL) by ultrasonication for 2 h to form a suspension. After stirring for 4 h, ethanol (800 mL) was added dropwise to the suspension. Subsequently, the black precipitates were filtered off, washed with ethanol several times, and then dried in vacuum at 40°C for 12 h. This collected composite was labeled LS-GNAs C. The LS-GNAs C was then heated in a tube furnace under an argon atmosphere according to the following temperature program: (1) keeping at room temperature (RT) for 1 h to degas, (2) heating at 10°C/min to 200°C, (3) holding at 200°C for 1 h, (4) heating at 10°C/min to 781°C, and (5) calcining at 781°C for 2 h. After cooling to RT naturally, the solid product, denoted as LS-GNAs H, was obtained. Because $Li_2S$ is soluble in anhydrous methanol, LS-GNAs H was thoroughly washed by methanol several times to remove $Li_2S$. The remaining carbon, denoted as LS-GNAs H-W, was finally dried at 30°C for 6 h. Ultimately, the $Li_2S$ content in LS-GNAs H was estimated to be 78.3 wt% by weight measurement before and after washing.

*Material characterization:* Thermogravimetry-mass spectrometry measurement was conducted using a Bruker TG-DTA2020SA/MS9610 instrument. The

morphology was characterized by a field emission scanning electron microscope (JEOL JSM-7001F) equipped with an energy-dispersive X-ray spectroscopy system. The X-ray diffraction patterns were recorded on a Rigaku Ultima Ⅳ X-ray diffractometer using a Cu Kα radiation source. Atomic force microscopy (AFM, SII SPI3800N/SPA400) was conducted to measure the thickness of the graphene materials. For the AFM measurements, the samples were dispersed in water by ultrasonication for 30 min and then placed on freshly cleaved mica surfaces before observation. The composition was investigated using an X-ray photoelectron spectroscope (ULVAC-PHI Quantera SXM).

*Electrochemical measurements:* Because lithium sulfide is very sensitive to moisture, all the cell preparation procedures were conducted in an argon-filled glovebox in which the moisture level was below 1 ppm. The LS-GNAs H–based electrode was prepared by grinding LS-GNAs H with carbon black (Super C65, TIMCAL) and polyvinylpyrrolidone (PVP, MW = 1200 kDa, JUNSEI) in a weight ratio of 76.6:13.4:10 ($Li_2S$:C:PVP = 60:30:10) for 50 min using *N*-methyl-2-pyrrolidinone as the solvent. The obtained slurry was uniformly deposited on an aluminum foil current collector by a doctor-blade technique and then dried in vacuum at 80°C for 16 h. The mass loading of active material was around 0.5 mg/cm$^2$. Under the same conditions, a $Li_2S$–GNAs mixture–based electrode was also prepared for comparison by mixing commercial $Li_2S$, GNAs, carbon black (Super C65), and PVP in a weight ratio of 60:16.6:13.4:10. For the electrolyte, tetraglyme (G4, Nippon Nyukazai) and lithium bis(trifluoromethanesulfonyl)amide (Li[TFSA], Solvey) were mixed in a molar ratio of 1:1. After the mixture was stirred at RT for 24 h, a homogeneous liquid denoted as $[Li(G4)_1][TFSA]$ was obtained. Next, 1,1,2,2-tetrafluoroethyl 2,2,3,3-tetrafluoropropyl ether (HFE) was added to the $[Li(G4)_1][TFSA]$ to obtain a $[Li(G4)_1][TFSA]$/HFE electrolyte, where the molar ratio of $[Li(G4)_1][TFSA]$:HFE is 1:4. Then, 2032-type coin cells (half-cells) were assembled using the $Li_2S$ cathode, a porous glass separator (GA55, Advantec), a lithium foil counter electrode, and the $[Li(G4)_1][TFSA]$/4HFE electrolyte. The coin cells were equilibrated at RT for 12 h before the electrochemical

measurements. The galvanostatic charge and discharge tests of the coin cells were conducted using a Nagano BTS-2004 battery testing system at 30°C. The cells were initially charged from the open circuit voltage to 4.40 V (vs. $Li/Li^+$) to activate the $Li_2S$ and then cycled in the voltage range of 1.50–3.50 V (vs. $Li/Li^+$). The specific capacity of the cell was calculated on the basis of the mass of $Li_2S$, and 1166 mA/g was defined as 1 C rate. Cyclic voltammetry measurement was performed using a Bio-Logic SAS VMP3 electrochemical workstation at a scan rate of 0.04 mV/s. Electrochemical impedance spectroscopy measurements were made for the fresh cells before cycling, using the same electrochemical workstation at the open circuit voltage (OCV) in the frequency range of 100 kHz to 4 Hz with a sinusoidal excitation amplitude of 5 mV.

## 2.3. Results and Discussion

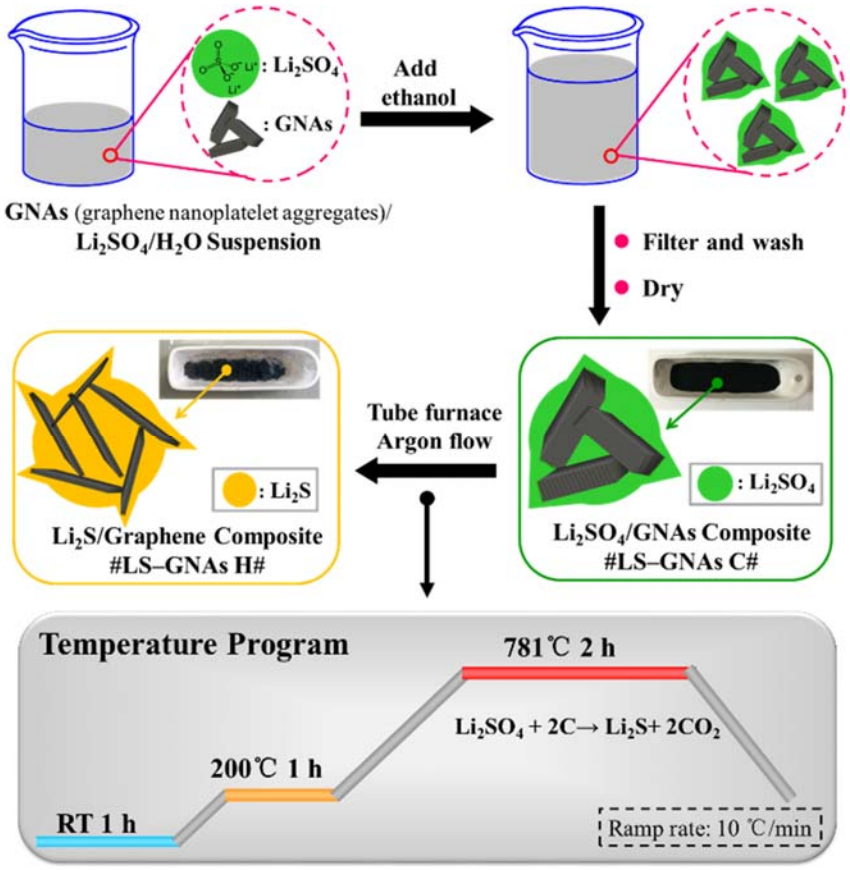


**Fig. 2.1.** Illustration of synthesis route for $Li_2S$/graphene composite.

This strategy was realized by one-pot pyrolysis of $Li_2SO_4$ and GNAs, as depicted in **Fig. 2.1**. First, a composite of $Li_2SO_4$/GNAs was obtained through a solvent/nonsolvent precipitation method (see the experimental section for details). More specifically, $Li_2SO_4 \cdot H_2O$ and GNAs (specific surface area: 750 $m^2/g$) were first dispersed into ultrapure water to form a suspension. Then ethanol as a precipitant of $Li_2SO_4$ was added dropwise into the suspension, which allows slow deposition of $Li_2SO_4$ onto the surface of the GNAs. After filtering, washing, and drying, the resultant black powder (**LS-GNAs C**) was subjected to pyrolysis at an elevated temperature. To set an appropriate pyrolysis temperature and elucidate the pyrolysis process of LS-GNAs C, thermogravimetry-mass spectrometry (TG-MS) measurement was conducted. As shown in **Fig. 2.2**, two clear weight loss steps were observed over the temperature range of 30-1000°C. The initial weight loss at around 84-134°C could originate from the removal of adsorbed water and mainly crystal water in $Li_2SO_4 \cdot H_2O$, as indicated by the significant signal of m/z 18 ($H_2O^+$), whereas the remarkable weight loss above 710°C could be assigned to the release of $CO_2$, as confirmed by the intense MS peak of m/z 44 ($CO_2^+$) at 781°C, originating from the chemical reaction $Li_2SO_4 + 2C \rightarrow 2CO_2 \uparrow + Li_2S$.[26] On the basis of the TG-MS results, LS-GNAs C was first heated at 200°C for 1 h to remove water and at 781°C for 2 h to complete the reaction between $Li_2SO_4$ and C. After cooling to room temperature (RT), the resulting solid product (**LS-GNAs H**) was ground into a fine powder for further experiments and analysis. Note that according to the above chemical reaction equation, an excess amount of GNAs is required to ensure sufficient graphene residue as the host to support active $Li_2S$ after pyrolysis. In our experiment, the $Li_2SO_4 \cdot H_2O$ and GNAs contents in LS-GNAs C were deliberately controlled as 1.60 and 0.48 g, respectively. After pyrolysis, LS-GNAs H was thoroughly washed in anhydrous methanol several times to remove $Li_2S$ (the resulting solid is denoted as LS-GNAs H-W). The $Li_2S$ content was estimated to be ~78.3 wt% by weight measurement of the residual graphene, which is very close to the expected theoretical value (~76.2 wt%).

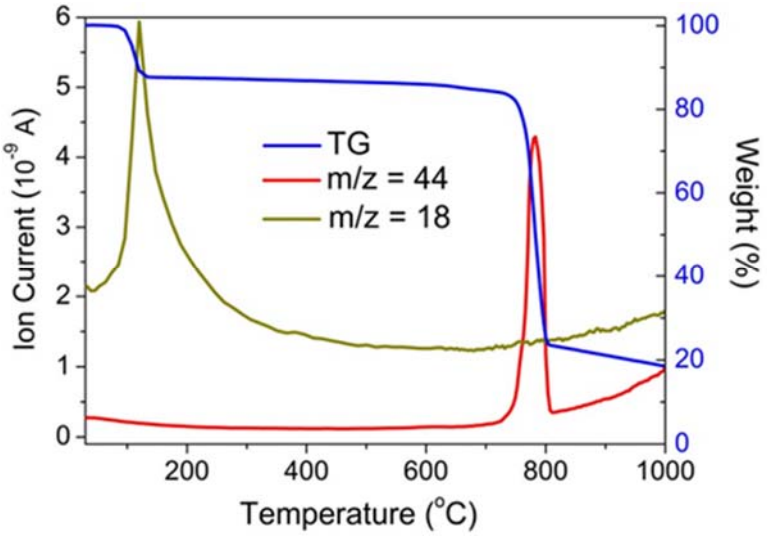


**Fig. 2.2.** TG-MS profiles of LS-GNAs C (ramp rate: 10 °C/min).

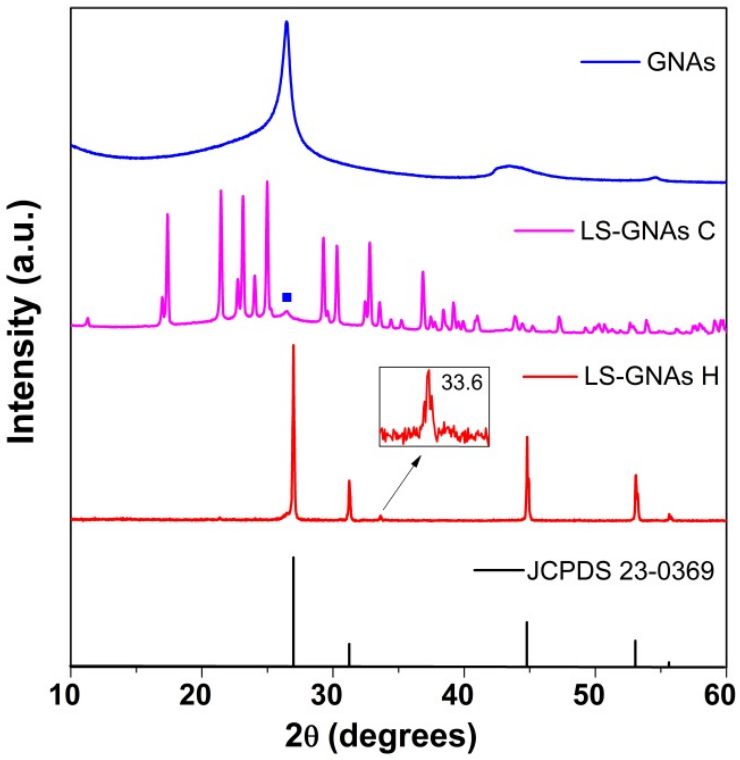


**Fig. 2.3.** XRD patterns of GNAs, LS-GNAs C, and LS-GNAs H.

The chemical composition and crystalline structure of the GNAs, LS-GNAs C, and LS-GNAs H were investigated by X-ray diffraction (XRD). As shown in **Fig. 2.3**, the XRD patterns of the GNAs show an intense peak centered at 26.5°, which can be indexed as the (002) reflection and corresponds to stacking of

graphene layers.[32, 33] This peak marked by the square is still remained in LS-GNAs C, and other sharp peaks agree very well with the diffractions for monoclinic $Li_2SO_4 \cdot H_2O$ (JCPDS 15-0873). However, the (002) peaks nearly disappeared for LS-GNAs H, whereas five intense peaks were observed at 27.0°, 31.2°, 44.8°, 53.1°, and 55.6°, corresponding to the (111), (200), (220), (311), and (222) reflections of $Li_2S$ with cubic structure, respectively (JCPDS 23-0369). This result strongly confirms the successful transformation from $Li_2SO_4$ to $Li_2S$ after pyrolysis. LS-GNAs H also contains trace amount of $Li_2O$, as indicated by a tiny diffraction peak at 33.6°, which can be assigned to the (111) reflection of cubic $Li_2O$ (JCPDS 77-2144). This is probably resulted from the oxygen-containing functional groups (carboxyl, epoxy, or hydroxyl) on the surface of the GNAs. These polar groups, however, may act as growth sites and help to immobilize $Li_2SO_4$ during precipitation, leading to improved contact between C and $Li_2S$.

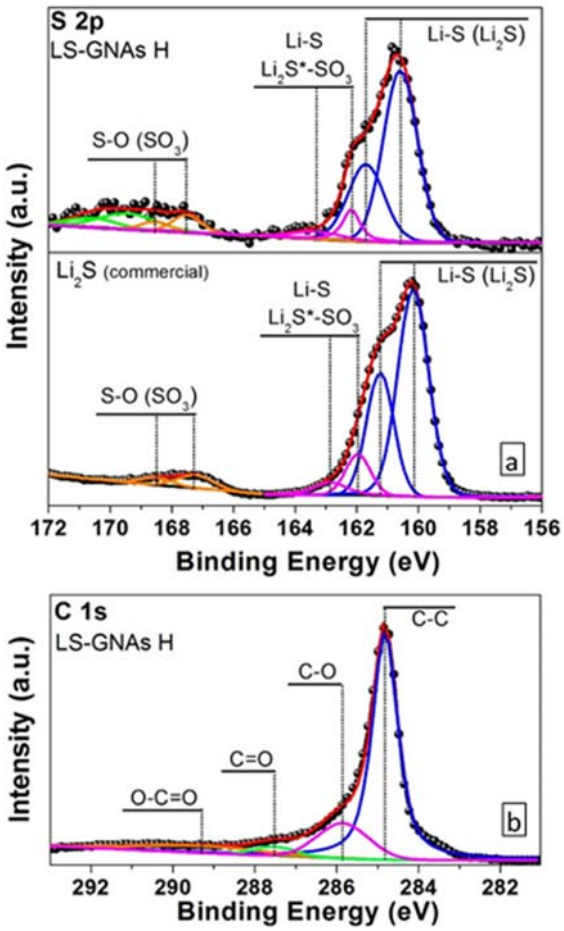

**Fig. 2.4.** (a) High-resolution S 2p XPS spectra of LS-GNAs H and commercial $Li_2S$. (b) C 1s XPS spectra of LS-GNAs H.

X-ray photoelectron spectroscopy (XPS) was employed to analyze the surface composition of LS-GNAs H. As expected, the S 2p spectra of LS-GNAs H are very similar to those of commercial $Li_2S$ (**Fig. 2.4a**); the only obvious difference is the additional signal above 169.0 eV for LS-GNAs H, which is probably due to the presence of a trace amount of unreacted $Li_2SO_4$. The S 2p spectra of LS-GNAs consist mainly of two signals at 160.6 and 161.7 eV, which can be ascribed to the S $2p_{3/2}$ and S $2p_{1/2}$ signals of Li–S bonding in $Li_2S$, respectively.[34] The other signals between 162.0 and 169.0 eV that are also observed in commercial $Li_2S$ can be ascribed to $Li_2S$*–$SO_3$ and $SO_3$.[34] It should be noted that nearly all of the S 2p signals of LS-GNAs H were shifted toward high energy compared with those of commercial $Li_2S$. As shown in **Fig. 2.4b**, the deconvoluted C 1s spectrum clearly reveals the presence of C–O (285.9 eV), C=O (287.5 eV), and O–C=O (289.3 eV) species in LS-GNAs H in addition to the dominant C–C (284.8 eV) composition,[35, 36] which may account for the possible strong interaction between $Li_2S$ and polar groups on the graphene matrix and thus the high-energy shift of the S 2p signals.

**Fig. 2.5** presents field emission scanning electron microscopy (FESEM) images of LS-GNAs H and LS-GNAs H-W. Clearly, the LS-GNAs H particles become quasi-spherical with an average size of 6.3 μm after pyrolysis, whereas the LS-GNAs C particles have irregular shapes and various particle sizes (**Fig. 2.6**). In addition, high-magnification FESEM images reveal that wrinkled laminar structures appear in the surface morphology of LS-GNAs H (**Fig. 2.5b** and **5c**). These lamellae are ascribed to the thin-layer graphene sheets resulting from in-situ etching of the GNAs during the chemical reaction at elevated temperature. The in-situ etching of the GNAs was further confirmed by the FESEM images of LS-GNAs H-W (after the $Li_2S$ in LS-GNAs H was removed by washing), which is found to consist of much thinner sheets than the aggregated structure of the raw GNAs (**Fig. 2.6**). Atomic force microscopy (AFM) images clarify that the GNAs were exfoliated from ca. 90 nm to < 1.3

nm after pyrolysis (**Fig. 2.7**). Energy-dispersive X-ray spectroscopy (EDS) elemental mappings of LS-GNAs H show a uniform distribution of carbon and sulfur throughout the LS-GNAs H particles (**Fig. 2.5d** and **5e**, respectively), implying that $Li_2S$ is homogeneously deposited on the surface of the graphene sheets in situ. It is noteworthy that the in situ formed $Li_2S$/graphene composite, wherein $Li_2S$ is immobilized by the 2D graphene host, provides high electronic conductivity because of the intimate contact between the graphene matrix and active material.

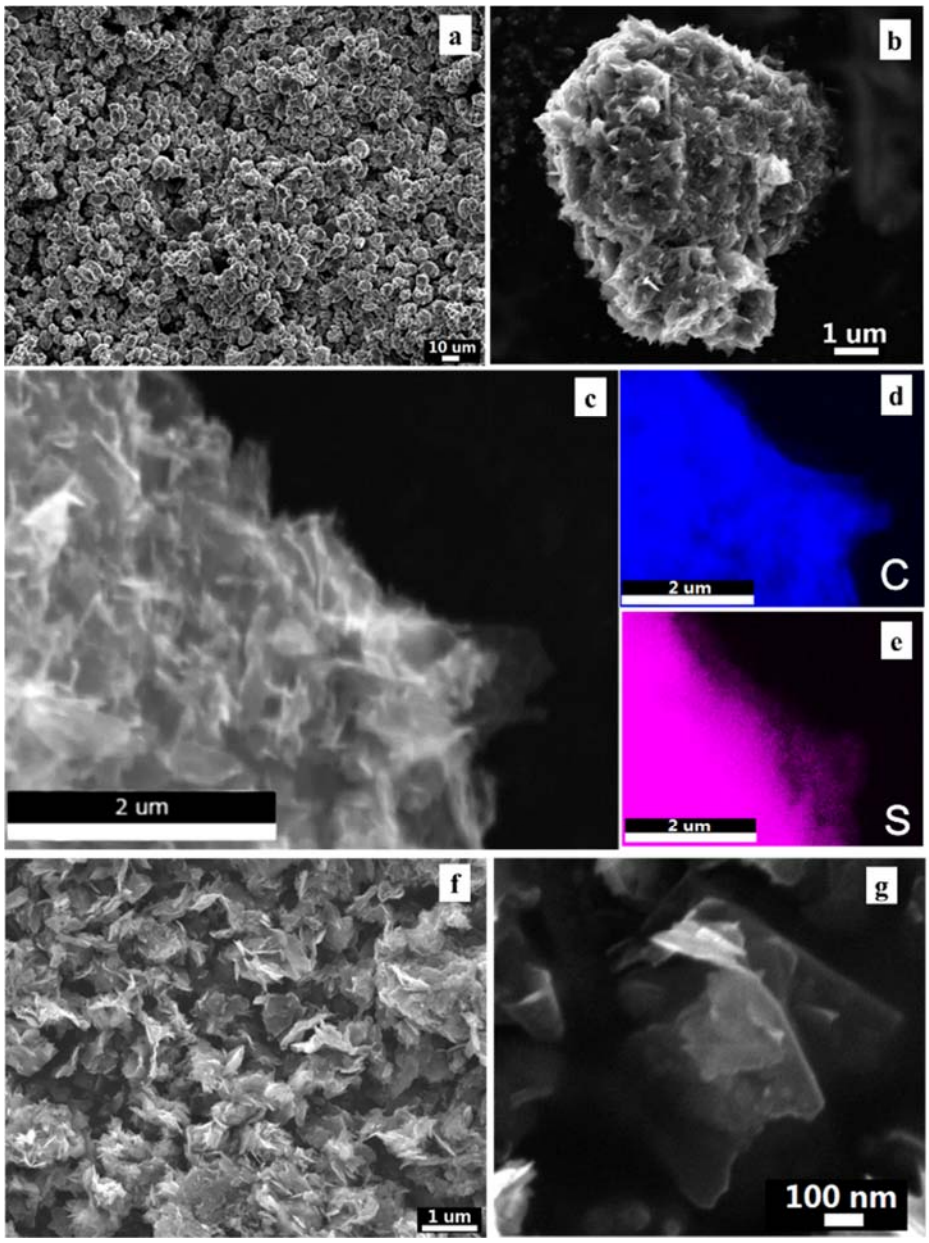

**Fig. 2.5.** FESEM images of LS-GNAs H at (a) low and (b, c) high magnifications. EDS elemental mappings of (d) carbon and (e) sulfur over image (c). (f, g) FESEM images of LS-GNAs H-W.

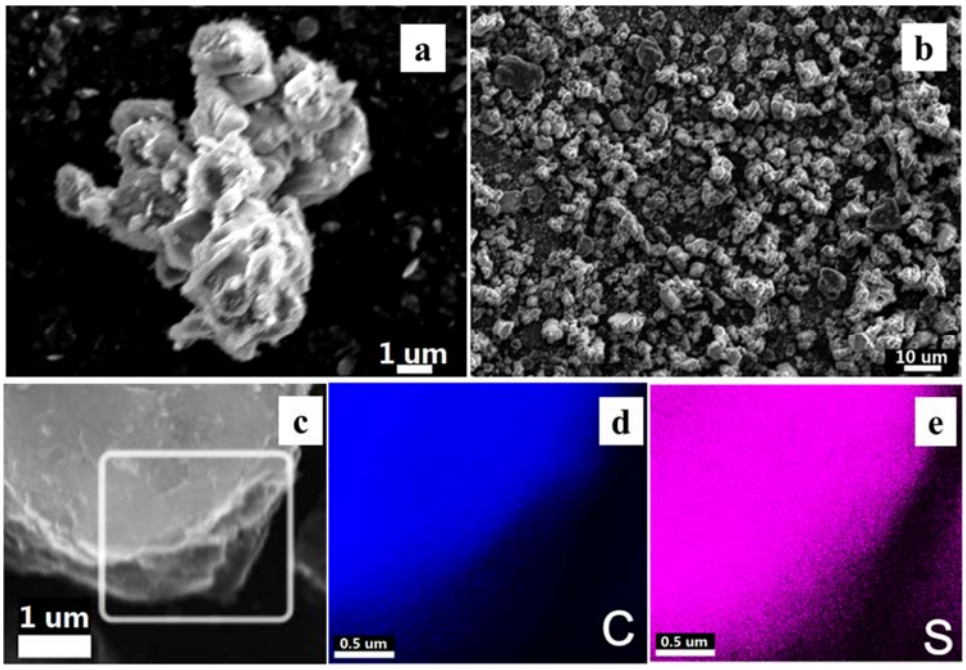


**Fig. 2.6.** FESEM images of (a) GNAs and (b) LS-GNAs C. (c) Enlarged FESEM image of LS-GNAs C particle and the corresponding energy-dispersive X-ray spectroscopy (EDS) elemental mappings of (d) carbon and (e) sulfur. GNAs consist of agglomerations of thick plates. The resultant LS-GNAs C particles have irregular shapes and particle sizes of 1.0–10.0 μm. Deposition of $Li_2SO_4$ results in a uniform distribution of $Li_2SO_4$ on the surface of the GNAs, as indicated by the homogeneous EDS signals of carbon and sulfur.

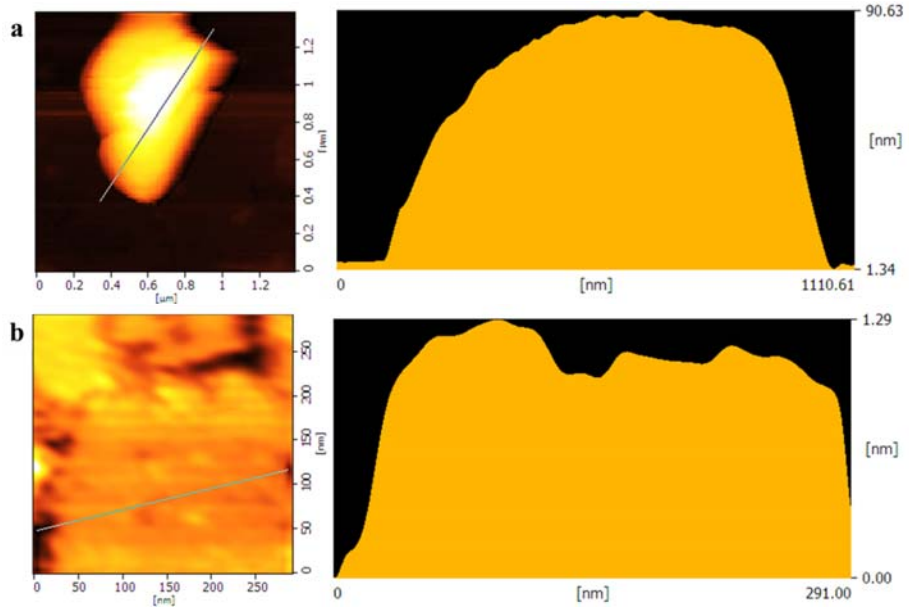

**Fig. 2.7.** Tapping-mode atomic force microscopy (AFM) images with the corresponding height profiles: (a) GNAs and (b) LS-GNAs H-W. Fig. 2.7a reveals that the thickness of the GNAs is around 89 nm, which is due to intrinsic agglomeration. Fig. 2.7b shows that the thicknesses of LS-GNAs H-W is between 1.0 and 1.3 nm, suggesting that the graphene sheets in this sample are thinner than those in the GNAs.

The electrochemical performance of the obtained $Li_2S$/graphene composite (LS-GNAs H) was evaluated in 2032-type coin cells. Simultaneously, an electrode based on the $Li_2S$–GNAs mixture was also prepared under the same conditions for comparison. The electrolyte employed in this work is a stable glyme–Li salt molten complex ([Li(G4)$_1$][TFSA]) diluted by a hydrofluoroether (HFE) with low donor ability and viscosity developed by our group.[7, 8, 37-42] This solvate ionic-liquid-based mixture could be used directly as the electrolyte in Li–S batteries without additional lithium salt, greatly suppressing the dissolution of lithium polysulfides compared to conventional organic electrolytes and giving rise to high Coulombic efficiency.[7, 31] **Fig. 2.8a** shows typical cyclic voltammograms of the LS-GNAs H–based electrode in [Li(G4)$_1$][TFSA]/4HFE for the first three cycles. For LS-GNAs H particles of micrometer size, the $Li_2S$ electrode must first be electrochemically activated by applying a high charging cutoff voltage to overcome the barrier of lithium extraction from insulating $Li_2S$.[18, 43] Therefore, the potential was swept from the open circuit voltage (OCV) to 4.4 V (versus Li/$Li^+$) initially and then swept between 3.5 and 1.5 V, which is also the operating voltage range of the cells. In the first anodic scan, an intense oxidation peak at 4.30 V accompanied by a broad shoulder at 3.85 V are observed, corresponding to activation of the $Li_2S$ electrode. In the cathodic scans, two sharp reduction peaks appear at approximately 2.27 and 1.97 V, which can be assigned to the transitions of sulfur to long-chain lithium polysulfide ($Li_2S_x$, $4 < x < 8$) and then to the end discharge product $Li_2S$, respectively.[28] A small oxidation peak at 2.41 V in the first cathodic scan is likely due to the oxidation of unactivated $Li_2S$ or some intermediate lithium polysulfides generated during $Li_2S$ activation. In contrast, only one oxidation peak located at 2.48 V exists during the subsequent anodic scans, which involve the direct conversion of $Li_2S$ into elemental sulfur. The cyclic voltammetry (CV) profiles of the LS-GNAs H

electrode agree well with those of the reported $Li_2S$ cathodes.[43] Note that LS-GNAs H displays much more intense and sharper CV peaks than the $Li_2S$–GNAs mixture **(Fig. 2.8b)**, revealing improved electronic conductivity and ion transport due to the possible structural advantage of LS-GNAs H. In contrast, the $Li_2S$–GNAs mixture exhibits a higher activation potential (4.38 V) and oxidation potential (2.79 V) and lower reduction potentials (2.09 V and 1.67 V) than LS-GNAs H, indicating severe electrochemical polarization of the $Li_2S$–GNAs mixture, which is probably associated with the poor electrochemical contact between the insulating $Li_2S$ and the GNAs.

The galvanostatic charge–discharge profiles of the LS-GNAs H–based electrode in the 1$^{st}$, 5$^{th}$, 10$^{th}$, and 20$^{th}$ cycles at a current rate of 1/12 C are presented in **Fig. 2.9a**. In the first charge process, the charge plateau (~4.19 V) is distinctly higher than that of the conventional sulfur cathode,[7] which can be attributed to the initial energy barrier from phase nucleation of polysulfides.[18] An initial charge capacity of 1116 mAh/g is achieved, which is close to the theoretical capacity of $Li_2S$ (1166 mAh/g). It is noteworthy that the subsequent charge curves exhibit a very flat, stable plateau around 2.32 V, indicating direct oxidation of $Li_2S$ to sulfur, whereas the discharge curves display two well-defined plateaus. The upper one, at 2.24 V, is related to the formation of long-chain lithium polysulfide, whereas the lower one, at 2.04 V, is related to the formation of lithium sulfide and lithium disulfide; the two peaks are in agreement with the two reduction peaks in the CV curves **(Fig. 2.8a)**. Significantly, the reduction and oxidation plateaus remain relatively constant over 20 cycles, suggesting a stable structure of LS-GNAs H and excellent cyclability of this electrode. To further reveal the structural stability of LS-GNA H, the cell after 40 cycles was disassembled, and the morphology of cathode was characterized by FESEM. As displayed in **Fig. 2.10**, the overall structure of $Li_2S$/graphene composite-based electrode was well retained when compared with the fresh electrode, indicating the excellent structural stability of the composite. Compared with the $Li_2S$–GNAs mixture, LS-GNAs H shows not only a higher charge–discharge capacity but also less polarization. As seen in **Fig. 2.9b**, the voltage hysteresis between

the discharge and charge curves decreased from 0.62 to 0.28 V.

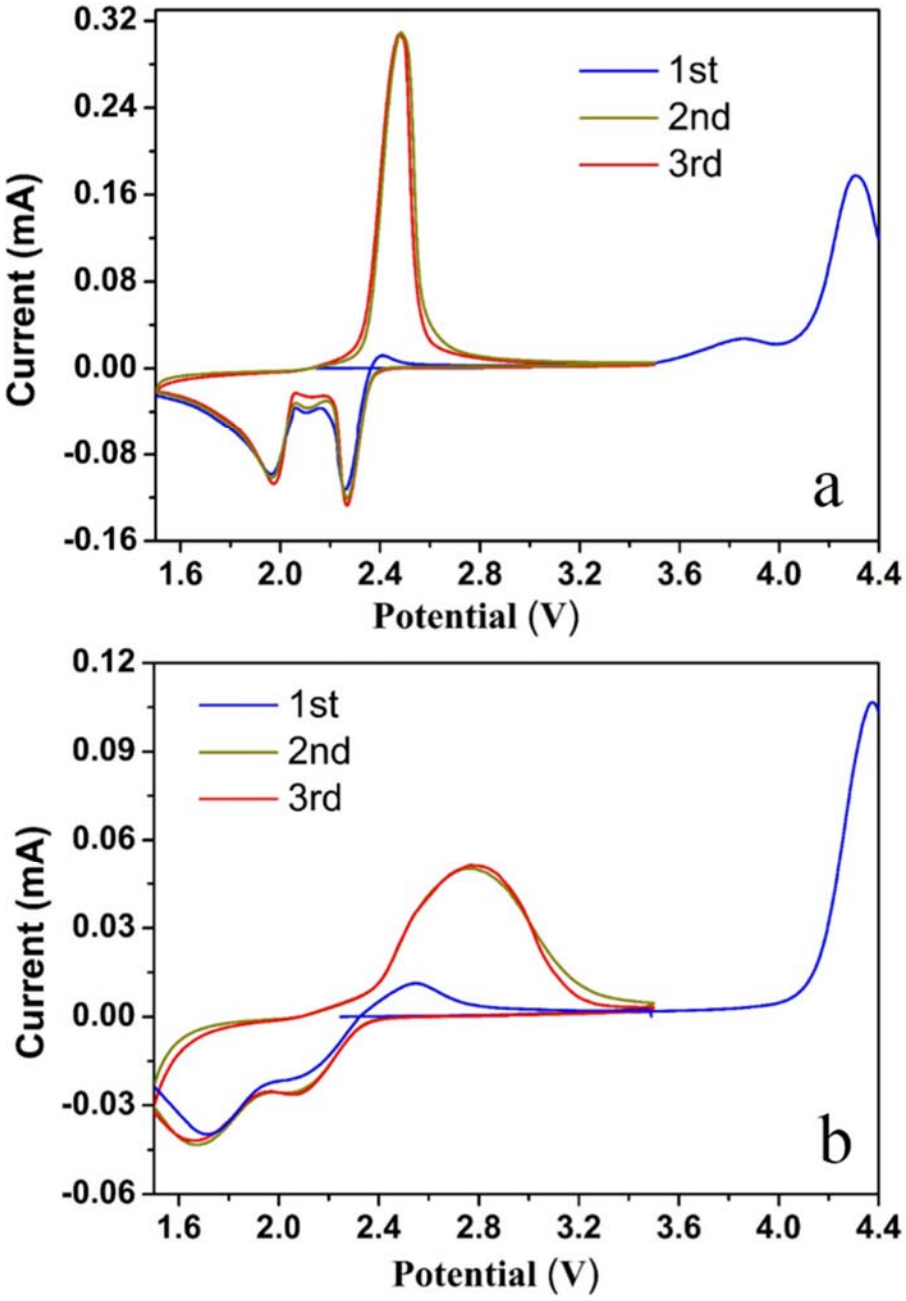


**Fig. 2.8.** Typical cyclic voltammograms of (a) LS-GNAs H and (b) $Li_2S$–GNAs mixture in $[Li(G4)_1][TFSA]$/4HFE at a scan rate of 0.04 mV/s. The potential was swept from the OCV to 4.4 V (versus $Li/Li^+$) initially and then swept between 3.5 and 1.5 V (versus $Li/Li^+$).

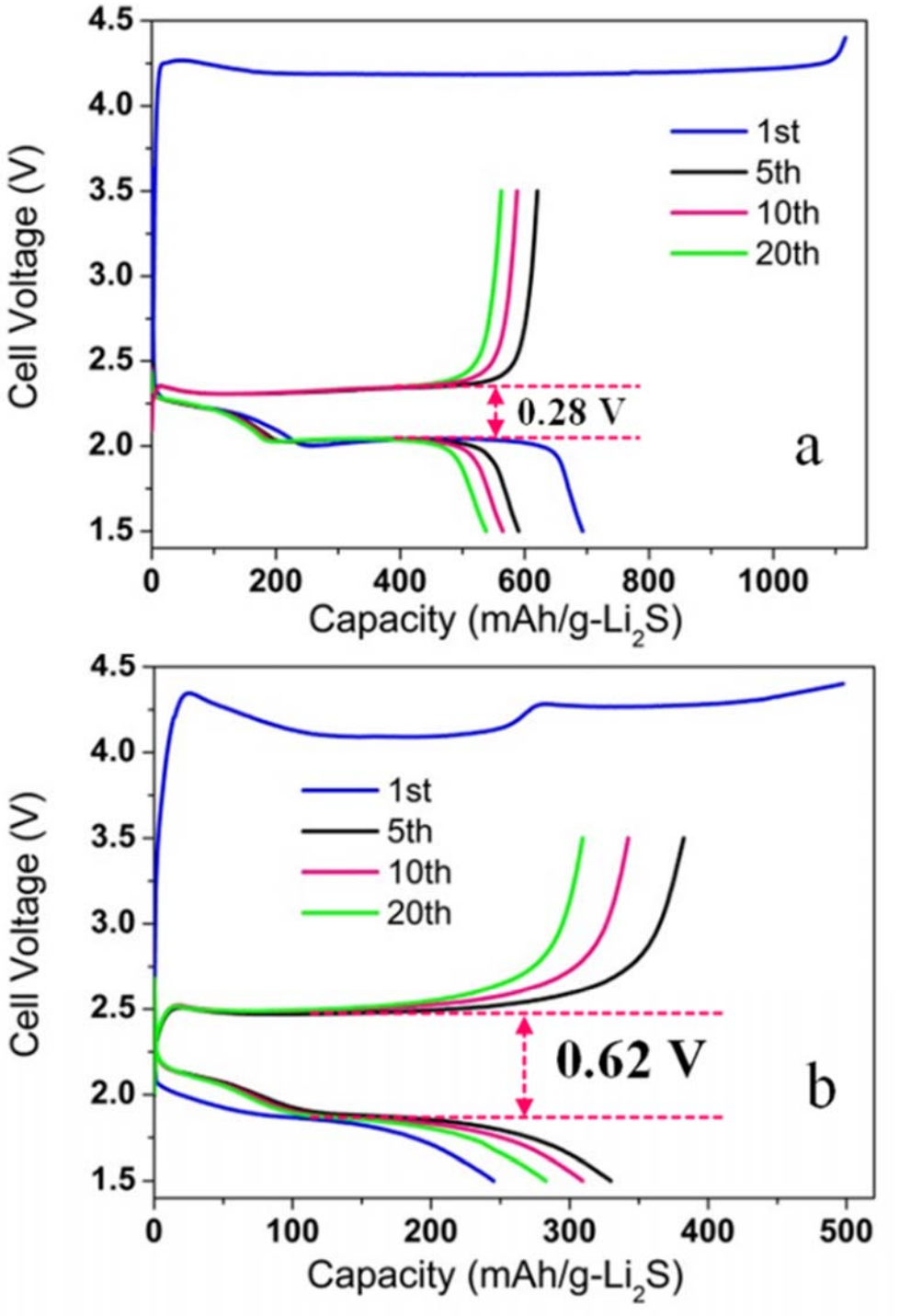


**Fig. 2.9.** Galvanostatic charge–discharge profiles of (a) LS-GNAs H and (b) $Li_2S$–GNAs mixture in the 1st, 5th, 10th, and 20th cycles at a current rate of 1/12 C (1 C = 1166 mA/g).

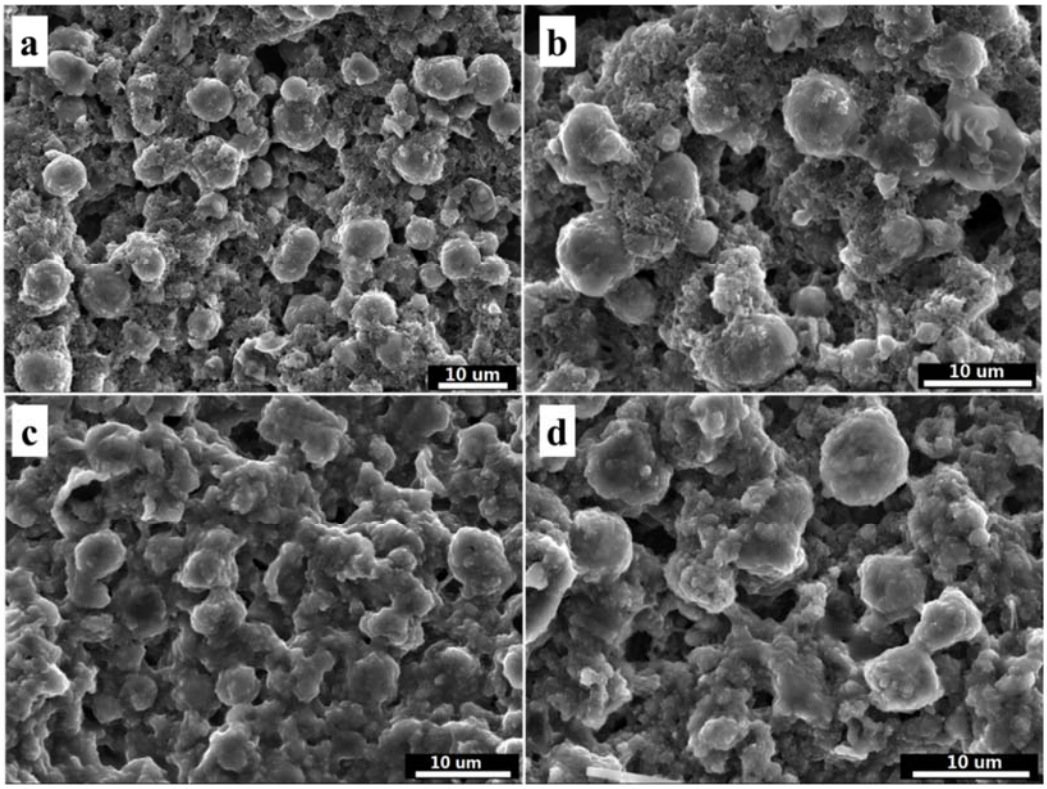


**Fig. 2.10.** FESEM images of (a, b) a fresh LS-GNAs H electrode before cycling and (c, d) the electrode after 40 cycles. For the electrode after 40 cycles, no large-sized $Li_2S$ agglomerations were observed, and abundant porous spaces were still preserved, which could enable the electrolyte channel for electrolyte immersion to be unblocked.

The cycling performance and Coulombic efficiency of LS-GNAs H at a current rate of 1/12 C are displayed in **Fig. 2.11a**, together with the results for the $Li_2S$–GNAs mixture for comparison. LS-GNAs H exhibits a higher initial discharge capacity (693 mAh/g) than the $Li_2S$–GNAs mixture (245 mAh/g), indicating that the utilization of active material increased dramatically. After 40 cycles, the discharge capacity of LS-GNAs H declines to 508 mAh/g, whereas the $Li_2S$–GNAs mixture can deliver only 260 mAh/g. Although it was not as high initially, the Coulombic efficiency of LS-GNAs H is still maintained around 95% after 2 cycles, showing an improvement over the $Li_2S$–GNAs mixture–based electrode. Moreover, the irreversible capacity of 5% still remains, probably arising from the initial electrochemical activation process of $Li_2S$, which may cause some potential adverse effects on the electrolyte.

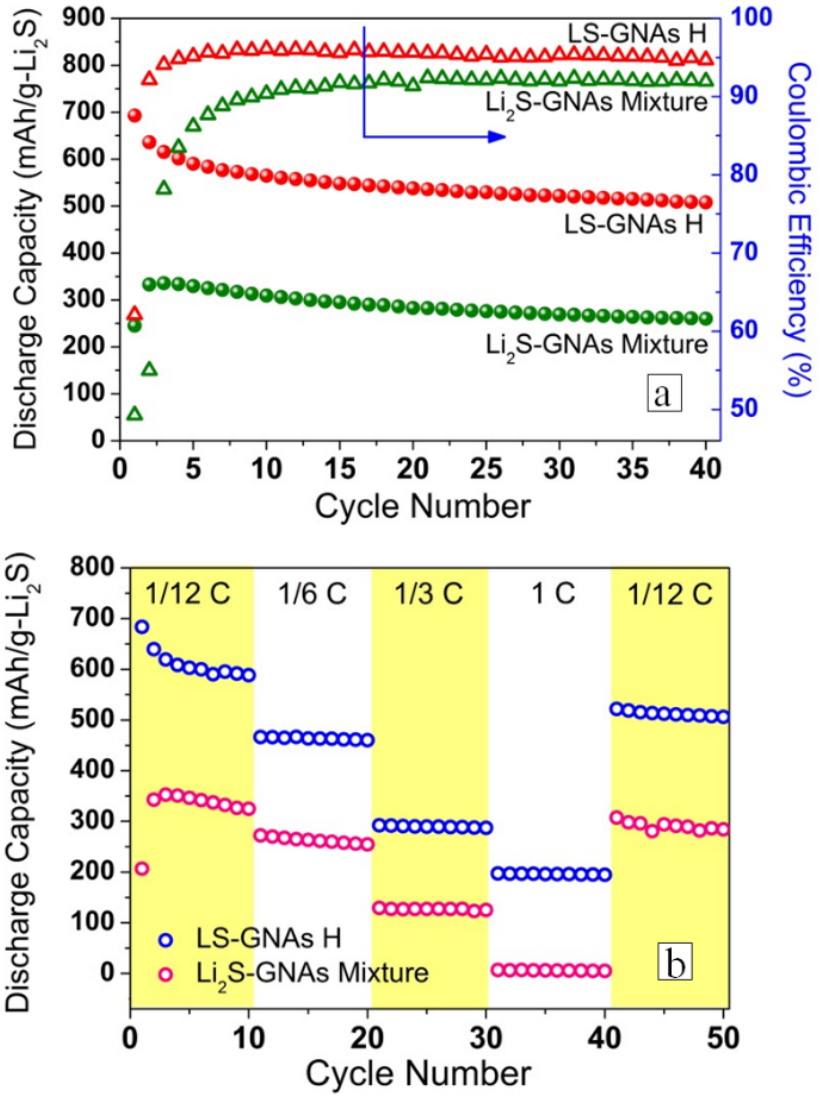


**Fig. 2.11** (a) Cycling performance and Coulombic efficiency of LS-GNAs H and $Li_2S$–GNAs mixture over 40 cycles at a current rate of 1/12 C. (b) Rate capability of LS-GNAs H and $Li_2S$–GNAs mixture at various discharge rates from 1/12 C to 1 C. The charge rate is fixed at 1/12 C (1 C = 1166 mA/g).

The rate capability of LS-GNAs H and the $Li_2S$–GNAs mixture at various discharge rates is investigated to further evaluate the kinetics of the electrodes; the data are presented in **Fig. 2.11b**. For the LS-GNAs H cathode, the stepwise discharge capacities at discharge rates of 1/12 C, 1/6 C, 1/3 C, and 1 C are 684–589, 466–460, 292–287, and 197–195 mAh/g, respectively, which are markedly higher than those of the $Li_2S$–GNAs mixture (nearly zero at 1 C), demonstrating better rate performance. When the current rate was changed back to 1/12 C, a

discharge capacity of 522 mAh/g was recovered for LS-GNAs H. This easy recovery of the discharge capacity after cycling under various conditions also implies that LS-GNAs H has good stability and reversibility.

**Table 1.** Content of different components in $Li_2S$/graphene composite-based electrode.

| Composite | Electrode | | | |
|---|---|---|---|---|
| $Li_2S$ Content (wt%) | $Li_2S$ (wt%) | Carbon (wt%) | | PVP (wt%) |
| | | Graphene | Carbon Black | |
| 69.5 | 60.0 | 26.3 | 3.7 | 10.0 |
| 78.3 | 60.0 | 16.6 | 13.4 | 10.0 |
| 82.4 | 60.0 | 12.8 | 17.2 | 10.0 |
| 86.4 | 60.0 | 9.4 | 20.6 | 10.0 |

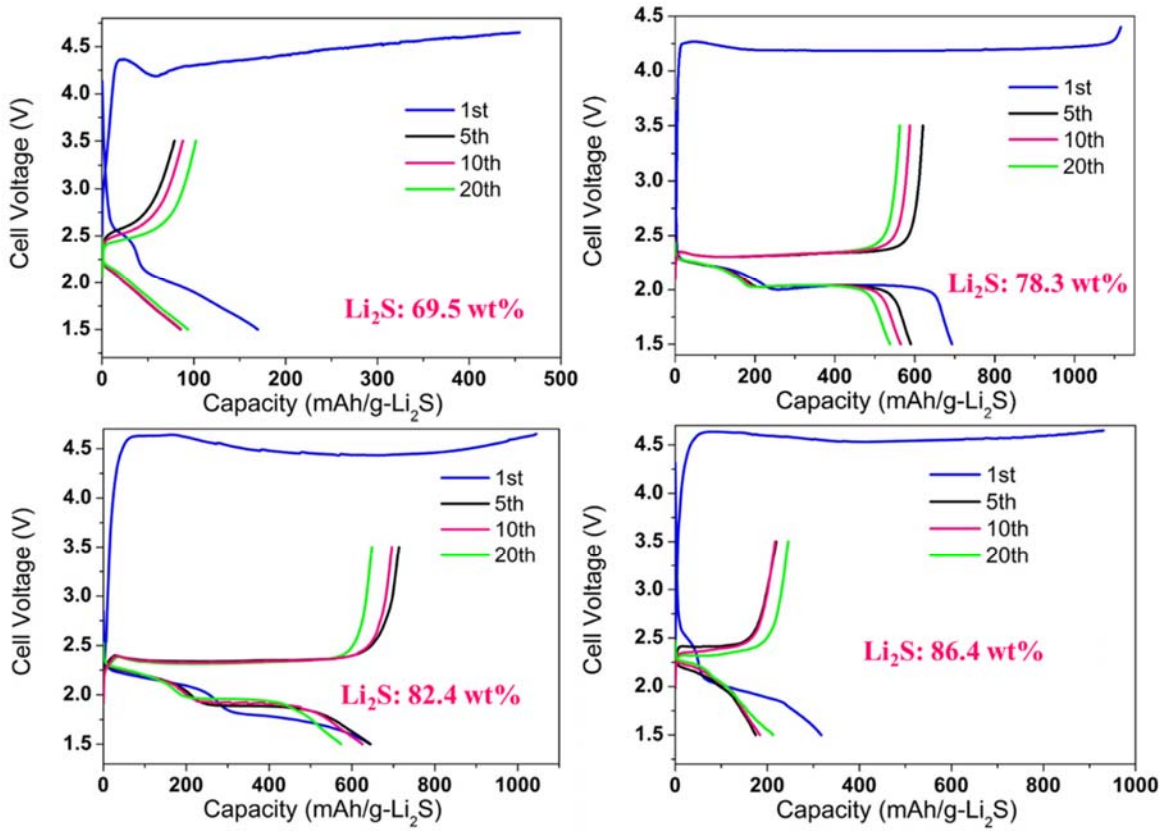


**Fig. 2.12.** Galvanostatic charge–discharge profiles of different $Li_2S$/graphene composites in the 1st, 5th, 10th, and 20th cycles at a current rate of 1/12 C (1 C = 1166 mA/g). Graphene can enhance electrical and mechanical connectivity between the individual $Li_2S$, while carbon black would improve the conductivity of the whole electrode. When the content of graphene

is low (e.g., the case of 86.4 wt% $Li_2S$ content in composite), some $Li_2S$ in the composite may agglomerate together, which require more energy to overcome the barrier of lithium extraction and lead to a poor utilization of $Li_2S$. Meanwhile, $Li_2S$/graphene composite with $Li_2S$ content of 69.5 wt%, demonstrated a very sluggish initial activation process of $Li_2S$ with a lower charge capacity of 455 mAh/g, due to the lack of carbon black (only 3.7 wt% of carbon black in the electrode).

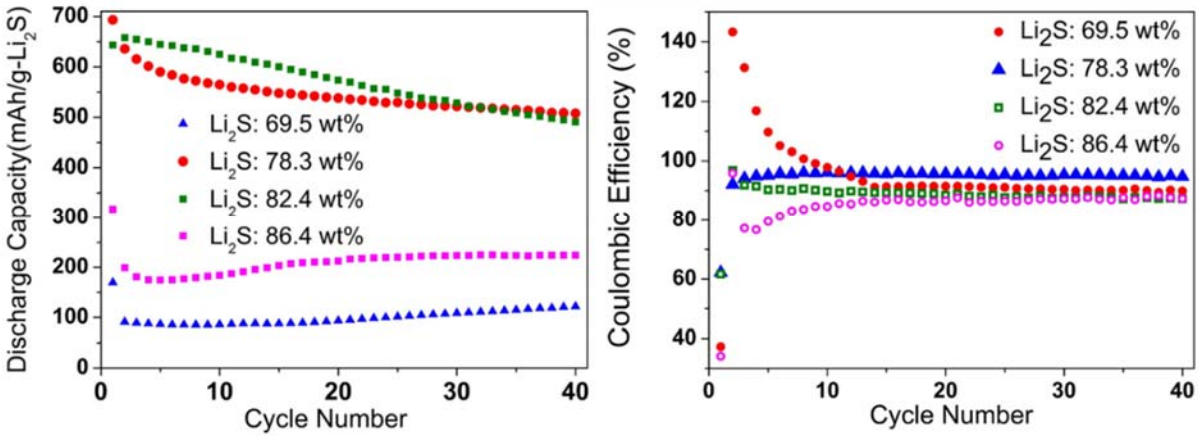


**Fig. 2.13.** Cycling performance and Coulombic efficiency of different $Li_2S$/graphene composites over 40 cycles at a current rate of 1/12 C.

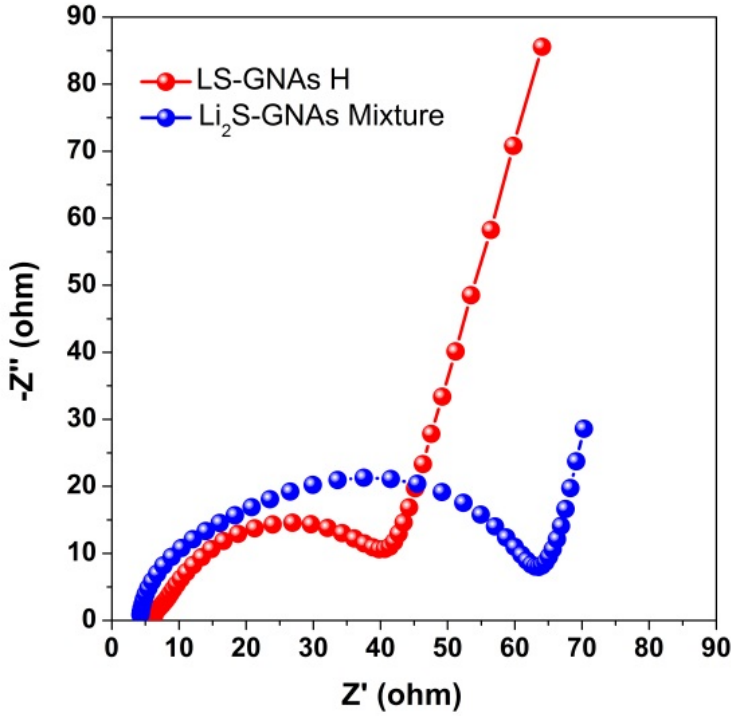


**Fig. 2.14.** Nyquist plots of LS-GNAs H and $Li_2S$–GNAs mixture before the initial charge.

To investigate the influence of the $Li_2S$ content in LS-GNA H on electrochemical performance, different composites were prepared by adjusting the amount of GNAs deliberately. During the fabrication of the electrode, carbon black was added to keep the same final composition of $Li_2S$, carbon and PVP in the electrode ($Li_2S$: C: PVP = 60:30:10), wherein the carbon included the graphene and carbon black. Compositions of different $Li_2S$/graphene composite-based electrodes are exhibited in **Table 1**. It is readily apparent that the $Li_2S$ content can affect the electrochemical performance, as indicated in **Fig. 2.12**. Base on the comparison of cycling performance and Coulombic efficiency among different composites (**Fig. 2.13**), the $Li_2S$ content of 78.3 wt% is the best composite composition for the electrochemical performance.

The fast reaction kinetics, low polarization, and greatly enhanced capacity and rate capability of LS-GNAs H compared with the $Li_2S$–GNAs mixture could be ascribed to the unique $Li_2S$/graphene structure. The $Li_2S$ formed in situ by chemical reaction between $Li_2SO_4$ and the GNAs at high temperature is probably deposited uniformly on the graphene sheets. The high conductivity of graphene as well as the intimate contact between the insulating electroactive material ($Li_2S$) and cathodic host is expected to improve the utilization of active material and contribute to the transport of electrons to the active material during the charge–discharge process. Electrochemical impedance spectroscopy (EIS) profiles of LS-GNAs H and the $Li_2S$–GNAs mixture confirmed this point (**Fig. 2.14**). Although they have nearly comparable bulk resistances corresponding to the electrolyte resistance (as determined by the left intersection of the semicircle with the *x* axis), the LS-GNAs H cathode exhibits a much lower charge transfer resistance ($R_{ct}$) for the electrochemical reaction on the electrode–electrolyte intersurface (as determined by the diameter of the semicircle).[44, 45] For $Li_2S$–GNAs mixture, the Nyquist plot seems to contain two semicircles, probably due to the different electrochemical environments in $Li_2S$–GNAs mixture, which are affected by the distribution of the conducting agent and large-sized $Li_2S$. The 2D graphene is also necessary for high cell performance, because when the GNAs were replaced by a benchmark Ketjenblack (KB, specific surface area: 1270

$m^2/g$), the obtained KB–$Li_2S$ composite (**LS-KB H**) exhibits a much lower discharge capacity than LS-GNAs H (**Fig. 2.15**).

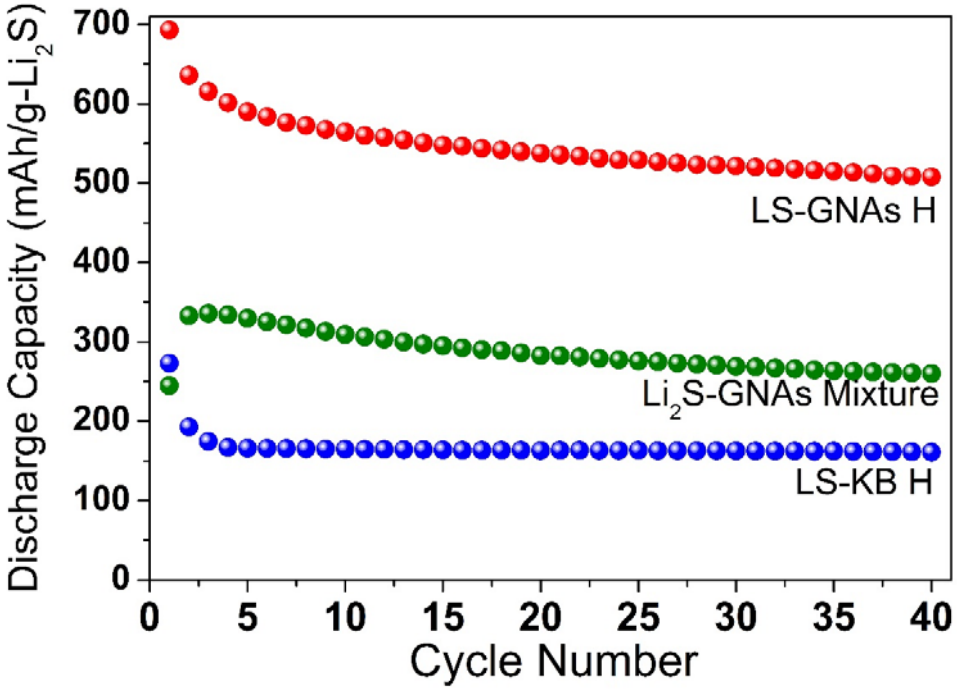


**Fig. 2.15.** Cycling performance of LS-GNAs H, $Li_2S$–GNAs mixture, and LS-KB H over 40 cycles at a current rate of 1/12 C.

## 2.4. Conclusions

In summary, we reported a very simple method of preparing a $Li_2S$/graphene composite through one-pot pyrolysis of lithium sulfate and GNAs without using expensive commercial $Li_2S$. This step can immobilize the active $Li_2S$ deposits in situ on the highly conductive host by intimate contact. XRD results showed that no impurities were formed except for a tiny amount of $Li_2O$. FESEM and EDS confirmed the homogenous distribution of C and S in the obtained composite. The in situ formed $Li_2S$/graphene could be used directly as cathodes for lithium–sulfur batteries, delivering greatly enhanced capacities, fast reaction kinetics, low polarization, and good cycling performance and rate capability as compared with a physical mixture of commercial $Li_2S$ and GNAs. For example, LS-GNAs H–based half-cells showed an initial discharge capacity of 693 mAh/g, a $40^{th}$ discharge capacity of 508 mAh/g, and a Coulombic efficiency of ca. 95%, which

are much higher than those of a mixture of commercial $Li_2S$ and GNAs. EIS analysis suggested that this improvement could be related to the reduced charge transfer resistance. Note, in addition, that the 2D layer structure of graphene plays an important role in transporting electrons and ions and thus maximizing the utilization of the active $Li_2S$, as suggested by a control experiment using a $Li_2S$/KB composite. The performance (e.g., areal capacity) of the battery based on this in-situ strategy might be further improved by reducing the particle size of the $Li_2S$/graphene composite,[24] introducing redox mediators to the electrolyte[46] to depress the active potential of $Li_2S$, or optimizing the type of binder and current collector.

## 2.5. References


[1] P. G. Bruce, S. A. Freunberger, L. J. Hardwick, J. M. Tarascon, *Nat. Mater.* **2012**, *11*, 19.

[2] A. Manthiram, Y. Fu, Y. S. Su, *Acc. Chem. Res.* **2013**, *46*, 1125.

[3] M. Barghamadi, A. Kapoor, C. Wen, *J. Electrochem. Soc.* **2013**, *160*, A1256.

[4] A. Manthiram, Y. Fu, S. H. Chung, C. Zu, Y. S. Su, *Chem. Rev.* **2014**, *114*, 11751.

[5] X. Ji, K. T. Lee, L. F. Nazar, *Nat. Mater.* **2009**, *8*, 500.

[6] M. K. Song, E. J. Cairns, Y. Zhang, *Nanoscale* **2013**, *5*, 2186.

[7] K. Dokko, N. Tachikawa, K. Yamauchi, M. Tsuchiya, A. Yamazaki, E. Takashima, J. W. Park, K. Ueno, S. Seki, N. Serizawa, M. Watanabe, *J. Electrochem. Soc.* **2013**, *160*, A1304.

[8] N. Tachikawa, K. Yamauchi, E. Takashima, J. W. Park, K. Dokko, M. Watanabe, *Chem. Commun.* **2011**, *47*, 8157.

[9] J. W. Park, K. Yamauchi, E. Takashima, N. Tachikawa, K. Ueno, K. Dokko, M. Watanabe, *J. Phys. Chem. C* **2013**, *117*, 4431.

[10] J. W. Park, K. Ueno, N. Tachikawa, K. Dokko, M. Watanabe, *J. Phys. Chem. C* **2013**, *117*, 20531.

[11] C. Zhang, A. Yamazaki, J. Murai, J. W. Park, T. Mandai, K. Ueno, K. Dokko, M. Watanabe, *J. Phys. Chem. C* **2014**, *118*, 17362.

[12] J. Kim, D. J. Lee, H. G. Jung, Y. K. Sun, J. Hassoun, B. Scrosati, *Adv. Funct. Mater.* **2013**, *23*, 1076.

[13] G. Xu, B. Ding, J. Pan, P. Nie, L. Shen, X. Zhang, *J. Mater. Chem. A* **2014**, *2*, 12662.

[14] S. S. Zhang, *J. Power Sources* **2013**, *231*, 153.

[15] K. Zhang, L. Wang, Z. Hu, F. Cheng, J. Chen, *Sci. Rep.* **2014**, *4*, 6467.

[16] Y. Yang, M. T. McDowell, A. Jackson, J. J. Cha, S. S. Hong, Y. Cui, *Nano Lett.* **2010**, *10*, 1486.

[17] M. Nagao, A. Hayashi, M. Tatsumisago, *J. Mater. Chem.* **2012**, *22*, 10015.

[18] Y. Yang, G. Zheng, S. Misra, J. Nelson, M. F. Toney, Y. Cui, *J. Am. Chem. Soc.* **2012**, *134*, 15387.

[19] K. Cai, M. K. Song, E. J. Cairns, Y. Zhang, *Nano Lett.* **2012**, *12*, 6474.

[20] J. Liu, H. Nara, T. Yokoshima, T. Momma, T. Osaka, *J. Power Sources* **2015**, *273*, 1136.

[21] F. Wu, J. T. Lee, A. Magasinski, H. Kim, G. Yushin, *Part. Part. Syst. Charact.* **2014**, *31*, 639.

[22] F. Wu, A. Magasinski, G. Yushin, *J. Mater. Chem. A* **2014**, *2*, 6064.

[23] J. Guo, Z. Yang, Y. Yu, H. D. Abruna, L. A. Archer, *J. Am. Chem. Soc.* **2013**, *135*, 763.

[24] C. Nan, Z. Lin, H. Liao, M. K. Song, Y. Li, E. J. Cairns, *J. Am. Chem. Soc.* **2014**, *136*, 4659.

[25] Z. Lin, C. Nan, Y. Ye, J. Guo, J. Zhu, E. J. Cairns, *Nano Energy* **2014**, *9*, 408.

[26] Z. Yang, J. Guo, S. K. Das, Y. Yu, Z. Zhou, H. D. Abruña, L. A. Archer, *J. Mater. Chem. A* **2013**, *1*, 1433.

[27] S. Evers, L. F. Nazar, *Chem. Commun.* **2012**, *48*, 1233.

[28] X. Yang, L. Zhang, F. Zhang, Y. Huang, Y. Chen, *ACS Nano* **2014**, *8*, 5208.

[29] H. Wang, Y. Yang, Y. Liang, J. T. Robinson, Y. Li, A. Jackson, Y. Cui, H. Dai, *Nano Lett.* **2011**, *11*, 2644.

[30] K. Han, J. Shen, C. M. Hayner, H. Ye, M. C. Kung, H. H. Kung, *J. Power Sources* **2014**, *251*, 331.

[31] S. Zhang, K. Ueno, K. Dokko, M. Watanabe, *Adv. Energy Mater.* **2015**, *5*, 1500117.

[32] G. Wang, J. Yang, J. Park, X. Gou, B. Wang, H. Liu, J. Yao, *J. Phys. Chem. C* **2008**, *112*, 8192.

[33] A. V. Murugan, T. Muraliganth, A. Manthiram, *Chem. Mater.* **2009**, *21*, 5004.

[34] Y. Diao, K. Xie, S. Xiong, X. Hong, *J. Electrochem. Soc.* **2012**, *159*, A1816.

[35] H. Huang, Y. Xia, X. Tao, J. Du, J. Fang, Y. Gan, W. Zhang, *J. Mater. Chem.* **2012**, *22*, 10452.

[36] C. Mattevi, G. Eda, S. Agnoli, S. Miller, K. A. Mkhoyan, O. Celik, D. Mastrogiovanni, G. Granozzi, E. Garfunkel, M. Chhowalla, *Adv. Funct. Mater.* **2009**, *19*, 2577.

[37] T. Tamura, K. Yoshida, T. Hachida, M. Tsuchiya, M. Nakamura, Y. Kazue, N. Tachikawa, K. Dokko, M. Watanabe, *Chem. Lett.* **2010**, *39*, 753.

[38] K. Ueno, K. Yoshida, M. Tsuchiya, N. Tachikawa, K. Dokko, M. Watanabe, *J. Phys. Chem. B* **2012**, *116*, 11323.

[39] K. Yoshida, M. Tsuchiya, N. Tachikawa, K. Dokko, M. Watanabe, *J. Phys. Chem. C* **2011**, *115*, 18384.

[40] K. Yoshida, M. Nakamura, Y. Kazue, N. Tachikawa, S. Tsuzuki, S. Seki, K. Dokko, M. Watanabe, *J. Am. Chem. Soc.* **2011**, *133*, 13121.

[41] K. Yoshida, M. Tsuchiya, N. Tachikawa, K. Dokko, M. Watanabe, *J. Electrochem. Soc.* **2012**, *159*, A1005.

[42] K. Ueno, J. W. Park, A. Yamazaki, T. Mandai, N. Tachikawa, K. Dokko, M. Watanabe, *J. Phys. Chem. C* **2013**, *117*, 20509.

[43] Y. Fu, Y. S. Su, A. Manthiram, *Adv. Energy Mater.* **2014**, *4*, 1300655.

[44] Y. S. Su, A. Manthiram, *Electrochim. Acta* **2012**, *77*, 272.

[45] L. Chen, Y. Liu, M. Ashuri, C. Liu, L. L. Shaw, *J. Mater. Chem. A* **2014**, *2*, 18026.

[46] S. Meini, R. Elazari, A. Rosenman, A. Garsuch, D. Aurbach, *J. Phys. Chem. Lett.* **2014**, *5*, 915.

# Chapter Three

Preparation of Ball-Milled $Li_2S$/Graphene Composite for High-Mass-Loading Cathode

**Abstract**

$Li_2S$ has recently emerged as a promising cathode material, due to its high theoretical specific capacity of 1166 mAh/g and its great potential in the development of lithium-ion sulfur batteries with a lithium-free anode such as graphite. In this part, a novel ball-milled $Li_2S$/graphene composite was introduced. This simple and efficient approach (high-energy ball milling) can not only reduce the particle size of the $Li_2S$/graphene composite, but also enhance the reaction kinetics of $Li_2S$. To improve the electrochemical performance of the $Li_2S$ cathode at high $Li_2S$ loading, carbon fiber paper was employed in place of the traditional aluminum foil current collector.

Part of the work presented in this chapter has been published as:

Zhe Li, Shiguo Zhang, Shoshi Terada, Xiaofeng Ma, Kohei Ikeda, Yutaro Kamei, Ce Zhang, Kaoru Dokko, Masayoshi Watanabe, Promising Cell Configuration for Next-Generation Energy Storage: $Li_2S$/Graphite Battery Enabled by a Solvate Ionic Liquid Electrolyte, ACS Applied Materials & Interfaces, 2016, 8, 16053–16062.

## 3.1. Introduction

Lithium sulfide ($Li_2S$) has recently emerged as a very promising cathodic material for lithium batteries, due to its high theoretical specific capacity of 1166 mAh/g and the possibility in conjunction with lithium-free anodes to address safety concerns. It is well known that the electronically and ionically insulating nature of $Li_2S$, as well as its high melting point (938°C), represent obstacles to its high electrochemical utilization and to its incorporation into conductive materials via the conventional melt-diffusion process, such as that used for sulfur. Therefore, a variety of approaches have been pursued to fabricate highly efficient $Li_2S$/carbon composites. However, most of the previously reported approaches directly employed expensive commercial $Li_2S$ powders,[1-7] or highly reactive organolithium reagents (lithium triethylborohydride or n-butyllithium) to react with sulfur,[8-12] and in both cases improving the procedures and performance remains challenging. Moreover, the $Li_2S$ loading in the reported cathodes is usually low (ca. 1.0 mg/cm$^2$),[1, 2, 4-7] which limits the energy density of the Li-S batteries.

To overcome these issues, we developed a $Li_2S$/graphene composite (LS-G), prepared by a facile, cost-effective, and scalable method involving one-pot pyrolysis of lithium sulfate ($Li_2SO_4$) and excess graphene nanoplatelet aggregates (GNAs).[13] Herein, the GNAs have a dual function. On one hand, the majority of the GNAs serve as carbon source to chemically reduce $Li_2SO_4$ and generate $Li_2S$ at 781°C ($Li_2SO_4 + 2C \rightarrow 2CO_2\uparrow + Li_2S$). On the other hand, the residual GNAs form thin graphene layers by in-situ etching that can immobilize the $Li_2S$, yielding a $Li_2S$/graphene composite with a close contact between the highly conductive two-dimensional (2D) host and the active material. In order to facilitate the activation of $Li_2S$ during the initial charge and further enhance the reaction kinetics of $Li_2S$, a very simple and efficient approach has been implemented, aimed at reducing the size of the $Li_2S$/graphene composite particles through a high-energy ball-milling process (**Fig. 3.1a**). In addition, traditional aluminum foil current collector will be replaced by a three-dimensionally porous current collector, carbon fiber paper (CFP), to improve the

electrochemical performance of the $Li_2S$ electrode at high mass loading. Herein, CFP as electron pathways can guarantee the efficient electron transport for $Li_2S$ and enhance the electronic conductivity of the entire electrode. Also, the sufficiency of porous spaces in electrode enabled by the unique architecture of CFP can provide excellent electrolyte absorption and numerous electrolyte channel, increasing the electrochemical sites for the reactions of active materials. As a result, the ball-milled $Li_2S$/graphene composite electrode exploiting this three-dimensionally porous current collector exhibits an excellent cell performance, even at a high $Li_2S$ loading of 2.2 mg/cm$^2$.

## 3.2. Experimental

*Preparation of ball-milled $Li_2S$/graphene composite:* A ball-milled $Li_2S$/graphene composite was prepared in three steps. First, 3.20 g of $Li_2SO_4 \cdot H_2O$ and 0.96 g of graphene nanoplatelet aggregates (GNAs, Strem Chemicals) were dispersed in 140 mL of ultrapure water. After ultrasonication and stirring for 6 h, 1600 mL of ethanol was added dropwise into the above suspension, allowing the slow precipitation of $Li_2SO_4$ onto the surface of the GNAs. Subsequently, the black $Li_2SO_4$/GNAs composite was filtered off, washed by ethanol several times, and dried for 12 h at 40°C in vacuum. In the second step, the $Li_2SO_4$/GNAs composite was subjected to pyrolysis in a tube furnace under flowing argon, using the following temperature program: (1) holding at room temperature (RT) for 1 h to degas, (2) heating to 200°C at 10°C/min, (3) keeping at 200°C for 1 h, (4) heating to 781°C at 10°C/min, (5) calcining at 781°C for 2 h, and (6) spontaneous cooling to RT. $Li_2S$ is generated in situ through one-pot pyrolysis ($Li_2SO_4 + 2C \rightarrow 2CO_2\uparrow + Li_2S$) and uniformly deposited on the residual graphene sheets, resulting in the $Li_2S$/graphene composite (LS-G). Finally, 0.40 g of the LS-G composite was mixed with 120 zirconia balls (grinding media, 4 mm in diameter), and then milled using a planetary ball mill (Fritsch Pulverisette 7) at a rotation speed of 600 rpm within an argon-filled glovebox, in which the moisture level was below 1 ppm. To avoid overheating of the sample, a ball-milling period of 10 min was followed by a rest period of 5 min. The ball-milled $Li_2S$/graphene composite was

collected after 192 cycles and hereafter denoted as LS-G BM. The $Li_2S$ content (80.6 wt%) in LS-G BM was measured by the weight method after washing away $Li_2S$ using anhydrous methanol.

*Preparation of $Li_2S$ cathodes:* All the $Li_2S$ cathodes were fabricated in an argon-filled glovebox ($H_2O$ level < 1 ppm). LS-G BM was mixed with carbon black (Super C65, TIMCAL) and polyvinylpyrrolidone (PVP, MW = 1200 kDa, JUNSEI) in *N*-methyl-2-pyrrolidinone (NMP) and ground for 50 min. The weight ratio of $Li_2S$, carbon (including graphene and carbon black), and PVP was set at 60:30:10. To compare with our previously reported LS-G cathode under the same conditions, this slurry was then uniformly coated onto an aluminum foil current collector (AFCC) via a doctor-blade technique, followed by drying in vacuum for 16 h at 80°C. The $Li_2S$ loading on the current collector was around 0.5 mg/cm$^2$. In order to prepare the composite cathode using carbon fiber paper (CFP, Toray Paper 060) as current collector, LS-G BM, carbon black, and PVP ($Li_2S$:C:PVP = 60:30:10) were dispersed into NMP and stirred for 48 h. The resultant low-viscosity slurry was then adsorbed by CFP via capillary force. After drying in vacuum at 80°C for 16 h, CFP-supported cathodes with controllable $Li_2S$ loadings ranging from 0.5 to 2.2 mg/cm$^2$ were obtained.

*Preparation of electrolytes:* $[Li(G4)_1][TFSA]$ was prepared by mixing the purified tetraglyme (G4, Nippon Nyukazai) and lithium bis(trif uoromethanesulfonyl)amide (Li[TFSA], Solvey) in a molar ratio of 1:1. Afterwards, HFE was added into the above mixture to obtain a homogeneous liquid (denoted as $[Li(G4)_1][TFSA]$/HFE) with a Li[TFSA] concentration of 1 mol/L at 30°C.

*Characterization:* The morphology and elemental distribution of the samples were investigated by field emission scanning electron microscopy (FESEM, JEOL JSM-7001F) equipped with an energy-dispersive X-ray spectroscopy (EDX) system. X-ray diffraction (XRD) measurements were performed by a Rigaku Ultima IV X-ray diffractometer using a Cu Kα radiation source. Since

$Li_2S$ is highly sensitive to moisture, during the XRD measurements the sample was sealed in an airtight chamber with a beryllium window.

*Electrochemical measurements:* The $Li_2S$/Li half cells were assembled into 2032-type coin cells using porous glass separators (GA55, Advantec). Before measuring the electrochemical properties, the cells were equilibrated for 12 h. The galvanostatic charge and discharge tests of the cells were performed at 30°C by a Nagano BTS-2004 battery testing system. In the cases of $Li_2S$/Li half cell, the cells were initially charged from the open circuit voltage (OCV) to 4.4 V to activate the $Li_2S$, and then operated in the voltage range of 1.5–3.5 V. The 1 C rate was set to 1166 mA/g, and the specific capacity of the cell was calculated in terms of the mass of $Li_2S$. Cyclic voltammetry (CV) was carried out on a Bio-Logic SAS VMP3 electrochemical workstation at a scan rate of 0.04 mV/s.

### 3.3. Results and Discussion

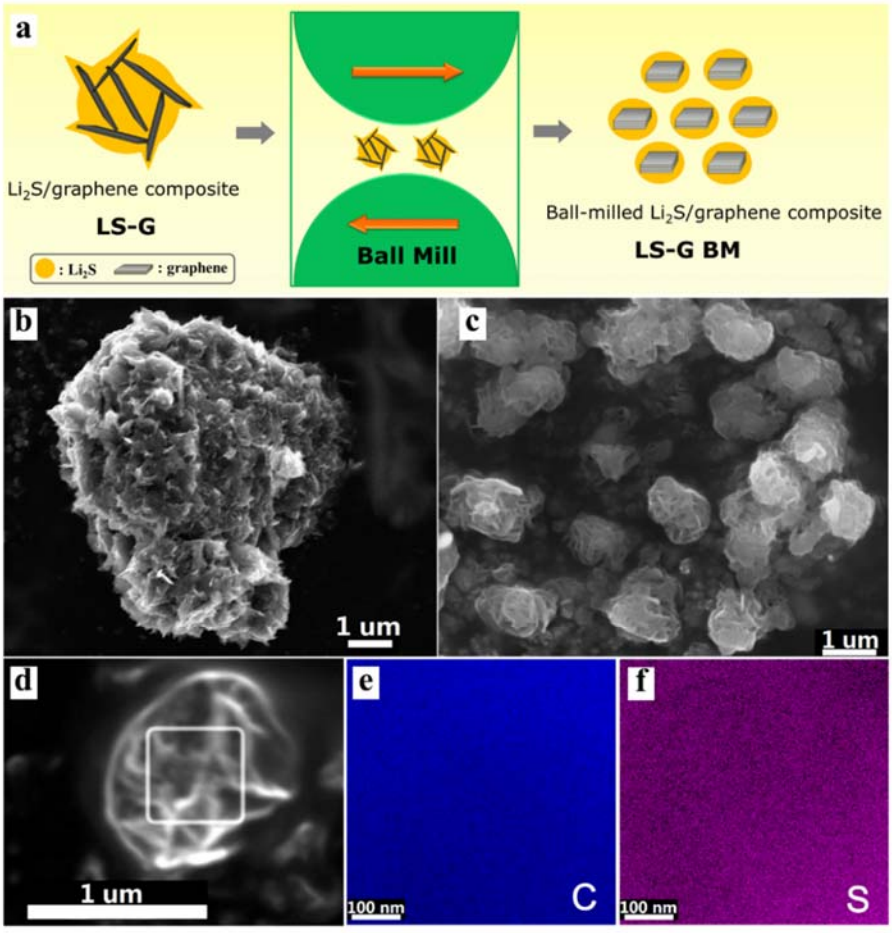

**Fig. 3.1**. (a) Schematic illustration of the preparation process of ball-milled $Li_2S$/graphene composite. Field emission scanning electron (FESEM) images of (b) $Li_2S$/graphene (LS-G) and (c, d) ball-milled $Li_2S$/graphene (LS-G BM) composites. Energy-dispersive X-ray spectroscopy (EDX) elemental mappings of (e) carbon and (f) sulfur over the region highlighted in image (d).

As shown in **Fig. 3.1b** and **1c**, the $Li_2S$/graphene composite obtained after ball-milling (LS-G BM) has a particle size of 0.3–1.1 μm, much smaller than the original LS-G (> 6.5 μm). The surface of LS-G BM particles (**Fig. 3.1d**) displays a crumpled morphology, which is due to the thin-layer graphene matrix. As indicated by the EDX elemental mapping (**Fig. 3.1e** and **1f**), carbon and sulfur are homogeneously distributed in LS-G BM, confirming that $Li_2S$ remains strongly attached to the graphene matrix surface after the ball milling. The XRD patterns of both LS-G and LS-G BM match very well the standard data for cubic $Li_2S$ (JCPDS 23-0369), showing that no impurities are generated during the ball-milling process (**Fig. 3.2)**. In agreement with the FESEM result, the peaks of LS-G BM are considerably broadened compared to LS-G, indicating a decrease in crystallite size of $Li_2S$, in turn due to the decrease in particle size of the $Li_2S$/graphene composite after ball milling.

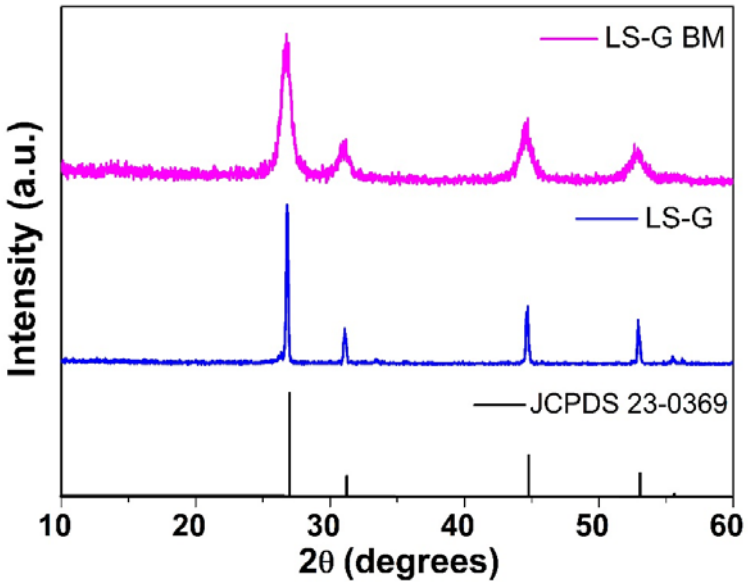


**Fig. 3.2**. X-ray diffraction patterns of $Li_2S$/graphene (LS-G) and ball-milled $Li_2S$/graphene (LS-G BM) composites.

To compare the cell performance of the composites before and after ball-milling, 2032-type half cells ([Li|electrolyte|$Li_2S$], $Li_2S$ loading: 0.5 mg/cm$^2$) were assembled using aluminum foil as current collector and a glyme-Li salt solvate IL diluted by HFE ([Li(G4)$_1$][TFSA]/4HFE) as electrolyte. Due to the particle size of the composites, an initial one-step electrochemical activation of the $Li_2S$ electrode is still required, which involves setting a higher charging cutoff voltage to overcome the initial barrier from phase nucleation of polysulfides.[3, 14] As shown in **Fig. 3.3a**, the galvanostatic charge-discharge curves at a current rate of 1/12 C clearly demonstrate an improved performance for LS-G BM compared to LS-G, as expected. Although the initial charge capacities of LS-G (1116 mAh/g) and LS-G BM (1154 mAh/g) cathodes are very close to each other, the LS-G BM cathode overcomes the energy barrier for lithium extraction with an initial charge plateau at 2.9 V, which is much lower than 4.2 V for the LS-G cathode under the same conditions. This is because the small particle size of LS-G BM ensures better contact between $Li_2S$, conductive host, and electrolyte, and increases the number of active sites for the electrochemical reactions. In the first discharge, the LS-G BM cathode could deliver a higher capacity of 812 mAh/g with slightly higher discharge plateaus than the LS-G cathode (**Fig. 3.3a**), also indicating increased utilization of $Li_2S$. Moreover, the subsequent charge-discharge behaviors of LS-G and LS-G BM cathodes are similar (**Fig. 3.3b**), resembling the behavior of the conventional sulfur cathode.[15, 16] The very flat and stable charge plateau at around 2.3 V in the fifth cycle is attributed to oxidative conversion of $Li_2S$ into elemental sulfur, whereas the two well-defined discharge plateaus correspond to the formation of long-chain lithium polysulfides ($Li_2S_x$, $4 < x < 8$) and of the end discharge product $Li_2S$.[17]

Typical cyclic voltammograms of LS-G and LS-G BM cathodes in the first three cycles are shown in **Fig. 3.3c**. A broad oxidation peak centered at 3.1 V was observed for LS-G BM in the first anodic scan, which is much lower than the activation peak for the LS-G cathode (4.3 V). In addition, the redox peaks of the LS-G BM cathode in the second and third cycles are much sharper and more

intense than those of LS-G, suggesting lower electrochemical polarization and faster electrochemical kinetics. Correspondingly, the LS-G BM cathode delivers higher capacities than LS-G over all 40 cycles (**Fig. 3.3d**). For example, a high discharge capacity of 600 mAh/g and a high Coulombic efficiency of ca. 98% were still obtained after 40 cycles at 1/12 C.

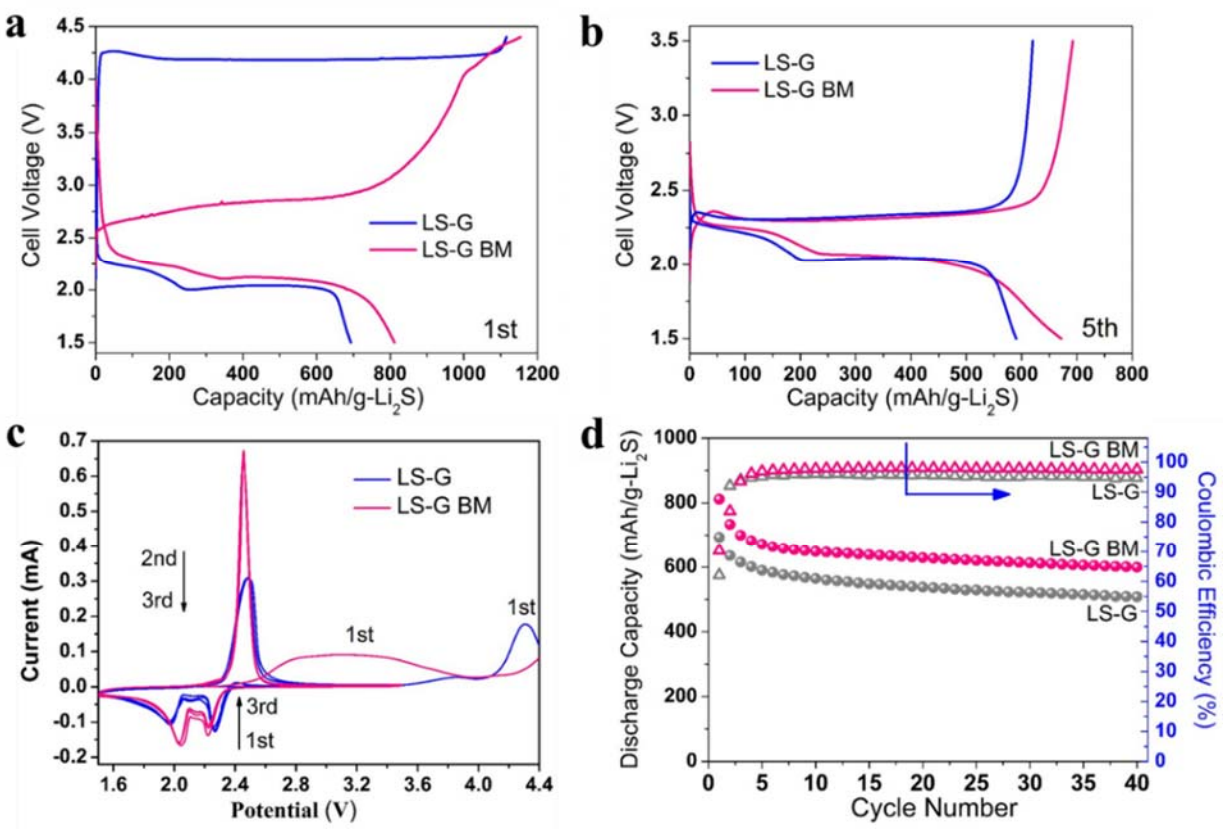


**Fig. 3.3**. Galvanostatic charge-discharge curves of $Li_2S$/Li half cells [Li metal |[ $Li(G4)_1$][TFSA]/HFE | $Li_2S$] (G4: tetraglyme, TFSA: bis(trifluoromethanesulfonyl)amide, HFE: 1,1,2,2-tetrafluoroethyl 2,2,3,3-tetrafluoropropyl ether) based on $Li_2S$/graphene (LS-G) and ball-milled (LS-G BM) cathodes on aluminum foil current collector (AFCC) in the (a) first and (b) fifth cycle at a current rate of 1/12 C (1 C = 1166 mA/g). (c) Typical cyclic voltammograms of $Li_2S$/Li half cells using LS-G and LS-G BM cathodes in the first three cycles at a scan rate of 0.04 mV/s. The potential was initially scanned from the open circuit voltage to 4.4 V (versus $Li/Li^+$), and then between 3.5 and 1.5 V (versus $Li/Li^+$). (d) Cycling performance and Coulombic efficiency of $Li_2S$/Li half cells using LS-G and LS-G BM cathodes over 40 cycles at 1/12 C. For the LS-G and LS-G BM cathodes, the $Li_2S$ loading on AFCC was ca. 0.5 mg/cm$^2$.

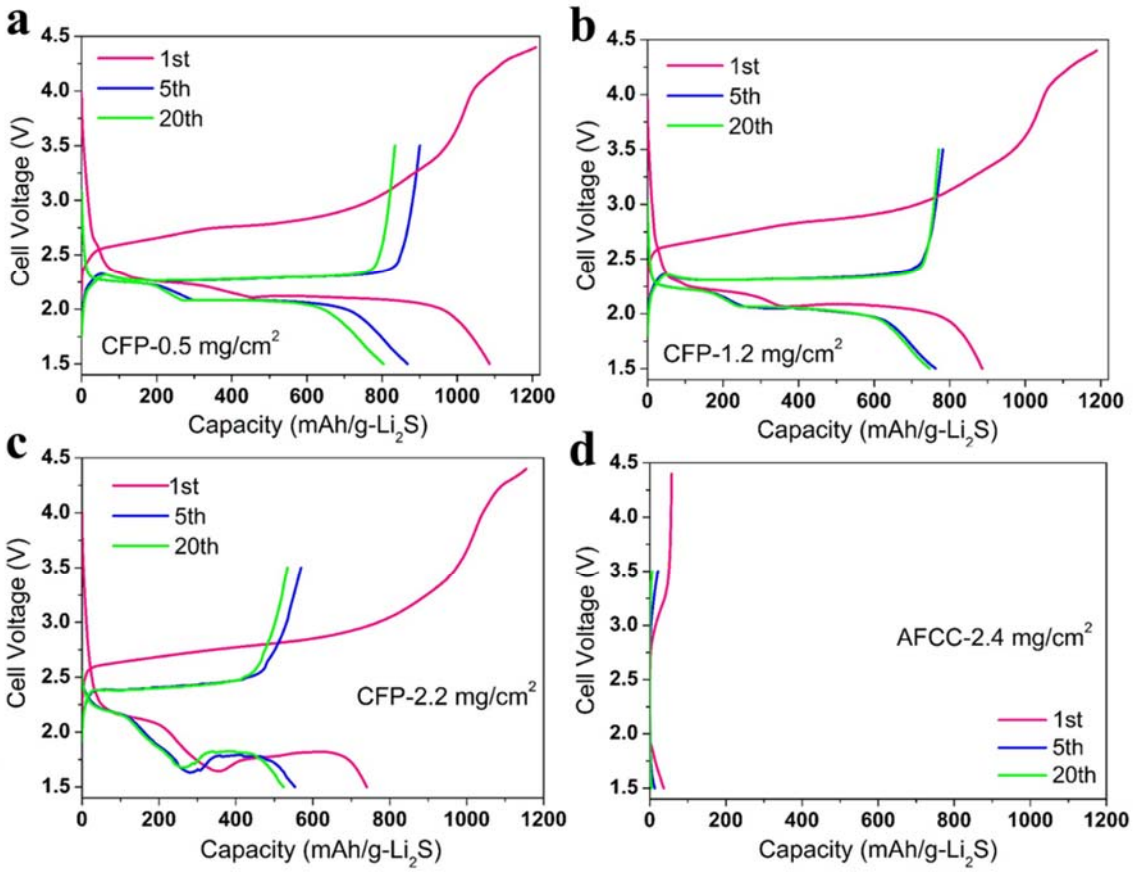


**Fig. 3.4**. Galvanostatic charge-discharge curves of $Li_2S$/Li half cells [Li metal | $[Li(G4)_1][TFSA]$/HFE | $Li_2S$] based on ball-milled $Li_2S$/graphene (LS-G BM) cathodes, using carbon fiber paper as current collector and with $Li_2S$ loadings of (a) 0.5, (b) 1.2, and (c) 2.2 mg/cm$^2$ at 1/12 C. (d) Charge-discharge curves of $Li_2S$/Li half cell based on the LS-G BM cathode using aluminum foil current collector at a $Li_2S$ loading of 2.4 mg/cm$^2$ at 1/12 C (1 C = 1166 mA/g).

Since a thick cathode is desirable for improving the energy density of a Li-S battery, the $Li_2S$ loading on the LS-G BM cathode was further increased to 2.4 mg/cm$^2$ using an AFCC. This thick cathode, however, delivered an extremely low discharge capacity of 5 mAh/g in the 20th cycle at 1/12 C (**Fig. 3.4d**), probably due to the increased electronic and ionic resistance resulting from the high $Li_2S$ loading on the flat current collector. In order to remove this issue, the AFCC was replaced by a three-dimensional (3D) porous current collector, CFP. The 3D porous network of the CFP is expected to ensure sufficient space for

high $Li_2S$ loading, as well as excellent electrolyte absorption and fast lithium ion migration, while the interconnected carbon fibers provide highly efficient electron transport pathways for insulating $Li_2S$. [18] As shown in Fig. 3.4a, the discharge capacity of the LS-G BM cathode with a $Li_2S$ loading of 0.5 mg/cm$^2$ on CFP is 1086 mAh/g in the first cycle, then declines to 868 mAh/g in the 5th cycle and to 803 mAh/g in the 20th cycle. These values are much higher than those obtained using an AFCC at the same $Li_2S$ loading (**Fig. 3.3d**). Even after further increasing the $Li_2S$ loading on CFP to 2.2 mg/cm$^2$ (**Fig. 3.4c**), the LS-G BM still exhibited an initial discharge capacity of 740 mAh/g and a 20th-cycle discharge capacity of 523 mAh/g. However, an enlarged voltage hysteresis between the discharge and charge curves was observed for the highest loading cathode (2.2 mg/cm$^2$). Such overpotential is larger for the discharge reaction. The thick $Li_2S$ cathode may induce Li-ion depletion inside the $Li_2S$ cathode because a large amount of the active materials is reduced to $Li_2S$ by the consumption of $Li^+$ from the electrolyte. Additionally, at variance with the thin electrodes, the thick cathode requires the paired lithium metal anode to undergo more intensive deposition and stripping during cycling, which can induce substantial morphological changes on the lithium metal surface and probably hinder the cell performance.

## 3.4. Conclusions

In summary, a novel $Li_2S$/graphene nano-composite (LS-G BM) was fabricated by applying high-energy ball milling to an in-situ formed $Li_2S$/graphene composite. This simple and efficient approach can not only reduce the particle size of the $Li_2S$/graphene composite, as confirmed by XRD and FESEM, but also enhance the reaction kinetics of $Li_2S$, which is probably due to an enhanced electrochemical contact between electrolyte and $Li_2S$. To improve the electrochemical performance of the LS-G BM cathode at high mass loading, carbon fiber paper (CFP) was exploited to replace the traditional aluminum foil current collector. At the $Li_2S$ loading of 2.2 mg/cm$^2$, the LS-G BM cathode with CFP in $[Li(G4)_1][TFSA]$/HFE electrolyte can deliver an initial discharge capacity of 740 mAh/g, and drop to 523 mAh/g in the 20th cycle.

## 3.5. References


[1] L. Chen, Y. Liu, M. Ashuri, C. Liu, L. L. Shaw, *J. Mater. Chem. A* **2014**, *2*, 18026.

[2] K. Cai, M. K. Song, E. J. Cairns, Y. Zhang, *Nano Lett.* **2012**, *12*, 6474.

[3] Y. Yang, G. Zheng, S. Misra, J. Nelson, M. F. Toney, Y. Cui, *J. Am. Chem. Soc.* **2012**, *134*, 15387.

[4] J. Liu, H. Nara, T. Yokoshima, T. Momma, T. Osaka, *J. Power Sources* **2015**, *273*, 1136.

[5] F. Wu, A. Magasinski, G. Yushin, *J. Mater. Chem. A* **2014**, *2*, 6064.

[6] C. Wang, X. Wang, Y. Yang, A. Kushima, J. Chen, Y. Huang, J. Li, *Nano Lett.* **2015**, *15*, 1796.

[7] Z. W. Seh, H. Wang, P. C. Hsu, Q. Zhang, W. Li, G. Zheng, H. Yao, Y. Cui, *Energy Environ. Sci.* **2014**, *7*, 672.

[8] K. Zhang, L. Wang, Z. Hu, F. Cheng, J. Chen, *Sci. Rep.* **2014**, *4*, 6467.

[9] C. Nan, Z. Lin, H. Liao, M. K. Song, Y. Li, E. J. Cairns, *J. Am. Chem. Soc.* **2014**, *136*, 4659.

[10] Z. Lin, C. Nan, Y. Ye, J. Guo, J. Zhu, E. J. Cairns, *Nano Energy* **2014**, *9*, 408.

[11] Y. Yang, M. T. McDowell, A. Jackson, J. J. Cha, S. S. Hong, Y. Cui, *Nano Lett.* **2010**, *10*, 1486.

[12] L. Suo, Y. Zhu, F. Han, T. Gao, C. Luo, X. Fan, Y. Hu, Sheng, C. Wang, *Nano Energy* **2015**, *13*, 467.

[13] Z. Li, S. Zhang, C. Zhang, K. Ueno, T. Yasuda, R. Tatara, K. Dokko, M. Watanabe, *Nanoscale* **2015**, *7*, 14385.

[14] Y. Fu, Y. S. Su, A. Manthiram, *Adv. Energy Mater.* **2014**, *4*, 1300655.

[15] K. Dokko, N. Tachikawa, K. Yamauchi, M. Tsuchiya, A. Yamazaki, E. Takashima, J. W. Park, K. Ueno, S. Seki, N. Serizawa, M. Watanabe, *J. Electrochem. Soc.* **2013**, *160*, A1304.

[16] C. Zhang, A. Yamazaki, J. Murai, J. W. Park, T. Mandai, K. Ueno, K. Dokko, M. Watanabe, *J. Phys. Chem. C* **2014**, *118*, 17362.

[17] X. Yang, L. Zhang, F. Zhang, Y. Huang, Y. Chen, *ACS nano* **2014**, *8*, 5208.

[18] S. H. Chung, A. Manthiram, *Electrochem. Commun.* **2014**, *38*, 91.

# Chapter Four

Development of Advanced $Li_2S$/Graphite Batteries Enabled by Solvate Ionic Liquid

## Abstract

Lithium-ion sulfur batteries with a [graphite|solvate ionic liquid electrolyte|lithium sulfide ($Li_2S$)] structure are developed to realize high performance batteries without the issue of lithium anode. $Li_2S$ has recently emerged as a promising cathode material, due to its high theoretical specific capacity of 1166 mAh/g and its great potential in the development of lithium-ion sulfur batteries with a lithium-free anode such as graphite. Unfortunately, the electrochemical $Li^+$ intercalation/deintercalation in graphite is highly electrolyte-selective: whereas the process works well in the carbonate electrolytes inherited from Li-ion batteries, it cannot take place in the ether electrolytes commonly used for Li-S batteries, because the cointercalation of solvent destroys the crystalline structure of graphite. Thus, only very few studies have focused on graphite-based Li-S full cells. In this work, simple graphite-based Li-S full cells were fabricated employing electrolytes beyond the conventional carbonates, in combination with highly loaded $Li_2S$/graphene composite cathodes ($Li_2S$ loading: 2.2 mg/cm$^2$). In particular, solvate ionic liquids can act as a single-phase electrolyte simultaneously compatible with both $Li_2S$ cathode and graphite anode, and can further improve the battery performance by suppressing the shuttle effect. Consequently, this lithium-ion sulfur batteries show a stable and reversible charge-discharge behavior, along with a very high Coulombic efficiency.



Part of the work presented in this chapter has been published as:

Zhe Li, Shiguo Zhang, Shoshi Terada, Xiaofeng Ma, Kohei Ikeda, Yutaro Kamei, Ce Zhang, Kaoru Dokko, Masayoshi Watanabe, Promising Cell Configuration for Next-Generation Energy Storage: $Li_2S$/Graphite Battery Enabled by a Solvate Ionic Liquid Electrolyte, ACS Applied Materials & Interfaces, 2016, 8, 16053–16062.

## 4.1. Introduction

The ever-increasing demand for electric vehicles and large-scale energy storage systems urgently requires high-energy-density energy storage devices beyond the current Li-ion batteries.[1] Lithium-sulfur (Li-S) batteries based on the lithium/sulfur redox reaction ($16Li + S_8 \rightarrow 8Li_2S$) are very attractive in this context, owing to their high theoretical specific capacity and energy of 1672 mAh/g and 2600 Wh/kg, respectively.[2-6] Sulfur is also naturally abundant, environmentally friendly, and inexpensive. Nevertheless, the commercialization of Li-S batteries has been hampered by the insulating nature of the cathode active material, the severe shuttle effect of polysulfides ($Li_2S_x$, $x$ = 2–8), the volumetric expansion (ca. 80%) going from $S_8$ to $Li_2S$, as well as by the short-circuit problem and capacity decay due to the formation of dendrite and dead lithium caused by the utilization of lithium metal anode.[7-9] The development of advanced composite cathodes or new potential electrolytes could help to circumvent the problems associated with the sulfur cathode, by improving the electronic conductivity of the cathode materials, suppressing the shuttle effect, and accommodating the volume change. Replacing the $S_8$ active material by $Li_2S$ could improve the mechanical stability of the composite cathode upon cycling, because the volume of the active material undergoes shrinkage ($Li_2S \rightarrow S_8$) rather than expansion ($S_8 \rightarrow Li_2S$) in the initial charge process. Most importantly, the known safety hazards associated to the lithium metal anode in liquid electrolytes could be addressed by pairing the $Li_2S$ cathode with certain Li-free anodes to form a lithium-ion full cell configuration.[10-14] A $Li_2S$ cathode has been coupled with high-capacity anodes such as Si or Sn,[12-14] but such anodes inevitably suffer from a severe volume change.[15] For example, the lithiation of a Si electrode involves a volume expansion of up to 400%, resulting in an unstable electrochemical interface, poor capacity retention, and even cracking and pulverization of Si upon cycling.[16]

Graphite represents a Li-free alternative easier to employ as the anode of a full cell, owing to its well-established $Li^+$ intercalation/deintercalation chemistry, exploited in commercial Li-ion batteries. The layered structure of graphite can

accommodate one Li per six C atoms and form Li-graphite intercalation compounds (Li-GICs) that involve only a very limited volume change (9−13%).[17] Unfortunately, the electrochemical $Li^+$ intercalation and deintercalation of graphite electrodes are highly electrolyte-selective, and cannot take place in the ether electrolytes most frequently utilized for Li-S batteries, such as mixtures of 1,3-dioxolane (DOL) and 1,2-dimethoxyethane (DME), because the cointercalation of solvent destroys the graphite crystalline structure.[18] In fact, most of the successful $Li^+$ intercalation and deintercalation of graphite electrodes reported to date were performed in carbonate electrolytes inherited from Li-ion batteries.[19] A small amount of ethylene carbonate (EC) is reductively decomposed at the graphite electrode in the initial charging process, and the decomposition products form a solid electrolyte interphase (SEI) layer on the graphite surface. The SEI acts as a passivation layer inhibiting the subsequent reductive decomposition of EC, as well as the cointercalation of solvent molecules into graphite.[20] The carbonate electrolytes used for Li-ion batteries, however, are chemically incompatible with most cathodes used in Li-S batteries, because carbonates can adversely react with polysulfides through nucleophilic attacks at either the ether or carbonyl carbon atoms on the carbonate molecules during the first discharge process.[21] Therefore, previous attempts to fabricate graphite-based Li-S full cells (graphite|electrolyte|$Li_2S$) necessarily employed special cathodes that were reported to be compatible with the carbonate-based electrolytes. For example, $Li_2S$ was confined in microporous carbons through vacuum infusion of sulfur vapor at 600ºC, followed by a complicated lithiation.[22] Although this cathode, coupled with a graphite anode, showed high Coulombic efficiency and long cycling stability in a conventional Li-ion battery electrolyte (1.0 M $LiPF_6$ + EC/DEC (1:1, v/v)), the microporous hosts can only support less than 30% active material and exhibit a low discharge voltage plateau (ca. 1.7 V), both of which strongly reduce the energy density. Another alternative method involves a very complicated full cell configuration consisting of a two-phase electrolyte system [graphite | electrolyte 1 (carbonate) || electrolyte 2 (ether) | $Li_2S$], wherein the carbonate electrolyte

(compatible with the graphite anode) and the ether electrolyte (compatible with the $Li_2S$ cathode) have to be separated by a ceramic lithium super ionic conductor (LISICON) film.[23] Therefore, there is great interest in developing an electrolyte suitable for the stable operation of graphite anode-based Li-S full cells with high capacity.

Here we report the fabrication of a simple graphite-based Li-S full cell with [graphite|[Li(G4)$_x$][TFSA]/HFE|$Li_2S$] (G4: tetraglyme, TFSA: bis(trifluoromethanesulfonyl)amide, HFE: 1,1,2,2-tetrafluoroethyl 2,2,3,3-tetrafluoropropyl ether, $x$ = 0.6, 0.8, 1) configuration, using solvate ionic liquids (ILs) diluted by HFE as a single-phase electrolyte. In particular, the solvate ILs are glyme-Li salt molten complexes diluted by a low-viscosity and nonpolar HFE cosolvent. Such electrolytes actually have a triple role. First, solvate ILs with high $Li^+$ transference numbers and high Li-ion concentration are compatible with the cathode of a Li-S battery.[24] Second, they are compatible with the graphite electrodes, and $Li^+$ can reversibly intercalate/deintercalate into the graphite anode without cointercalation of solvent molecules.[20, 25] Third, the shuttle effect is greatly reduced because polysulfides have a very low solubility in solvate ILs diluted by HFE.[24, 26-31] By combining the present "three-in-one" electrolyte discovered by us with an in-situ formed and high-loading $Li_2S$/graphene composite cathode, here we show that a Li-S full cell based on a graphite anode exhibits stable and reversible charge-discharge behavior, along with very high Coulombic efficiency.

## 4.2. Experimental

*Preparation of $Li_2S$ cathodes:* All the $Li_2S$ cathodes were fabricated in an argon-filled glovebox ($H_2O$ level < 1 ppm). In order to prepare the composite cathode using carbon fiber paper (CFP, Toray Paper 060) as current collector, ball-milled $Li_2S$/graphene composite (LS-G BM), carbon black, and PVP ($Li_2S$:C:PVP = 60:30:10) were dispersed into NMP and stirred for 48 h. The resultant low-viscosity slurry was then adsorbed by CFP via capillary force.

After drying in vacuum at 80°C for 16 h, CFP-supported cathodes with a $Li_2S$ loading of 2.2 mg/cm$^2$ were obtained.

*Preparation of graphite anode.* Artificial graphite (90 wt%, Hitachi Chemical), acetylene black (AB, 3 wt%, Denki Kagaku Kogyo), and poly(vinylidene fluoride) (PVDF, 7 wt%, Kureha) were mixed in NMP to form a slurry, which was coated onto a Cu foil current collector and then dried in an oven for 12 h at 80°C. Prior to use, the obtained graphite electrodes were compressed to enhance the electrical conductivity, and further dried in vacuum for 24 h at 80°C. The graphite loading on the electrode was 4.5 mg/cm$^2$.

*Preparation of electrolytes:* [Li(G4)$_1$][TFSA] was prepared by mixing the purified tetraglyme (G4, Nippon Nyukazai) and lithium bis(trif uoromethanesulfonyl)amide (Li[TFSA], Solvey) in a molar ratio of 1:1. Afterwards, HFE was added into the above mixture to obtain a homogeneous liquid (denoted as [Li(G4)$_1$][TFSA]/HFE) with a Li[TFSA] concentration of 1 mol/L at 30°C. Li[TFSA] and G4 in different molar ratios ([Li(G4)$_{0.8}$][TFSA]/HFE and [Li(G4)$_{0.6}$][TFSA]/HFE) were also prepared under the same conditions, with the Li[TFSA] concentration fixed to 1 mol/L. For comparison, a traditional electrolyte with 1 mol/L Li[TFSA] in a mixture of 1,3-dioxolane (DOL) and 1,2-dimethoxyethane (DME) (1:1, v/v) was also prepared (hereafter denoted as LiTFSA-DOL/DME).

*Characterization:* The density and viscosity of the electrolyte were determined by a SVM3000 viscometer (Anton Paar). The ionic conductivity of the electrolyte was evaluated by complex impedance spectroscopy in a frequency range of 500 kHz to 10 Hz using an AC impedance analyzer (VMP2, Princeton Applied Research) with amplitude of 10 mV. A conductivity cell with two platinized Pt electrodes (CG-511B, TOA Electronics) was utilized for these measurements, and the cell constant was estimated using a standard 0.01 mol/L aqueous solution of KCl at 25°C. The sample cell was thermally equilibrated in a temperature-controlled chamber for at least 60 min at 30°C.

*Electrochemical measurements:* The Li/graphite half cells and $Li_2S$/graphite full cells were assembled into 2032-type coin cells using porous glass separators (GA55, Advantec). Before measuring the electrochemical properties, the cells were equilibrated for 12 h. The galvanostatic charge and discharge tests of the cells were performed at 30°C by a Nagano BTS-2004 battery testing system. In the case of the Li/graphite half cell, the cells were charged and discharged in the voltage range of 0–2.0 V (vs. $Li/Li^+$), and 372 mA/g was defined as 1 C rate. In the cases of $Li_2S$/graphite full cell, the cells were initially charged from the open circuit voltage (OCV) to 4.2 V to activate the $Li_2S$, and then operated in the voltage range of 0.5–3.5 V. The 1 C rate was set to 1166 mA/g, and the specific capacity of the cell was calculated in terms of the mass of $Li_2S$. Cyclic voltammetry (CV) was carried out on a Bio-Logic SAS VMP3 electrochemical workstation at a scan rate of 0.04 mV/s.

## 4.3. Results and Discussion

To eliminate the negative effect of the lithium anode and take advantage of the thick $Li_2S$ cathode, a full [graphite|electrolyte|$Li_2S$] cell was fabricated using a LS-G BM cathode (CFP, $Li_2S$ loading: 2.2 mg/cm$^2$), a $[Li(G4)_1][TFSA]$/HFE electrolyte, and a graphite anode, as depicted in **Fig. 4.1a**. The CV profiles in the first three cycles clearly demonstrate that the full cell can deliver a stable and reversible charge-discharge performance (**Fig. 4.1b**). The oxidation peak around 1.9 V in the initial anodic scan corresponds to the lithium extraction process from $Li_2S$ and is apparently lower than the activation voltage for the $Li_2S$/Li half cell; this happens because $Li^+$ ions are intercalated into the graphite electrode and form lithium-graphite intercalation compounds (Li-GICs).[20] Two obvious activation peaks are also observed at around 2.8 and 3.5 V in the initial anodic scan, probably due to the different electrochemical environments of the insulating $Li_2S$. It can be expected that small $Li_2S$ particles are easily activated, whereas accessing the electrolytes is more difficult for large particles or for those trapped between the graphene layers. In the subsequent anodic scans, only one broad peak was observed around 2.4 V, which can be assigned to the typical oxidation process of $Li_2S$. In contrast, two peaks at 1.9 and 2.1 V, due to the

stepwise reduction of elemental sulfur, can be observed during all cathodic scans. **Fig. 4.1c** depicts the charge-discharge curves of the $Li_2S$/graphite full cell with the $[Li(G4)_1][TFSA]$/HFE electrolyte in the first, fifth, and 20th cycle. The two well-defined discharge plateaus and the charge plateaus observed for this full cell are in good agreement with the redox peaks observed in the CV curves (**Fig. 4.1b**). The full cell delivered an initial discharge capacity of 628 mAh/g at 1/12 C and maintained a capacity of 463 mAh/g with a Coulombic efficiency of 97% after 20 cycles. Without question, the successful charge-discharge of LS-G BM is originated from the stable and reversible $Li^+$ intercalation/deintercalation of graphite electrodes in $[Li(G4)_1][TFSA]$/HFE.[20] Unlike the solvate IL-based electrolyte, the most commonly used LiTFSA-DOL/DME electrolyte could not be recharged at all under the same conditions (**Fig. 4.1d**). Even though a high capacity of 990 mA h $g^{-1}$ was obtained in the first charge, the subsequent charging and discharging processes delivered quite low discharge capacities. The deterioration is mainly ascribed to the cointercalation of ether solvent into graphite and thus the exfoliation of graphite.[18, 20] It should be noted that the solvate IL, being a polysulfide-insoluble electrolyte, can greatly reduce the shuttle effect, in addition to being compatible with both the graphite anode and $Li_2S$ cathode.

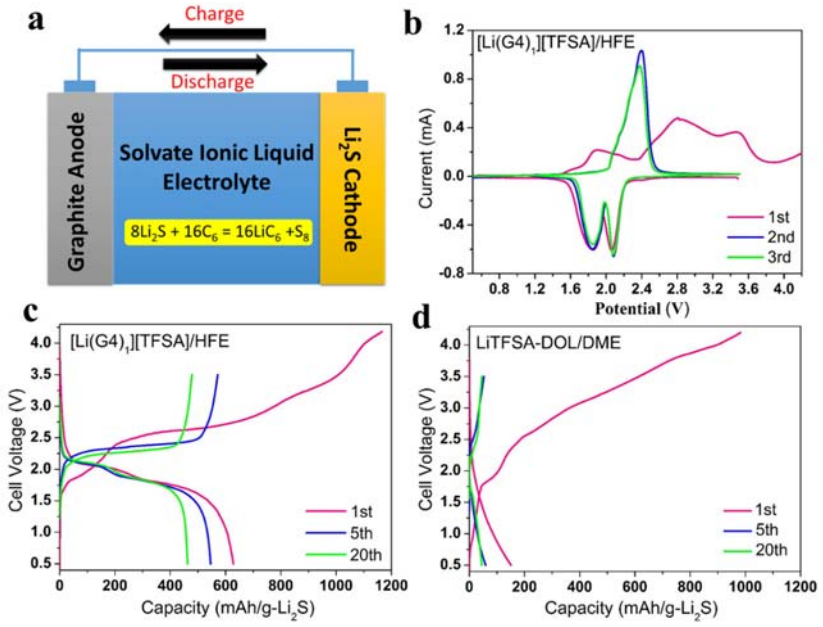

**Fig. 4.1**. (a) Schematic illustration of $Li_2S$/graphite full cell configuration using a single solvate ionic liquid (IL) electrolyte. (b) Typical cyclic voltammetry curves of $Li_2S$/graphite full cell using ball-milled $Li_2S$/graphene (LS-G BM) cathode, graphite anode, and $[Li(G4)_1][TFSA]$/HFE (G4: tetraglyme, TFSA: bis(trifluoromethanesulfonyl)amide, HFE: 1,1,2,2-tetrafluoroethyl 2,2,3,3-tetrafluoropropyl ether) electrolyte, in the first three cycles at a scan rate of 0.04 mV/s. The potential was scanned first from the open circuit voltage (OCV) to 4.2 V and then between 3.5 and 0.5 V. (c, d) Galvanostatic charge-discharge curves of $Li_2S$/graphite full cells with (c) $[Li(G4)_1][TFSA]$/HFE and (d) LiTFSA-DOL/DME (DOL = 1,3-dioxolane and DME = 1,2-dimethoxyethane) electrolytes. The full cells were initially charged from the OCV to 4.2 V at 1/48 C, and then cycled in the voltage range of 0.5–3.5 V at 1/12 C. All full cells are based on LS-G BM cathodes, using carbon fiber paper (CFP) as current collector. The $Li_2S$ loading on CFP is ~ 2.2 mg/cm$^2$, and the graphite loading on the anode is ~ 4.5 mg/cm$^2$.

**Table 4.1**. Viscosities ($\eta$), densities ($d$), ionic conductivities ($\sigma$) and Li[TFSA] concentrations ($c$) of $[Li(G4)_x][TFSA]$/HFE electrolytes at 30 °C.

| | $\eta$ (mPa·s) | $d$ (g/cm$^3$) | $\sigma$ (mS/cm) | $c_{Li[TFSA]}$ (mol/L) |
|---|---|---|---|---|
| $[Li(G4)_1][TFSA]$/HFE | 5.03 | 1.49 | 5.65 | 1 |
| $[Li(G4)_{0.8}][TFSA]$/HFE | 4.73 | 1.51 | 3.82 | 1 |
| $[Li(G4)_{0.6}][TFSA]$/HFE | 4.45 | 1.53 | 2.03 | 1 |

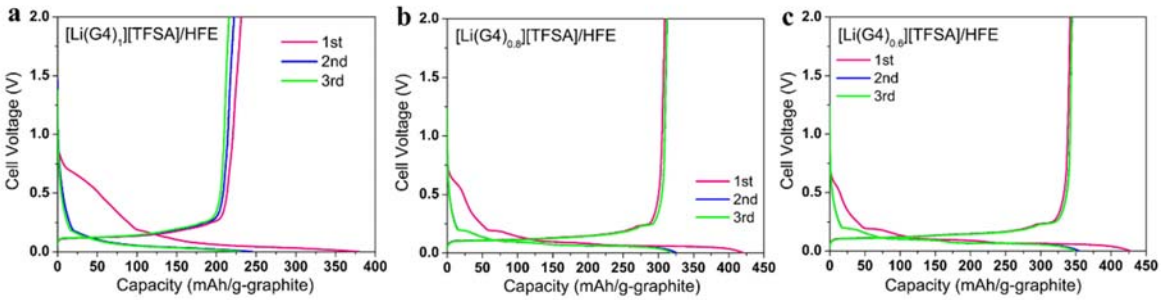


**Fig. 4.2.** Galvanostatic charge-discharge curves of Li/graphite half cells with (a) $[Li(G4)_1][TFSA]$/HFE, (b) $[Li(G4)_{0.8}][TFSA]$/HFE and (c) $[Li(G4)_{0.6}][TFSA]$/HFE electrolytes in the first three cycles at a current rate of 1/20 C (1 C = 372 mA/g). The graphite loading on graphite electrode is ~4.5 mg/cm$^2$, and the Li/graphite half-cells were cycled in the voltage range of 0–2.0 V.

In our previous work, we investigated the electrochemical intercalation of $Li^+$ into graphite electrodes, in electrolytes based on triglyme (G3), $[Li(G3)_x][TFSA]$ ($x \geq 1$).[25] The activity (concentration) of free G3 has a significant impact on the

$Li^+$ ion intercalation into a graphite electrode. Cointercalation of G3 and $Li^+$ takes place in $[Li(G3)_x][TFSA]$ electrolytes containing excess G3 ($x > 1$). In contrast, in $[Li(G3)_1][TFSA]$, in which $Li^+$ is preferentially solvated by G3 and forms $[Li(G3)]^+$ complex cations in the electrolyte, cointercalation is significantly limited, and desolvation of the solvate $[Li(G3)_1]^+$ cation occurs at the graphite/electrolyte interface to form Li-GIC.[25] Based on these considerations, we prepared a series of concentrated electrolytes in which Li[TFSA] and G4 were mixed in molar ratios of 1:1, 1:0.8, and 1:0.6, respectively. HFE was further added to lower the viscosity and increase the conductivity of the electrolytes. The concentration of Li[TFSA] ($c_{Li[TFSA]}$) in the resulting solutions was fixed at 1 mol/L at 30°C ($[Li(G4)_x][TFSA]$/HFE, $x = 0.6$, 0.8, 1). It should be noted that the diluted cosolvent, HFE, scarcely participates in the solvation and affects the intercalation/deintercalation process, because of its low donor ability and relatively low permittivity.[25] The basic physicochemical properties such as viscosity, density, and ionic conductivity of these electrolytes are summarized in **Table 4.1**. The electrochemical properties of graphite in these electrolytes were first investigated by constructing half cells [graphite | electrolyte | Li] using lithium metal as the counter electrode. In these systems, the $Li^+$ intercalation into the graphite electrodes is regarded as "charging process" and **Fig. 4.2** shows the charge-discharge curves. Clearly, both the charge and discharge capacities of the graphite electrodes increase with decreasing G4/Li[TFSA] molar ratio. For example, $[Li(G4)_{0.6}][TFSA]$/HFE and $[Li(G4)_{0.8}][TFSA]$/HFE can deliver charge capacities of 349 and 319 mAh/g at 1/20 C in the third cycle, respectively, which are apparently higher than the capacity of $[Li(G4)_1][TFSA]$/HFE (231 mAh/g). The enhanced capacities in solvate ILs containing excess Li[TFSA] could be due to the significantly reduced activity (concentration) of free G4 in these electrolytes. We reported that cointercalation of glyme and $Li^+$ ion into the graphite takes place during charging process in the electrolyte containing excess glyme ($x > 1$ in $[Li(glyme)_x][TFSA]$).[20,25] The conitercalation is irreversible and decreases the capacity of the electrode.[20] The cointercalation can be suppressed by decreasing

the activity (concentration) of free glyme in the electrolyte.[25] Instead, the desolvation of $Li^+$ occurs at the interface between graphite and electrolyte and $Li^+$ ion is reversibly intercalated into the graphite.[25] The absence of free G4 in solutions of $x \leq 1$ ($x$ in $[Li(G4)_x][TFSA]$/HFE) could benefit the desolvation of $Li^+$ ions at the graphite/electrolyte interface, suppressing the irreversible capacity of the graphite electrode. With decreasing the G4 in the electrolyte, the irreversible capacity is suppressed and the reversible capacity approaches the theoretical capacity of the graphite (372 mAh/g) (**Fig. 4.2**). In the cell with $[Li(G4)_x][TFSA]$/HFE ($x \leq 1$), the desolvation of $Li^+$ takes place at the graphite anode and the solvation of $Li^+$ occurs at the counter electrode during charging (**Fig. 4.3**). Simultaneously, the ligand exchange of $[Li(G4)]^+$ happens in the bulk of electrolyte solution.[29]

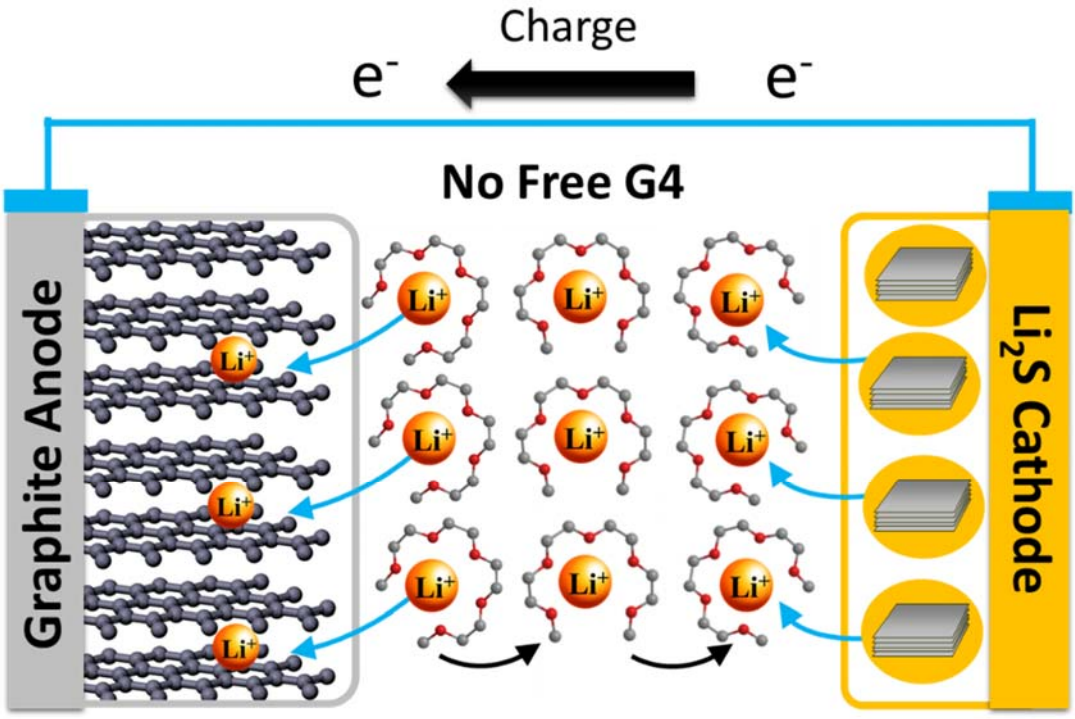


**Fig. 4.3**. Schematic illustration of charging process in $Li_2S$/graphite full cell using solvate ionic liquid (IL) electrolytes ([Li(G4)x][TFSA]/HFE, x = 0.6, 0.8, 1).

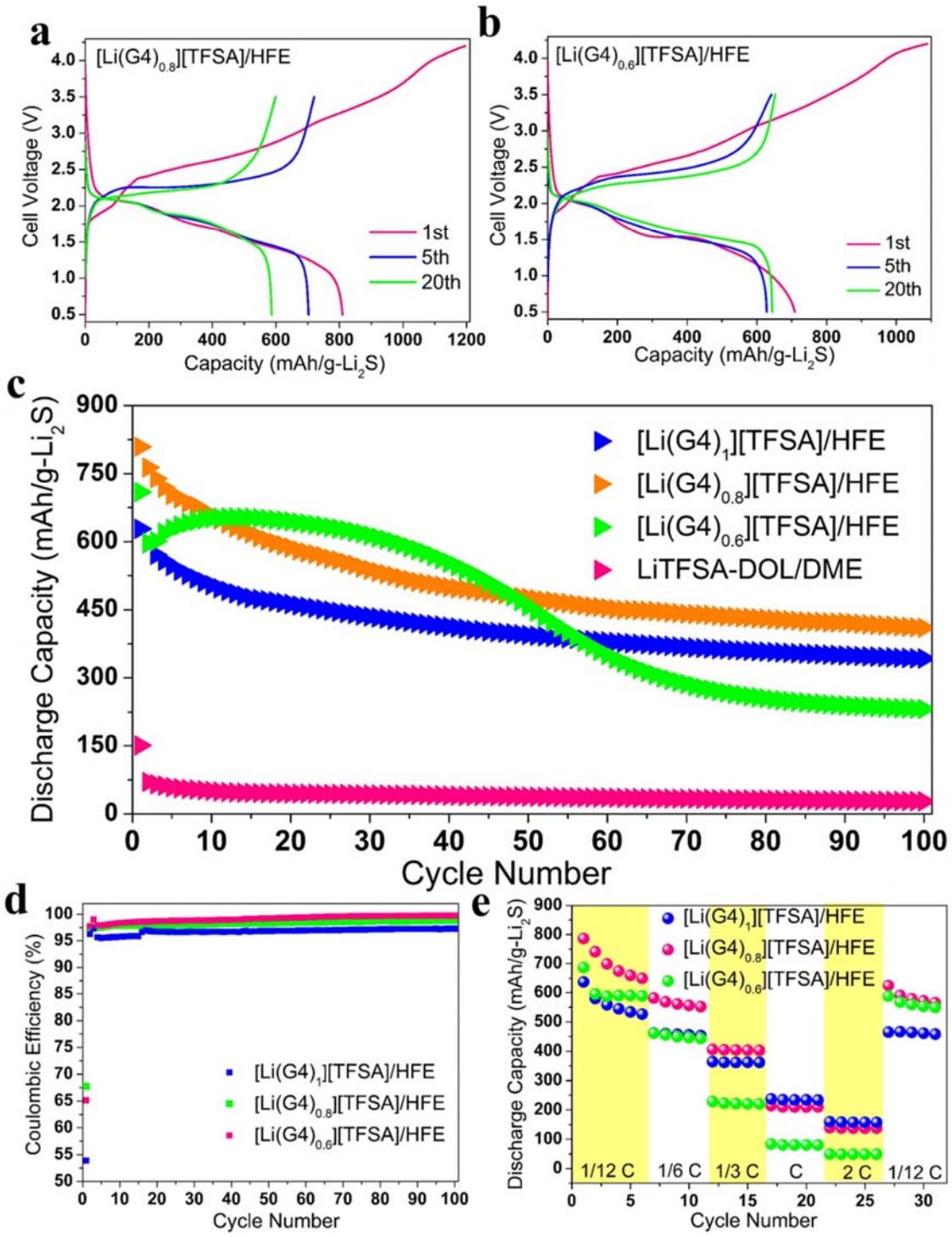


**Fig. 4.4**. Galvanostatic charge-discharge curves of $Li_2S$/graphite full cells with (a) $[Li(G4)_{0.8}][TFSA]$/HFE and (b) $[Li(G4)_{0.6}][TFSA]$/HFE electrolyte in the first, fifth, and 20th cycles. (c) Cycling performance and (d) Coulombic efficiency of $Li_2S$/graphite full cells with different electrolytes over 100 cycles. The full cells were initially charged at 1/48 C, and then

cycled at 1/12 C. (e) Rate capability of $Li_2S$/graphite full cells at various rates from 1/12 C to 2 C. All the full cells are based on ball-milled $Li_2S$/graphene (LS-G BM) cathodes using carbon fiber paper (CFP) as current collector. The $Li_2S$ loading on CFP is ~ 2.2 mg/cm$^2$, and the graphite loading on the anode is ~ 4.5 mg/cm$^2$.

$Li_2S$/graphite full cells ([graphite|electrolyte|$Li_2S$]) employing the $[Li(G4)_{0.8}][TFSA]$/HFE and $[Li(G4)_{0.6}][TFSA]$/HFE electrolytes were also assembled (**Fig. 4.3**), and their charge-discharge profiles are displayed in **Fig. 4.4a** and **4.4b**. Initial discharge capacities of 809 and 709 mAh/g, and 20th-cycle discharge capacities of 586 and 644 mAh/g were delivered using $[Li(G4)_{0.8}][TFSA]$/HFE and $[Li(G4)_{0.6}][TFSA]$/HFE electrolytes, respectively, which are higher than in the case of the $[Li(G4)_1][TFSA]$/HFE electrolyte. This trend could be attributed to the improved kinetics of $Li^+$ intercalation/deintercalation at the anode side enabled by the low G4/Li[TFSA] ratio. However, when we compare the charge-discharge curves in the 20th cycle (**Fig. 4.5**), the $[Li(G4)_{0.6}][TFSA]$/HFE electrolyte exhibits a slightly larger voltage hysteresis. This effect is probably caused by the low ionic conductivity (2.03 mS/cm) of the electrolyte, which could lead to a somewhat sluggish redox reaction of $Li_2S$ at cathode side and then to a large polarization. $[Li(G4)_1][TFSA]$/HFE and $[Li(G4)_{0.8}][TFSA]$/HFE electrolytes could maintain discharge capacities of 343 and 410 mAh/g at 1/12 C after 100 cycles (**Fig. 4.4c**), respectively. In contrast, in the case of the $[Li(G4)_{0.6}][TFSA]$/HFE electrolyte, only a small discharge capacity of 231 mAh/g, with a very severe polarization, was obtained in the 100th cycle (**Fig. 4.5**), and an increased rate of capacity fade after 30 cycles was also observed, both of which are likely associated with the low ionic conductivity and slow lithium ion diffusion of $[Li(G4)_{0.6}][TFSA]$/HFE. As shown in **Fig. 4.5**, the polarization for charge and discharge of the cell with $[Li(G4)_{0.6}][TFSA]$/HFE was increased after 20 cycles. This increase of the polarization might originate from the change of porous structure $Li_2S$ cathode. As mentioned before, volumetric expansion (ca. 80%) from $S_8$ to $Li_2S$ proceeds in the porous cathode during discharging of the cell. The repetition of volume expansion and shrinkage of the active material would change the porous

structure, and this might increase the resistance for the ionic conduction in the porous cathode. With decreasing the ionic conductivity of the electrolyte, the polarization due to the increase of resistance of porous cathode becomes severer. This might cause the increased rate of capacity fade of the cell with $[Li(G4)_{0.6}][TFSA]$/HFE after 30 cycles. In any case, all the $Li_2S$/graphite full cells demonstrated high Coulombic efficiencies over 100 cycles (**Fig. 4.4d**) thanks to the reduced dissolution of polysulfides in solvate ILs. In particular, the $[Li(G4)_{0.6}][TFSA]$/HFE electrolyte manifested a Coulombic efficiency of up to 100%, which is higher than that of $[Li(G4)_{0.8}][TFSA]$/HFE (99%) and $[Li(G4)_1][TFSA]$/HFE (97%). The rate capabilities of $Li_2S$/graphite full cells with different electrolytes at variable current rate were also investigated. The corresponding results reflect the fact that the electrochemical performance of the full cell is determined by both the ionic conductivity of the electrolyte and the $Li^+$ intercalation/deintercalation properties at the graphite anode. As shown in **Fig. 4.4e**, the stepwise discharge capacities of $[Li(G4)_{0.8}][TFSA]$/HFE at low current rates of 1/12 C, 1/6 C, and 1/3 C are 786–650, 581–552, and 406–403 mAh/g, respectively, which are significantly higher than those of both $[Li(G4)_1][TFSA]$/HFE and $[Li(G4)_{0.6}][TFSA]$/HFE. The best rate capability of $[Li(G4)_{0.8}][TFSA]$/HFE at low current rates could be due to its balanced $Li^+$ intercalation properties (**Fig. 4.2**) and ionic conductivity. However, upon further increasing the current rate to 1 C and 2 C, $Li(G4)_{0.8}][TFSA]$/HFE exhibits slightly lower discharge capacities than $[Li(G4)_1][TFSA]$/HFE. This effect could be ascribed to its relatively low ionic conductivity, which cannot ensure the fast lithium ion migration and thus limits the redox reaction of $Li_2S$ at higher current rates. Despite its superior $Li^+$ intercalation properties, $[Li(G4)_{0.6}][TFSA]$/HFE showed the lowest capacities at nearly all high current rates, which is undoubtedly due to its very low ionic conductivity. Further studies are currently underway to investigate the capacity decay issue and improve the full cell performance.

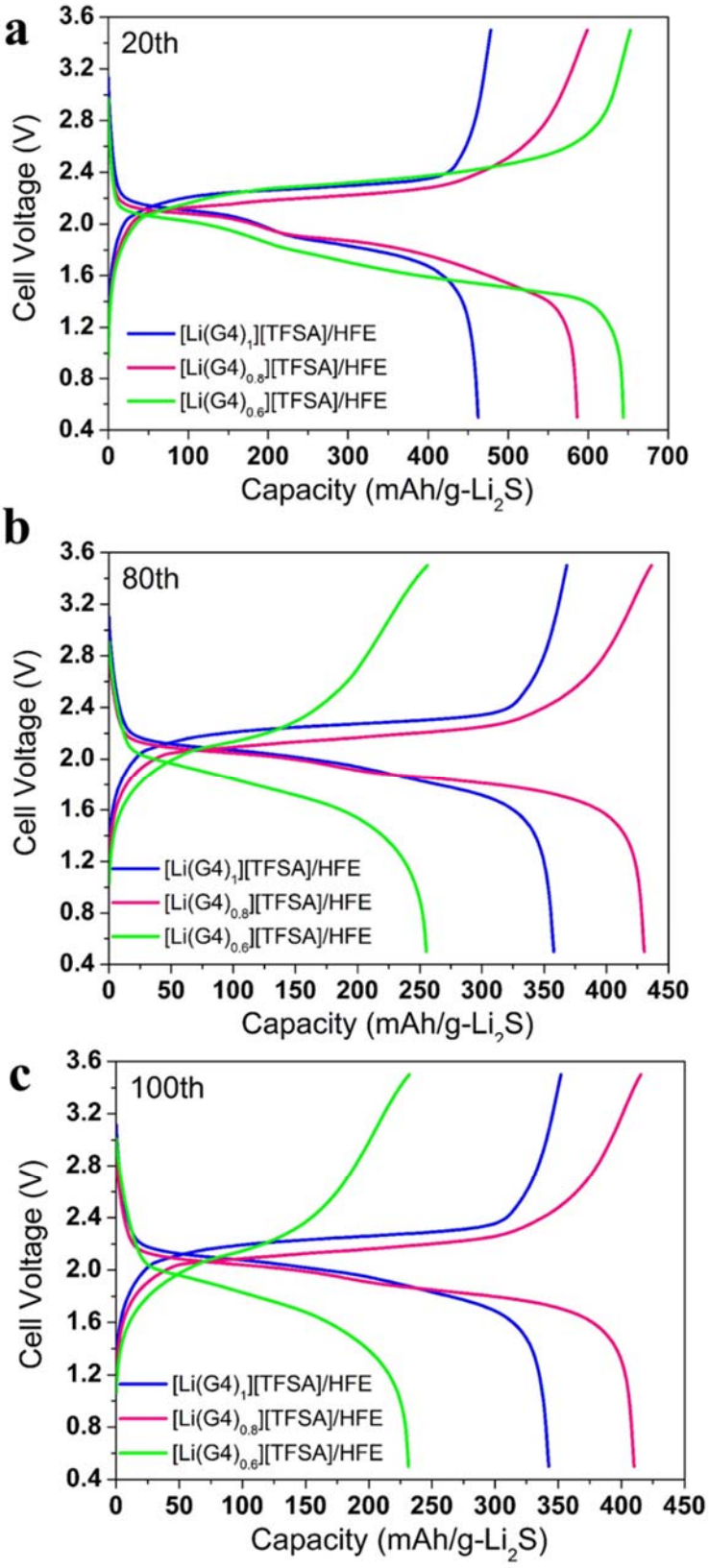


**Fig. 4.5.** Galvanostatic charge-discharge curves of $Li_2S$/graphite full cells with different

electrolytes in the (a) 20th, (b) 80th and (b) 100th cycles. The $Li_2S$ loading on the LS-G BM cathode is ~2.2 mg/cm$^2$, and the graphite loading on anode is ~4.5 mg/cm$^2$. The full cells were initially charged at 1/48 C, and then cycled at 1/12 C (1 C = 1166 mA/g).

## 4.4. Conclusions

Based on the favorable charge-discharge behavior of both Li/$Li_2S$ and Li/graphite half cells, Li-S full cells [graphite|electrolyte|$Li_2S$] were constructed by combining a thick LS-G BM cathode ($Li_2S$ loading: 2.2 mg/cm$^2$), a solvate ionic-liquid-based electrolyte, and a graphite anode, without any complicated cell architecture.[23] In this system, solvate IL, acting as a single-phase electrolyte, can enable the effective $Li^+$ intercalation and deintercalation of graphite electrodes and simultaneously inhibit the severe shuttle effect of lithium polysulfides. For example, the high-loading $Li_2S$/graphene composite cathode in [$Li(G4)_1$][TFSA]/HFE electrolyte can deliver an initial discharge capacity of 628 mAh/g at 1/12 C rate and maintain a capacity of 463 mAh/g with a Coulombic efficiency of 97% after 20 cycles. The composition of solvate ILs ([$Li(G4)_x$][TFSA]/HFE, $x$ = 0.6, 0.8, 1) was further optimized by varying the molar ratio between G4 and LiTFSA. The ionic conductivity and the $Li^+$ intercalation/deintercalation properties of the electrolytes were found to greatly affect the battery performance. Among all concentrated electrolytes examined, [$Li(G4)_{0.8}$][TFSA]/HFE, possessing both a balanced conductivity and intercalation/deintercalation capability, exhibited the highest first- and 20th-cycle discharge capacities of 809 and 586 mAh/g, respectively, in conjunction with a high Coulombic efficiency of up to 99%. At variance with the reported carbonate electrolyte, which is specific to microporous carbon cathodes,[22] the solvate ILs presented here are compatible with nearly all Li-S cathodes. We believe that the present research could trigger new attempts to fabricate lithium-ion sulfur cells.

## 4.5. References


[1] P. G. Bruce, S. A. Freunberger, L. J. Hardwick, J. M. Tarascon, *Nat. Mater.* **2012**, *11*, 19.

[2] X. Ji, K. T. Lee, L. F. Nazar, *Nat. Mater.* **2009**, *8*, 500.

[3] A. Manthiram, Y. Fu, Y. S. Su, *Acc. Chem. Res.* **2013**, *46*, 1125.

[4] M. K. Song, E. J. Cairns, Y. Zhang, *Nanoscale* **2013**, *5*, 2186.

[5] S. S. Zhang, *J. Power Sources* **2013**, *231*, 153.

[6] S. Urbonaite, T. Poux, P. Novák, *Adv. Energy Mater.* **2015**, *5*, 1500118.

[7] C. Nan, Z. Lin, H. Liao, M. K. Song, Y. Li, E. J. Cairns, *J. Am. Chem. Soc.* **2014**, *136*, 4659.

[8] Z. W. Seh, H. Wang, P. C. Hsu, Q. Zhang, W. Li, G. Zheng, H. Yao, Y. Cui, *Energy Environ. Sci.* **2014**, *7*, 672.

[9] F. Wu, J. T. Lee, F. Fan, N. Nitta, H. Kim, T. Zhu, G. Yushin, *Adv. Mater.* **2015**, *27*, 5579.

[10] A. Manthiram, Y. Fu, S. H. Chung, C. Zu, Y. S. Su, *Chem. Rev.* **2014**, *114*, 11751.

[11] Y. Son, J. S. Lee, Y. Son, J. H. Jang, J. Cho, *Adv. Energy Mater.* **2015**, *5*, 1500110.

[12] Y. Yang, M. T. McDowell, A. Jackson, J. J. Cha, S. S. Hong, Y. Cui, *Nano Lett.* **2010**, *10*, 1486.

[13] K. Zhang, L. Wang, Z. Hu, F. Cheng, J. Chen, *Sci. Rep.* **2014**, *4*, 6467.

[14] J. Hassoun, B. Scrosati, *Angew. Chem. Int. Ed.* **2010**, *49*, 2371.

[15] C. M. Park, J. H. Kim, H. Kim, H. J. Sohn, *Chem. Soc. Rev.* **2010**, *39*, 3115.

[16] H. Wu, G. Zheng, N. Liu, T. J. Carney, Y. Yang, Y. Cui, *Nano Lett.* **2012**, *12*, 904.

[17] Y. Ma, B. Ding, G. Ji, J. Y. Lee, *ACS nano* **2013**, *7*, 10870.

[18] D. Lv, P. Yan, Y. Shao, Q. Li, S. Ferrara, H. Pan, G. L. Graff, B. Polzin, C. Wang, J. G. Zhang, J. Liu, J. Xiao, *Chem. Commun.* **2015**, *51*, 13454.

[19] D. Aurbach, Y. Talyosef, B. Markovsky, E. Markevich, E. Zinigrad, L. Asraf, J. S. Gnanaraj, H. J. Kim, *Electrochim. Acta* **2004**, *50*, 247.

[20] H. Moon, R. Tatara, T. Mandai, K. Ueno, K. Yoshida, N. Tachikawa, T. Yasuda, K. Dokko, M. Watanabe, *J. Phys. Chem. C* **2014**, *118*, 20246.

[21] J. Gao, M. A. Lowe, Y. Kiya, H. D. Abruña, *J. Phys. Chem. C* **2011**, *115*, 25132.

[22] S. Zheng, Y. Chen, Y. Xu, F. Yi, Y. Zhu, Y. Liu, J. Yang, C. Wang, *ACS nano* **2013**, *7*, 10995.

[23] L. Wang, Y. Wang, Y. Xia, *Energy Environ. Sci.* **2015**, *8*, 1551.

[24] K. Dokko, N. Tachikawa, K. Yamauchi, M. Tsuchiya, A. Yamazaki, E. Takashima, J. W. Park, K. Ueno, S. Seki, N. Serizawa, M. Watanabe, *J. Electrochem. Soc.* **2013**, *160*, A1304.

[25] H. Moon, T. Mandai, R. Tatara, K. Ueno, A. Yamazaki, K. Yoshida, S. Seki, K. Dokko, M. Watanabe, *J. Phys. Chem. C* **2015**, *119*, 3957.

[26] J. W. Park, K. Ueno, N. Tachikawa, K. Dokko, M. Watanabe, *J. Phys. Chem. C* **2013**, *117*, 20531.

[27] J. W. Park, K. Yamauchi, E. Takashima, N. Tachikawa, K. Ueno, K. Dokko, M. Watanabe, *J. Phys. Chem. C* **2013**, *117*, 4431.

[28] N. Tachikawa, K. Yamauchi, E. Takashima, J. W. Park, K. Dokko, M. Watanabe, *Chem. Commun.* **2011**, *47*, 8157.

[29] K. Yoshida, M. Nakamura, Y. Kazue, N. Tachikawa, S. Tsuzuki, S. Seki, K. Dokko, M. Watanabe, *J. Am. Chem. Soc.* **2011**, *133*, 13121.

[30] K. Ueno, J. W. Park, A. Yamazaki, T. Mandai, N. Tachikawa, K. Dokko, M. Watanabe, *J. Phys. Chem. C* **2013**, *117*, 20509.

[31] S. Zhang, K. Ueno, K. Dokko, M. Watanabe, *Adv. Energy Mater.* **2015**, *5*, 1500117.

# Chapter Five

Development of an Advanced $Li_2S$/Amorphous Silicon Battery

## Abstract

A lithium-sulfur cell consisting of Si nanoflake negative electrode, $Li_2S$/graphene composite positive electrode, and a non-flammable solvate ionic liquid electrolyte, was developed. This cell configuration allows us to escape from the use of Li metal electrode and to avoid the dendritic deposition of Li metal at the negative electrode during charging, leading to the highly safe and stable operation of the cell. The solvate ionic liquid electrolyte solution was composed of tetraglyme, lithium bis(trif uoromethanesulfonyl)amide, and a hydrofluoroether, and the solubility of lithium polysulfides, which are reaction intermediates of the positive electrode, is very low in the electrolyte solution, resulting in the high Coulombic efficiency of discharge/charge and long cycle life of the Si/$Li_2S$ cell.

Part of the work presented in this chapter has been published as:

Zhe Li, Yutaro Kamei, Masakazu Haruta, Toshio Takenaka, Akira Tomita, Takayuki Doi, Shiguo Zhang, Kaoru Dokko, Minoru Inaba, and Masayoshi Watanabe, Si/$Li_2S$ Battery with Solvate Ionic Liquid Electrolyte, Electrochemistry, in press.

## 5.1. Introduction

Li-S batteries have attracted much attention owing to their high energy density.[1-4] Assuming the complete conversion of S to $Li_2S$ ($S_8 + 16Li^+ + 16e^- \rightarrow 8Li_2S$), the sulfur can offer a theoretical specific capacity of 1672 mAh/g and the theoretical specific energy density of 2600 Wh/kg on the basis of the reaction, $16Li + S_8 \rightarrow 8Li_2S$. However, the S cathode has been suffered from several issues. The insulating nature of electroactive species from $S_8$ to $Li_2S$ causes the low discharge and charge capacities compared with the theoretical capacity. The nanostructured carbon-sulfur composite electrodes have been developed to make intimate contact between sulfur and conductive carbon.[2, 5] The intimate contact is effective in collecting current from sulfur, leading to the high utilization of sulfur and high capacity of the electrode. Another issue is the dissolution of lithium polysulfides, which are reaction intermediates of sulfur cathode. This results in the low discharge-charge cycle stability and the low coulombic efficiency of discharge/charge.[5, 6] We reported that ionic liquid and solvate ionic liquid electrolytes suppress the dissolution of lithium polysulfides.[7-11] Tetraglyme (G4, $CH_3{-}O{-}(CH_2{-}CH_2{-}O)_4{-}CH_3$) and Li[TFSA] (TFSA: bis(trif uoromethanesulfonyl)amide) form a complex in 1:1 molar ratio. This complex of [Li(G4)][TFSA] keeps liquid state at room temperature and is a representative solvate ionic liquid consisting of a $[Li(G4)]^+$ complex cation and a $[TFSA]^-$ anion.[12] The electrolyte solution of [Li(G4)][TFSA] mixed with a hydrofluoroether (HFE), having low viscosity and donor ability, enables the stable and long term operation of Li-S cells.[6, 7] Furthermore, the solvate ionic liquid electrolyte [Li(G4)][TFSA]/HFE is non-flammable and favorable for the achieving the thermal stability of the cells.

The safety issue of Li-S cell should be also addressed. The dendritic growth of lithium metal anode proceeds in the cell during the charging especially at high current densities. This brings about the internal short circuit of the cell that causes serious problems for the safe use of Li-S batteries and hinders their large-scale practical applications.[13-15] A strategy to tackle this challenging issue is to

adopt $Li_2S$ (a theoretical specific capacity of 1166 mAh/g) as an alternative cathode material and Li-free anode materials. We recently developed a $Li_2S$/graphene nanocomposite electrode, which exhibits a high discharge capacity of ca. 700 mAh/g and good cycle stability.[16, 17] The use of $Li_2S$ cathode enables us to select Li-free anodes such as graphite, tin, and silicon, circumventing the formation of lithium dendrites and thus increasing the cell safety.[5, 18-23] Among the various anode materials, Si as a Li-alloying metal is one of the most promising candidates owing to the wide abundance and extremely high capacity of 3580 mAh/g.[24, 25] However, the large volume change of Si during the lithiation and delithiation process could cause the mechanical degradation (cracking or pulverization) and then the poor electrochemical properties.[24, 26] Recently, amorphous Si nanoflake powder (Si LeafPowder®, denoted as Si-LP) with thickness of 50-200 nm was developed.[27, 28] The short Li diffusion length facilitates the uniform distribution of Li in thin Si-LP during the alloying and de-alloying. This is favorable for the relaxation of the stress of volume change of Si, leading to the suppression of mechanical degradation of Si-LP and a good charge-discharge cycle stability. Herein we report the battery performance of Si-LP/$Li_2S$ cell with a non-flammable solvate ionic liquid electrolyte.

## 5.2. Experimental

$Li_2S$/graphene composite was fabricated according to the method reported elsewhere.[16, 17] In brief, $Li_2SO_4$/graphene nanoplatelet aggregates (GNAs) composite was first formed by a solvent/nonsolvent precipitation method, which permitted the uniform deposition of $Li_2SO_4$ onto the surface of the GNAs. The weight ratio of $Li_2SO_4 \cdot H_2O$ and GNAs was 10:3. The resultant $Li_2SO_4$/GNAs composite was then transferred to a tube furnace with an argon atmosphere, and heated at 200 °C for 1 h to remove water and at 781°C for 2 h to ensure the sufficient reaction between $Li_2SO_4$ and C ($Li_2SO_4 + 2C \rightarrow 2CO_2\uparrow + Li_2S$). Because the amount of GNAs was excess, the remaining graphene sheets could then serve as a highly conductive two-dimensional (2D) host to anchor the in-

situ generated $Li_2S$ by intimate contact, and $Li_2S$/graphene composite was obtained. Finally, in order to reduce its particle size, $Li_2S$/graphene composite (0.40 g) was milled with 120 zirconia balls (4 mm in diameter) through a Fritsch Pulverisette 7 planetary ball mill at 600 rpm in an argon-filled glovebox ($H_2O$ level < 1 ppm). The ball-milled $Li_2S$/graphene composite, carbon black (Super C65, TIMCAL), and polyvinylpyrrolidone (PVP, MW = 1200 kDa, JUNSEI) were dispersed into *N*-methyl-2-pyrrolidinone and stirred for 48 h. The mass ratio of $Li_2S$, carbon (including graphene and carbon black), and PVP was 60:30:10. This slurry was absorbed by a carbon fiber paper (CFP, Toray Paper 060), and then, dried in vacuum for 16 h at 80 °C. The $Li_2S$ loading of the CFP-supported $Li_2S$ electrode sheet was ca. 2.2 mg/cm$^2$.

The Si-LP (OIKE & Co., Ltd.) was synthesized by electron beam vapor deposition.[27, 28] The thickness of Si-LP was 100 nm. A homogenous slurry was formed by mixing the Si-LP (83.3 wt%), Ketjenblack (5.6 wt%), and carboxymethyl cellulose sodium salt (11.1 wt%) in water, which was then pasted onto a copper foil. After drying overnight at 80°C under vacuum, the composite electrode sheet with a Si loading of 0.9 mg/cm$^2$ was obtained.

[Li(G4)][TFSA] was prepared by a simple mixing of purified G4 (Nippon Nyukazai) and Li[TFSA] (Solvey) in 1:1 molar ratio. The obtained [Li(G4)][TFSA] was mixed with a HFE (1,1,2,2-tetrafluoroethyl 2,2,3,3-tetrafluoropropyl ether, $CF_2H{-}CF_2{-}O{-}CH_2{-}CF_2{-}CF_2H$, Daikin Industries) in a molar ratio of 1:4. Using this [Li(G4)][TFSA]/4HFE electrolyte, Li/Si half cell and Si/$Li_2S$ full cell (2032-type coin cell) were assembled. The CFP-supported $Li_2S$ electrode sheet and the Si composite electrode sheet were cut into disks (16 mm diameter) and subjected to battery tests. Li metal foil (Honjo Metal) was used as the counter electrode of Li/Si cell. A porous glass filter (GA55, Advantec) was used as a separator between negative and positive electrodes. Prior to the electrochemical measurements, the cells were kept for 12 h at room temperature to ensure the complete penetration of electrolyte through the porous composite electrodes. The galvanostatic charge and discharge tests were carried

out using a battery testing system (BTS-2004, Nagano) at 30 °C. Cyclic voltammetry measurement was conducted at a scan rate of 0.025 mV/s on a Bio-Logic SAS VMP3 electrochemical workstation. The morphologies of electrodes were observed by a field emission scanning electron microscope (JEOL JSM-7001F).

## 5.3. Results and Discussion

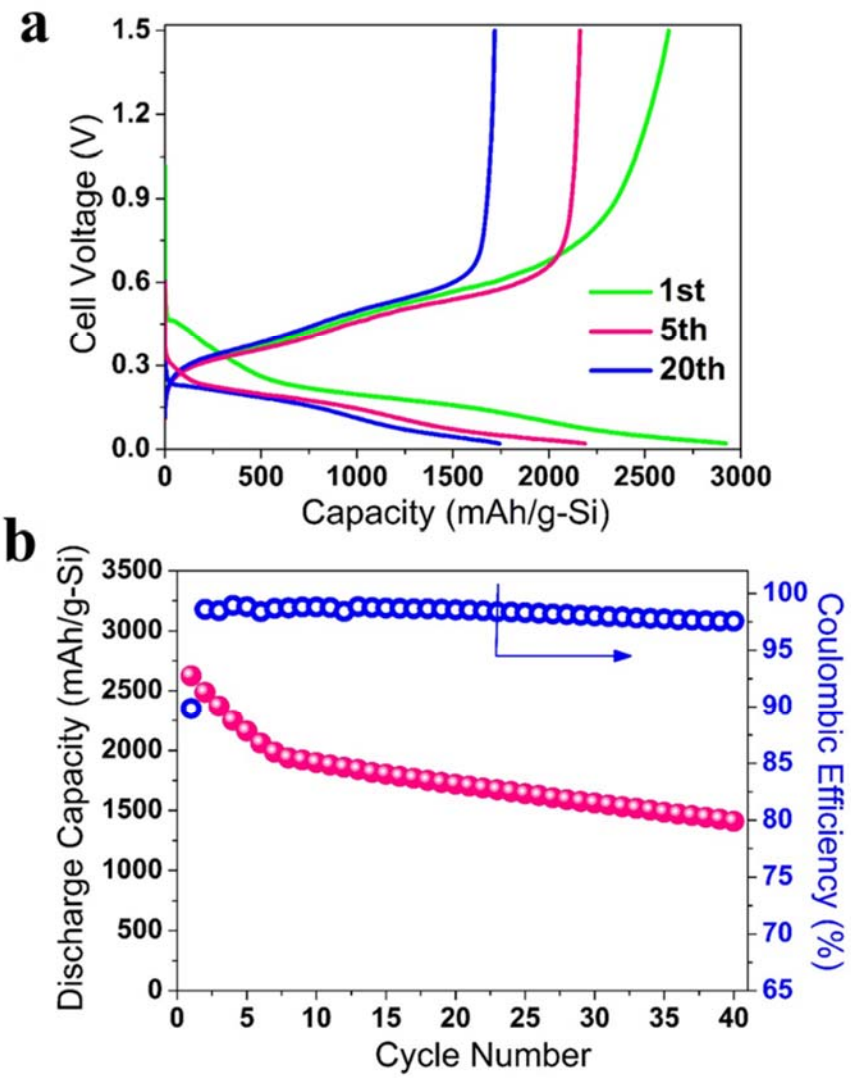


**Fig. 5.1.** (a) Galvanostatic charge-discharge curves of [Li metal|[Li(G4)][TFSA]/4HFE|Si] cell at a rate of 1/12 C (1 C = 3580 mA/g). The cell was cycled between 1.5 and 0.02 V (versus $Li/Li^+$). (b) Cycling performance and Coulombic efficiency of the cell over 40 cycles

at 1/12 C.

**Fig. 5.1** presents the galvanostatic charge-discharge curves, cycling performance, and Coulombic efficiency of Li/Si half cell at 1/12 C. In this system, the charging process corresponds to the Li-alloying reaction with Si. The cell was first charged to 0.02 V, and then discharged to 1.5 V. This amorphous Si electrode exhibits a typical charge-discharge behavior without any obvious plateaus in the solvate ionic liquid electrolyte (**Fig. 5.1a**).[27] The initial discharge capacity of the Si electrode was 2625 mAh/g. After 40 cycles, a discharge capacity of 1410 mAh/g with a Coulombic efficiency of 98% was preserved. The discharge capacity fade of the Si electrode was slightly faster than the previously reported one,[27] which was probably caused by the higher Si loading (0.9 mg/cm$^2$).

A Si/$Li_2S$ cell was prepared exploiting a solvate ionic liquid electrolyte. The $Li_2S$/graphene composite cathode was supported by three-dimensionally porous current collector (carbon fiber paper). [16, 17] To evaluate the validity of this cell configuration ([Si|[Li(G4)][TFSA]/4HFE|$Li_2S$]), cyclic voltammograms (CVs) in the first three cycles were measured (**Fig. 5.2**). The cell voltage was initially swept to 4.2 V to overcome the energy barrier of lithium extraction from insulating $Li_2S$.[29] Thus, the broad current peak located at 2.9 V in the first positive scan correspond to the electrochemical activation process of $Li_2S$. In the subsequent positive scans, the charging current peak around 2.4 V is identified as the reactions of $Li_2S$ to S. Moreover, in all the negative scan, there are two clear discharging current peaks at 1.7 and 1.3 V, which are attributed to the conversion of sulfur to high-order lithium polysulfide ($Li_2S_x$, $4< x < 8$) and then to $Li_2S_2$/$Li_2S$, respectively. The CVs with obvious charge and discharge current peaks reflect the reversible electrochemical reaction between the $Li_2S$ and amorphous silicon, $15Li_2S + 8Si = 2Li_{15}Si_4 + 15S$. Here, the lithiated phase that formed at negative electrode is assumed to be $Li_{15}Si_4$.[25]

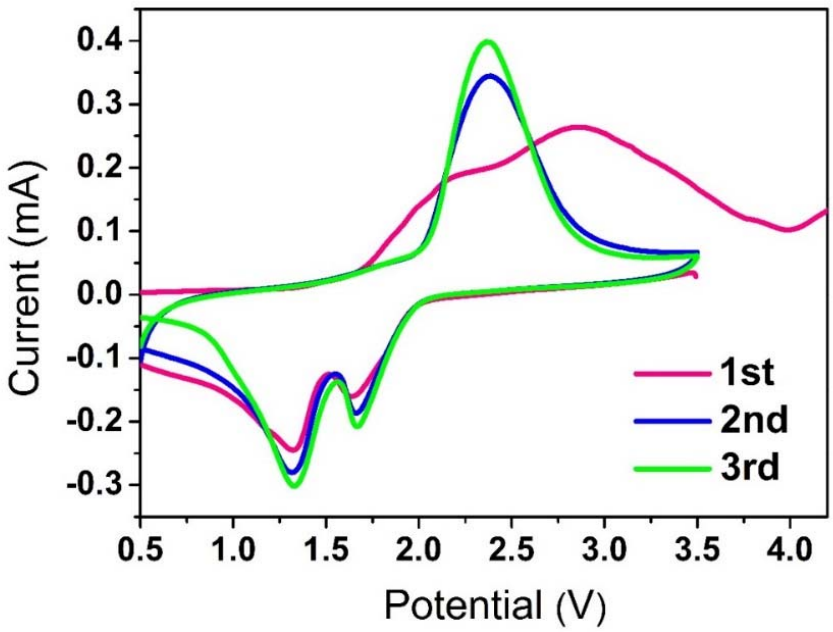


**Fig. 5.2** Typical cyclic voltammograms of the lithium-ion sulfur battery [Si|[Li(G4)][TFSA]/4HFE|$Li_2S$] in the first three cycles at a scan rate of 0.025 mV/s. The potential was swept from the open circuit voltage to 4.2 V initially, and then between 3.5 and 0.5 V.

The galvanostatic charge-discharge profiles of [Si|[Li(G4)][TFSA]/4HFE|$Li_2S$] cell are shown in **Fig. 5.3a**. The specific capacity was calculated based on the mass of $Li_2S$. The full cell delivered the initial charge capacity of 1188 mAh/g, which is close to the theoretical value of $Li_2S$ (1166 mAh/g), suggesting that the $Li_2S$ was sufficiently activated. However, the initial discharge capacity was only 702 mAh/g. This irreversible capacity was probably due to (i) the volumetric shrinkage of $Li_2S$ during the first charge, which loosens the electrical contact between the active material and conductive carbon and (ii) the consumption of lithium at Si anode side during the initial cycle (**Fig. 5.1a**). Additionally, in the $5^{th}$ and $20^{th}$ cycles, a very flat charge plateau at 2.1 V and two well-defined discharge plateaus at 1.8 and 1.4 V are observed. This is consistent with the CV profiles shown in **Fig. 5.2**. After 40 cycles, the full cell maintained a discharge capacity of 403 mAh/g with a Coulombic efficiency of 96% (**Fig. 5.3b**). The relatively high Coulombic efficiency of discharge/charge suggests that the

shuttle effect was effectively suppressed in the cell owing to the very low solubility of lithium polysulfides in the [Li(G4)][TFSA]/4HFE electrolyte.[7, 23] In our previous study, a graphite/$Li_2S$ full cell exploiting the [Li(G4)][TFSA]/4HFE electrolyte showed an average capacity fade of 0.86% per cycle,[17] which is lower than that of present Si/$Li_2S$ full cell (1.06% per cycle). The capacity fade of Si electrode was ascribed to the large volume change of Si (ca. 280%) and the irreversible side reaction of electrolyte at the Si electrode surface [30]. In contrast, the volume change of graphite electrode during Li intercalation is relatively small (ca. 10%), and the irreversible side reaction of electrolyte is rather suppressed. To improve the charge-discharge cycle stability of Si/$Li_2S$ full cell, the stabilization of passivation layer (solid electrolyte interphase) of Si electrode and the suppression of irreversible decomposition of electrolyte may be needed. Further researches are underway in our group and will be reported in due course.

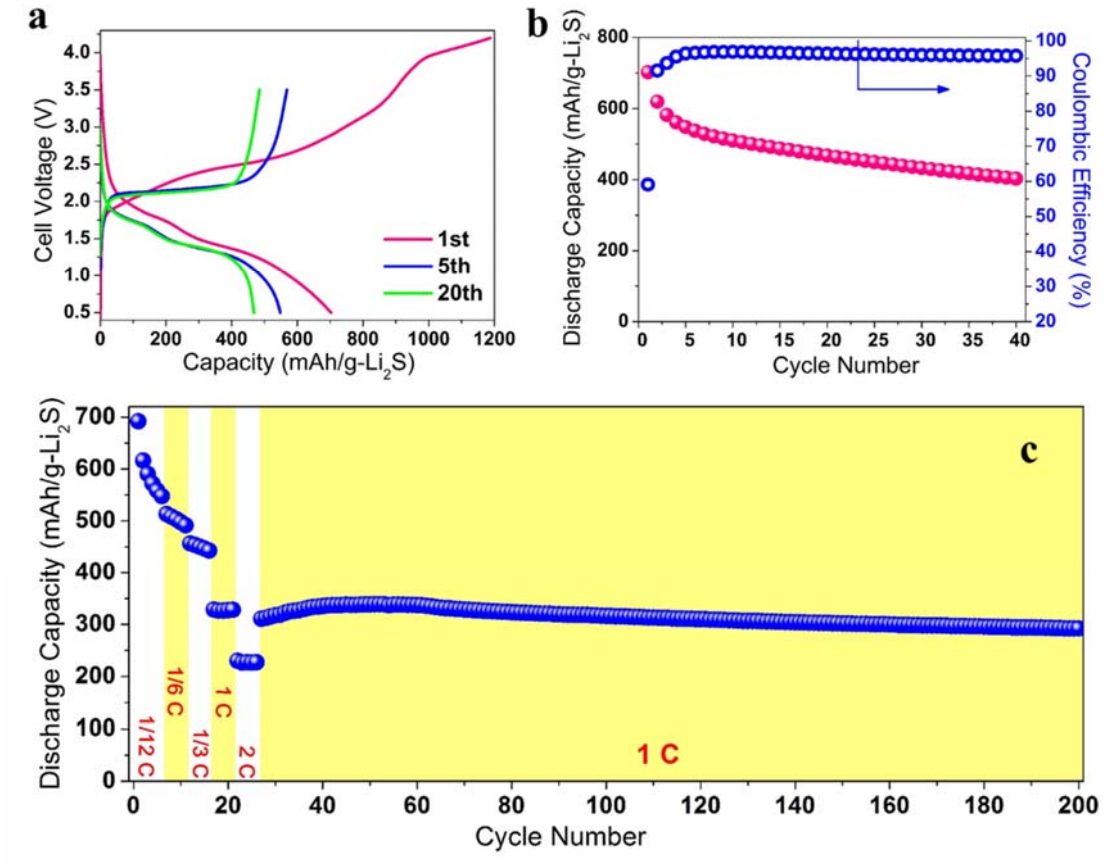

**Fig. 5.3.** (a) Galvanostatic charge-discharge curves of [Si|[Li(G4)$_1$][TFSA]/4HFE|$Li_2S$] cell. The cell was initially charged to 4.2 V at 1/48 C and then discharged and charged between 0.5 and 3.5 V at 1/12 C rate (1 C = 1166 mA/g) in the subsequent cycles. (b) Cycling performance and Coulombic efficiency of Si/$Li_2S$ cell over 40 cycles at 1/12 C. (c) Rate capability of Si/$Li_2S$ cell measured in the range of 1/12−2 C. The cycle durability measurement was conducted at 1 C.

To evaluate the rate capability of Si/$Li_2S$ full cell, the charge and discharge rates were changed from 1/12 C to 2 C as shown in **Fig. 5.3c**. The full cell delivered discharge capacities of 692, 513, 456, 329 and 230 mAh/g at rates of 1/12, 1/6, 1/3, 1 and 2 C, respectively. The 200$^{th}$ discharge capacity of Si/$Li_2S$ cell was 292 mAh/g at 1 C rate (**Fig. 5.3c**), implying a good cycle stability at high current rate. This rate capability and cycle performance of the cell are attributed to the short Li diffusion length in the Si-LP, the intimate contact between $Li_2S$ and graphene, and the relatively high ionic conductivity of [Li(G4)][TFSA]/4HFE electrolyte. The short Li diffusion length in the Si-LP is favorable for the charge and discharge of negative electrode at high current densities. The intimate contact between $Li_2S$ and graphene decreases the resistance of the composite cathode and facilitates the redox reaction of insulating $Li_2S$. The high ionic conductivity of electrolyte reduces the internal resistance of the cell.

The Si/$Li_2S$ cell was disassembled after 200 cycles to characterize the surface of the electrodes (**Fig. 5.4**). For the cycled $Li_2S$ positive electrode, the morphology of $Li_2S$/graphene composite particle and the abundant porous spaces provided by carbon fiber network was well preserved. For the cycled Si negative electrode, some agglomerations of Si flakes are observed, however, no obvious cracks can be seen on the Si-LP, suggesting that the stress of volume change during lithation/delithiation was well defused within the Si-LP thanks to its two-dimensional morphology.

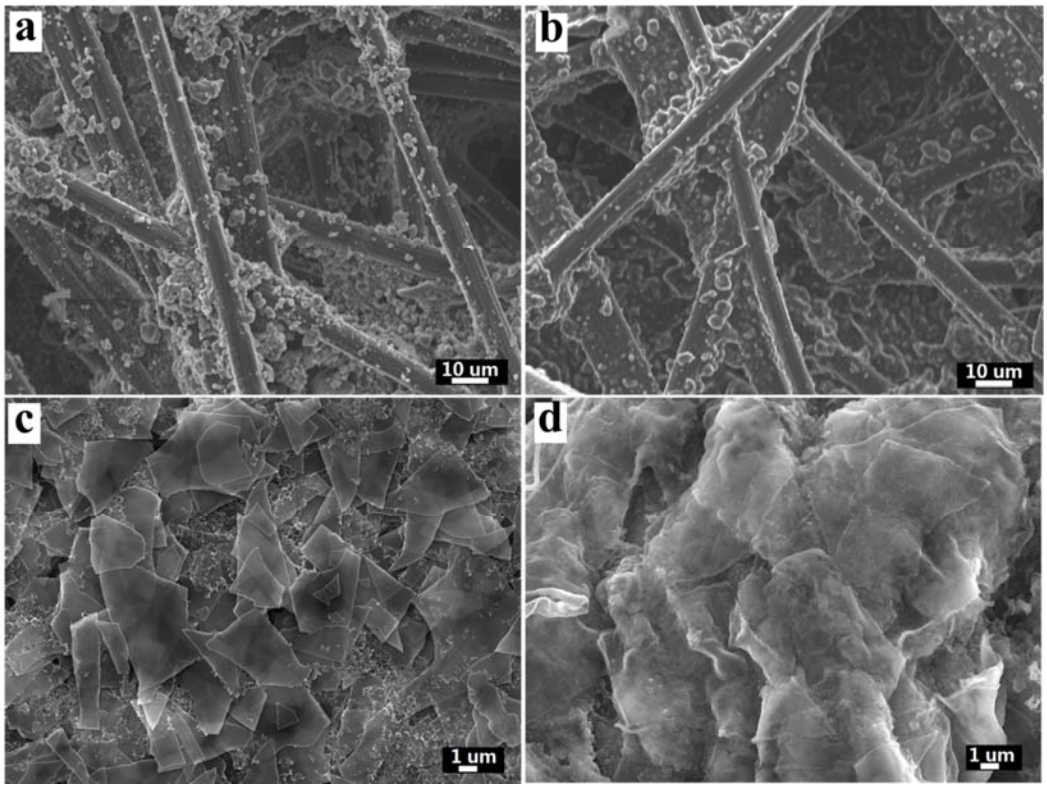


**Fig. 5.4.** Field emission scanning electron microscopy (FESEM) images of (a) fresh $Li_2S$ cathode, (b) $Li_2S$ cathode after 200 cycles, (c) fresh Si anode, and (d) Si anode after 200 cycles.

## 5.4. Conclusions

We prepared and tested a lithium-ion sulfur battery consisting of Si-LP negative electrode, $Li_2S$/graphene positive electrode, and a solvate ionic liquid electrolyte. The Si/$Li_2S$ cell maintained a discharge capacity of 292 mAh/g at 1 C rate after 200 cycles. The stable operation of the Si/$Li_2S$ cell was enabled by the benefits of (i) the ball-milled $Li_2S$/graphene composite with decreased particle size of $Li_2S$ and an intimate contact between the graphene and $Li_2S$, which facilitates the electrochemical reaction of insulating $Li_2S$ in the positive electrode, (ii) the two-dimensional morphology of the Si-LP, which helps to defuse the stress of volume change of Si during the Li-alloying/dealloying process in the negative electrode, and (iii) the solvate ionic liquid, which functions as a polysulfide-insoluble electrolyte and restrains the shuttle effect in the cell effectively. To

achieve higher energy density of Si/$Li_2S$ cell, the densities of $Li_2S$/graphene and Si electrodes should be increased. Further developments are ongoing and will be reported elsewhere.

## 5.5. References


[1] P. G. Bruce, S. A. Freunberger, L. J. Hardwick, J. M. Tarascon, *Nat. Mater.* **2012**, *11*, 19.

[2] A. Manthiram, Y. Fu, Y. S. Su, *Acc. Chem. Res.* **2013**, *46*, 1125.

[3] M. K. Song, E. J. Cairns, Y. Zhang, *Nanoscale* **2013**, *5*, 2186.

[4] S. Urbonaite, T. Poux, P. Novák, *Adv. Energy Mater.* **2015**, *5*, 1500118.

[5] A. Manthiram, Y. Fu, S. H. Chung, C. Zu, Y. S. Su, *Chem. Rev.* **2014**, *114*, 11751.

[6] S. Zhang, K. Ueno, K. Dokko, M. Watanabe, *Adv. Energy Mater.* **2015**, *5*, 1500117.

[7] K. Dokko, N. Tachikawa, K. Yamauchi, M. Tsuchiya, A. Yamazaki, E. Takashima, J. W. Park, K. Ueno, S. Seki, N. Serizawa, M. Watanabe, *J. Electrochem. Soc.* **2013**, *160*, A1304.

[8] C. Zhang, A. Yamazaki, J. Murai, J. W. Park, T. Mandai, K. Ueno, K. Dokko, M. Watanabe, *J. Phys. Chem. C* **2014**, *118*, 17362.

[9] H. Moon, T. Mandai, R. Tatara, K. Ueno, A. Yamazaki, K. Yoshida, S. Seki, K. Dokko, M. Watanabe, *J. Phys. Chem. C* **2015**, *119*, 3957.

[10] J. W. Park, K. Ueno, N. Tachikawa, K. Dokko, M. Watanabe, *J. Phys. Chem. C* **2013**, *117*, 20531.

[11] J. W. Park, K. Yamauchi, E. Takashima, N. Tachikawa, K. Ueno, K. Dokko, M. Watanabe, *J. Phys. Chem. C* **2013**, *117*, 4431.

[12] K. Yoshida, M. Nakamura, Y. Kazue, N. Tachikawa, S. Tsuzuki, S. Seki, K. Dokko, M. Watanabe, *J. Am. Chem. Soc.* **2011**, *133*, 13121.

[13] C. Nan, Z. Lin, H. Liao, M. K. Song, Y. Li, E. J. Cairns, *J. Am. Chem. Soc.* **2014**, *136*, 4659.

[14] F. Wu, J. T. Lee, F. Fan, N. Nitta, H. Kim, T. Zhu, G. Yushin, *Adv. Mater.* **2015**, *27*, 5579.

[15] Z. W. Seh, H. Wang, P. C. Hsu, Q. Zhang, W. Li, G. Zheng, H. Yao, Y. Cui, *Energy Environ. Sci.* **2014**, *7*, 672.

[16] Z. Li, S. Zhang, C. Zhang, K. Ueno, T. Yasuda, R. Tatara, K. Dokko, M. Watanabe, *Nanoscale* **2015**, *7*, 14385.

[17] Z. Li, S. Zhang, S. Terada, X. Ma, K. Ikeda, Y. Kamei, C. Zhang, K. Dokko, M. Watanabe, *ACS Appl. Mater. Interfaces* **2016**, under review.

[18] Y. Son, J. S. Lee, Y. Son, J. H. Jang, J. Cho, *Adv. Energy Mater.* **2015**, *5*, 1500110.

[19] S. Zheng, Y. Chen, Y. Xu, F. Yi, Y. Zhu, Y. Liu, J. Yang, C. Wang, *ACS nano* **2013**, *7*, 10995.

[20] L. Wang, Y. Wang, Y. Xia, *Energy Environ. Sci.* **2015**, *8*, 1551.

[21] J. Hassoun, B. Scrosati, *Angew. Chem. Int. Ed.* **2010**, *49*, 2371.

[22] K. Zhang, L. Wang, Z. Hu, F. Cheng, J. Chen, *Sci. Rep.* **2014**, *4*, 6467.

[23] Y. Yang, M. T. McDowell, A. Jackson, J. J. Cha, S. S. Hong, Y. Cui, *Nano Lett.* **2010**, *10*, 1486.

[24] C. M. Park, J. H. Kim, H. Kim, H. J. Sohn, *Chem. Soc. Rev.* **2010**, *39*, 3115.

[25] T. D. Hatchard, J. R. Dahn, *J. Electrochem. Soc.* **2004**, *151*, A838.

[26] H. Wu, G. Zheng, N. Liu, T. J. Carney, Y. Yang, Y. Cui, *Nano Lett.* **2012**, *12*, 904.

[27] M. Haruta, Y. Masuo, T. Moriyasu, A. Tomita, C. Sakakibara, A. Kamei, M. Hirota, T. Takenaka, T. Doi, M. Inaba, *Electrochemistry* **2015**, *83*, 837.

[28] M. Saito, T. Yamada, C. Yodoya, A. Kamei, M. Hirota, T. Takenaka, A. Tasaka, M. Inaba, *Solid State Ionics* **2012**, *225*, 506.

[29] Y. Yang, G. Zheng, S. Misra, J. Nelson, M. F. Toney, Y. Cui, *J. Am. Chem. Soc.* **2012**, *134*, 15387.

[30] M.N. Obrovac, L.J. Krause, *J. Electrochem. Soc.*, **2007**, *154*, A103.

# Chapter Six

Concluding Remarks and Future Directions

## 6.1. General Conclusions

In chapter one, progress and challenge of Li−S batteries have been introduced in the light of the previous studies and current trend in the fundamental and application perspectives. To circumvent the issues and face the challenges in Li–S batteries, $Li_2S$ as a promising cathode-active material has been investigated extensively by researchers. In this chapter, the preparation methods of $Li_2S$-C composite have been summarized in detail, which included ball-milling method, solution-based route and chemistry approach. Moreover, in previous works, $Li_2S$ cathodes have been coupled with graphite, Si and Sn anodes to realize the rechargeable full cells, which were also introduced. Finally, the aim and outline of this study were proposed.

In chapter two, a very simple method of preparing a $Li_2S$/graphene composite through one-pot pyrolysis of lithium sulfate and graphene nanoplatelet aggregates (GNAs) without using expensive commercial $Li_2S$ was developed. This step can immobilize the active $Li_2S$ deposits in situ on the highly conductive host by intimate contact. The in situ formed $Li_2S$/graphene could be used directly as cathodes for lithium–sulfur batteries, delivering greatly enhanced capacities, fast reaction kinetics, low polarization, and good cycling performance and rate capability as compared with a physical mixture of commercial $Li_2S$ and GNAs.

In chapter three, a novel composite was fabricated by applying high-energy ball milling to this in-situ formed $Li_2S$/graphene composite. This simple and efficient approach (high-energy ball milling) can not only reduce the particle size of the $Li_2S$/graphene composite, but also enhance the reaction kinetics of $Li_2S$. In addition, traditional aluminium foil current collector was replaced by a three-dimensionally porous current collector (carbon fiber paper), to improve the electrochemical performance of the $Li_2S$ electrode at high mass loading. As a result, the ball-milled $Li_2S$/graphene composite electrode exploiting the three-dimensionally porous current collector exhibited an excellent cell performance, even at a high $Li_2S$ loading of 2.2 mg/cm$^2$.

In chapter four, simple graphite-based Li-S full cells were fabricated by employing solvate ionic liquid electrolytes, in combination with highly loaded $Li_2S$/graphene composite cathodes ($Li_2S$ loading: 2.2 mg/cm$^2$). The composition of electrolyte ([Li(G4)$_x$][TFSA]/HFE, $x$ = 0.6, 0.8, 1) was further optimized by varying the molar ratio between G4 and LiTFSA. The ionic conductivity and the $Li^+$ intercalation/deintercalation properties of the electrolytes were found to greatly affect the battery performance. Among all concentrated electrolytes examined, [Li(G4)$_{0.8}$][TFSA]/HFE, possessing both a balanced conductivity and intercalation/deintercalation capability, exhibited the highest first- and 20th-cycle discharge capacities of 809 and 586 mAh/g, respectively, in conjunction with a high Coulombic efficiency of up to 99%.

In chapter five, a high-performance full cell comprised of an amorphous Si anode, a solvate ionic liquid electrolyte and a thick $Li_2S$ cathode ($Li_2S$ loading: 2.2 mg/cm$^2$) was developed. This full cell maintained a discharge capacity of 292 mAh/g at 1 C rate after 200 cycles. The stable operation of the Si/$Li_2S$ cell was enabled by the benefits of (i) the ball-milled $Li_2S$/graphene composite with decreased particle size of $Li_2S$ and an intimate contact between the graphene and $Li_2S$, which facilitates the electrochemical reaction of insulating $Li_2S$ in the positive electrode, (ii) the two-dimensional morphology of the Si-LP, which helps to defuse the stress of volume change of Si during the Li-alloying/dealloying process in the negative electrode, and (iii) the solvate ionic liquid, which functions as a polysulfide-insoluble electrolyte and restrains the shuttle effect in the cell effectively.

## 6.2. Future Directions

Although a facile, low-cost, scalable, and environmentally friendly method for preparing the $Li_2S$-C composite was proposed in this study, and advanced $Li_2S$ cathode/Li-free anode cells were assembled successfully, issues associated with the battery energy density still need to be solved. Possible strategies that can improve the energy density are shown as follows:

(a) Introduce the redox mediators to the electrolyte to depress the active potential of $Li_2S$.
(b) Develop novel high-efficient $Li_2S$-C composites by this one-pot pyrolysis method.
(c) Utilize other three-dimensionally porous current collectors and improve the $Li_2S$ loading.
(d) Increase the density of cathode material and decrease the electrolyte uptake.

Moreover, we believe that the $Li_2S$ cathode/Li-free anode battery is a promising cell configuration for next-generation energy storage, and the present research could trigger new attempts to fabricate the lithium-ion sulfur cells.

**List of Publications:**

1. **Zhe Li**, Shiguo Zhang, Ce Zhang, Kazuhide Ueno, Tomohiro Yasuda, Ryoichi Tatara, Kaoru Dokko, Masayoshi Watanabe, One-pot pyrolysis of lithium sulfate and graphene nanoplatelet aggregates: in situ formed $Li_2S$/graphene composite for lithium–sulfur batteries, *Nanoscale*, **2015**, 7, 14385-14392.
2. **Zhe Li**, Shiguo Zhang, Shoshi Terada, Xiaofeng Ma, Kohei Ikeda, Yutaro Kamei, Ce Zhang, Kaoru Dokko, Masayoshi Watanabe, Promising Cell Configuration for Next-Generation Energy Storage: $Li_2S$/Graphite Battery Enabled by a Solvate Ionic Liquid Electrolyte, *ACS Applied Materials & Interfaces*, **2016**, 8, 16053–16062.
3. **Zhe Li**, Yutaro Kamei, Masakazu Haruta, Toshio Takenaka, Akira Tomita, Takayuki Doi, Shiguo Zhang, Kaoru Dokko, Minoru Inaba, and Masayoshi Watanabe, Si/$Li_2S$ Battery with Solvate Ionic Liquid Electrolyte, *Electrochemistry*, in press.